UNIVERSIDAD COMPLUTENSE DE MADRID
FACULTAD DE MEDICINA

TESIS DOCTORAL

Papel de las C-JUN cinasas N-terminales (JNK) en el desarrollo de cáncer de vías biliares

Role of-JUN N-terminal kinases (JNK1/2) in the development of cancer of the biliary tract

MEMORIA PARA OPTAR AL GRADO DE DOCTOR

PRESENTADA POR

Chaobo Chen

DIRECTORES

Javier Cubero Palero
Yulia A. Nevzorova

Madrid

UNIVERSIDAD COMPLUTENSE DE MADRID

FACULTAD DE MEDICINA

TESIS DOCTORAL

PAPEL DE LAS C-JUN CINASAS N-TERMINALES (JNK) EN EL DESARROLLO DE CÁNCER DE VÍAS BILIARES

MEMORIA PARA OPTAR AL GRADO DE DOCTOR

PRESENTADA POR

CHAOBO CHEN

DIRECTORES

FRANCISCO JAVIER CUBERO PALERO

YULIA A. NEVZOROVA

Madrid

08.12.2020

COMPLUTENSE UNIVERSITY

SCHOOL OF MEDICINE

DOCTORAL THESIS

ROLE OF C-JUN N-TERMINAL KINASES (JNK1/2) IN THE DEVELOPMENT OF CANCER OF THE BILIARY TRACT

MEMORY TO OPT FOR THE DEGREE OF DOCTOR

PRESENTED BY

CHAOBO CHEN

Directors

Francisco Javier Cubero Palero

Yulia A. Nevzorova

Madrid

08.12.2020

UNIVERSIDAD COMPLUTENSE DE MADRID

FACULTAD DE MEDICINA

Departamento de Inmunología, Oftalmología y ORL

TESIS DOCTORAL

PAPEL DE LAS C-JUN CINASAS N-TERMINALES (JNK) EN EL DESARROLLO DE CÁNCER DE VÍAS BILIARES

ROLE OF C-JUN N-TERMINAL KINASES (JNK1/2) IN THE DEVELOPMENT OF CANCER OF THE BILIARY TRACT

CHAOBO CHEN

Madrid
08.12.2020

Directors: Francisco Javier Cubero Palero
Yulia A. Nevzorova

UNIVERSIDAD COMPLUTENSE DE MADRID

FACULTAD DE MEDICINA

Departamento de Inmunología, Oftalmología y ORL

TESIS DOCTORAL

PAPEL DE LAS C-JUN CINASAS N-TERMINALES (JNK) EN EL DESARROLLO DE CÁNCER DE VÍAS BILIARES

ROLE OF C-JUN N-TERMINAL KINASES (JNK1/2) IN THE DEVELOPMENT OF CANCER OF THE BILIARY TRACT

CHAOBO CHEN

Madrid
08.12.2020

Directors: Francisco Javier Cubero Palero
Yulia A. Nevzorova

Acknowledgements

Sincerely, I need to thank everyone who helped me! Without the help, encouragement, guidance and support of many people, it would be impossible for me to complete this thesis dissertation.

First of all, I would like to thank Prof. Francisco Javier Cubero for granting me the opportunity to study in the Department of Immunology at the Complutense University School of Medicine in Madrid, Spain. This has provided me with excellent research conditions. Prof. Francisco Javier Cubero, just like a godfather who presents me as a child at baptism and promises to take responsibility for me via his professional education. Thanks a lot, under his supervision, guidance together with advice during the project is progressing and throughout the whole study periods, I have made big progress that I never thought before. Sincerely, I would also prefer to thank Prof. Cubero for all his friendly activity and all constructive discussions, as well as deep thinking idea combined with creative direction to me. Furthermore, during my studies, I am grateful to Prof. Cubero for giving me full confidence and encouragement, and also helping me to improve my awareness of high-quality papers. Additionally, I would like to thank him for his continuous support and corrections to complete my thesis. The most precious thing is that he respects Chinese students from the beginning to the end, and is never biased, so he gives us, Chinese foreigners, a warm environment. This is why I have all respect and gratitude to my Dear tutor Javier from the heart. In my heart, he is not only my director but also a great navigator to help me open the new world of science.

Secondly, I would like to thank the former Director of the Department and current Vicedean of Research José Ramón Regueiro Gonzalez-Barros and also Prof. Eduardo Martínez-Naves for allowing me to conduct research and study opportunities in the Department of Immunology. It provides a nice environment for me to make the experimental results smoothly.

Thanks to Prof. Yulia A. Nevzorova for her help and support during my project, so that I can quickly master the experimental methods of immunohistochemistry. At the same time, she also help me revise and improve the thesis.

Thanks to Drs. Fengjie Hao, Kang Zheng, and Feifei Guo, who helped me develop experimentally targeted gene knockout mice from the very beginning, and helped me to improve the technology of experiments as well as the guidance for my scientific research ideas in the project.

In particular, I would like to thank my dear Dr. Hui Ye, for all kinds of her help and support during the whole project in my Ph.D. studying period. In this passed three-year studying, she not only helped me to take care of the experimental mice, but also encouraged me to try to adjust the thinking mode so that I could improve the efficiency of my project. These enabled me to complete good experimental results within a fixed time. Furthermore, we are not only work-partners in our research projects, but also help each other in our daily life. Especially during the quarantine period of the coronavirus-19 (COVID-19) pandemic, we encouraged each other and overcame the difficulty successfully.

Thanks to Beatriz Martín Adrados for helping me successfully complete the cell gene knockout and for guiding me during the completion of the project. Also, I am very grateful to Beatriz for her help so that I can easily conduct and complete part of the experiments. At the same time, I am very grateful to show sincerely gratitude to Beatriz for her continuing enthusiastic and generous supports.

Thanks to Prof. Agustín Tortajada Alonso. With his help, I successfully realized the technique of preparing and extracting plasmids. Additionally, I shall thank to Beatriz Amorós Pérez, because her help whenever I asked for, she would not hesitate to show me a hand to solve the problems, with super nice support as well. I would like to thank them all. During my study here, I am very grateful for their friendship and generosity.

I would like to thank Dr. Raúl Torres, CNIO Research Center and Dr. Igor Aurrekoetxea, of the Medicine School University of the Basque Country for enabling me to successfully master the CRISPR Cas9 cell gene knockdown technology and the methods of plasmid preparation, extraction and use.

Thanks to all the members in our laboratory, Arantza Lamas Paz, Olga

Estévez Vázquez, Laura Morán Blanco, Raquel Benedé Ubieto, Marina Mazariegos León, Carlos Sanz García. They have provided me with a lot of help during my study, giving the laboratory a particularly harmonious atmosphere, and it is super extremely pleasant to work with them.

I also want to thank Prof. Gang Zhao for his continuing support and all kind advice before I came here as well as during my three years' PhD study.

I would like to sincerely thank Wuxi Xishan People's Hospital, for whose sufficient financial support, and all my colleagues in the Department of General Surgery for their encouragement, support and help.

Finally, I sincerely thank my parents for their encouragement and help, my dear love Jing Hu for giving me the strongest financial background and continuing support without any complaint, as well as my daughter Yunzhu Chen (Racy) and son Yulin Chen (Kevin) for their encouragement, completely understanding and spiritual support. I also want to thank my brothers and sisters, relatives and all of my kind friends.

Index

Table of contents

1. Resumen/Abstract

1.1 Resumen

El colangiocarcinoma (CCA) es un cáncer de las vías biliares maligno agresivo, y que constituye el segundo tumor primario de hígado más común. En Europa, se diagnostican alrededor de 13.000 nuevos casos de CCA por año. Sin embargo, la patogenia de CCA sigue siendo difícil de entender y la falta de herramientas de diagnóstico y tratamiento impiden un mejor resultado para los pacientes. En el presente estudio, utilizamos un nuevo modelo animales de CCA, para entender el mecanismo molecular. En el presente trabajo, planteamos la hipótesis de que la disfunción sinérgica de Jnk1 y Jnk2 en los hepatocitos impulsa el desarrollo de la colangiocarcinogénesis. Ratones con deleción específica de Jnk1/2 en hepatocitos $Jnk^{\Delta hepa}$ y ratones floxeados control ($Jnk^{f/f}$) fueron sacrificaron en diferentes puntos de tiempo durante la progresión de la enfermedad hepática. Así mismo, diferentes modelos experimentales tóxicos (TAA, DE/TAA, DEN/CCl_4) fueron utilizados. De manera interesante, los ratones $Jnk^{\Delta hepa}$ mostraron progresivamente una mayor expresión de BiP/GR78, XBP1 empalmado y regulación a la baja de pIRE1α, lo que sugiere que la activación de XBP1 asociada con BiP podría desencadenar la cistogénesis hepática y las primeras etapas de CCA. Simultáneamente, tras daño tóxico o en modelo genético de cáncer, en comparación con los ratones $Jnk^{f/f}$, los marcadores séricos de daño hepático (ALT, AST, LDH) aumentaron significativamente en los ratones $Jnk^{\Delta hepa}$ tratad Estos resultados se acompañaron de un aumento significativo de células TUNEL-positivas, hiperproliferación de células hepáticas (Ki 67), fibrogénesis, depósito de colágeno y α-actina del músculo liso (αSMA) y citocinas proinflamatorias (por ejemplo, *Tnf-α*, *Tgf-β1*, *IL-6*). De acuerdo con esta detección, se produjo una activación prominente de necroptosis (RIP1/RIP3/MLKL) en el daño hepático $Jnk^{\Delta hepa}$. Concomitantemente, los biomarcadores de células ovales hepáticas y epitelio biliar (CK19, AFP, SOX9,

YAP1, MUCIN2, Notch1) se regularon significativamente al alza. Finalmente, la sobreexpresión de c-MYC puede ser carcinogénica para desencadenar la formación de CCA en el grupo experimental $Jnk^{\Delta hepa}$ en comparación con el hígado $Jnk^{f/f}$. En resumen, nuestros datos indican que la combinación de funciones de JNK en los hepatocitos es esencial para la homeostasis de los hepatocitos. La pérdida de función de JNK1/2 puede promover la activación de la XBP1 asociada con BiP involucrada en ER-estrés, desencadenar cistogénesis hepática y etapas tempranas de CCA. La sobreexpresión de JNK1/2 promueve la formación de HCC, mientras que la falta de JNK1/2 promueve la formación de CCA en la estimulación hepática crónica. Colectivamente, las JNK juegan un papel vital en el equilibrio de la diferenciación y transformación de hepatocitos y colangiocitos. Nuestra investigación reveló la nueva función de JNK en el destino de los hepatocitos y colangiocitos, abriendo una nueva vía terapéutica para el tratamiento de la CCA.

1.2 Abstract

Cholangiocarcinoma (CCA) is an aggressive malignant bile duct cancer, and the second most common primary liver tumor In Europe, around 13,000 new CCA cases were diagnosed per year. However, the pathogenesis of CCA remains elusive and lack of diagnostic as well as treatment tools impede a better outcome for patients. In the present study, we use a new animal model of CCA, to understand the molecular mechanism. In the present work, we hypothesize that the synergistic dysfunction of Jnk1 and Jnk2 in hepatocytes drives the development of cholangiocarcinogenesis. Mice with specific deletion of *Jnk1/2* in hepatocytes ($Jnk^{\Delta hepa}$) and floxed ($Jnk^{f/f}$) control mice were sacrificed at different time points during liver disease progression. Likewise, different toxicity treatments (i.e., TAA, DEN/TAA and DEN/CCl4) and experimental models were used. Interestingly, $Jnk^{\Delta hepa}$ mice showed progressively higher expression of BiP/GR78, combined with spliced XBP1, and down-regulation of pIRE1α, suggesting that BiP-associated activation of XBP1 could trigger liver cystogenesis and early stages of CCA. Simultaneously, after toxicity damage or in the genetic model of cancer, compared to the $Jnk^{f/f}$ mice, the serum markers of liver damage (ALT, AST, LDH) significantly increased in $Jnk^{\Delta hepa}$ mice after the treatments. These results were accompanied by a significantly increased number of TUNEL-positive cells, hyperproliferation of liver cells (Ki 67), fibrogenesis, deposition of collagen and α-smooth muscle actin (αSMA), and pro-inflammatory cytokines (e.g., *Tnf-α*, *Tgf-β1*, *IL-6*). In line with these detection, prominent activation of necroptosis (RIP1/RIP3/MLKL) occurred in $Jnk^{\Delta hepa}$ liver damage. Concomitantly, the biomarkers of liver oval cells and biliary epithelium (CK19, AFP, SOX9, YAP1, MUCIN2, Notch1) were significantly upregulated. Finally, the overexpression of c-MYC may be carcinogenic to trigger the formation of CCA in the $Jnk^{\Delta hepa}$ experimental group compared to the $Jnk^{f/f}$ liver. In summary, our data indicate that the combination of JNK functions in hepatocytes is essential for hepatocyte

homeostasis. Loss function of JNK1/2 may promote the activation of the XBP1 associated with BiP involved in ER-stress, trigger hepatic cystogenesis and early stages of CCA. Overexpression of JNK1/2 promotes formation of HCC, while the lack of JNK1/2 promotes the formation of CCA in chronic liver stimulation. Collectively, JNKs play a vital role in balancing the differentiation and transformation of hepatocytes and cholangiocytes. Our research revealed the new function of JNK in the fate of hepatocytes and cholangiocytes, opening a novel therapeutic avenue for the treatment of CCA.

2. Abbreviations

2.1. List of Abbreviations

Abbreviation	Significance
ADPKD	Autosomal dominant polycystic kidney disease
ADPLD	Autosomal dominant polycystic liver disease
AFP	Alpha-fetoprotein
aHSCs	Activated hepatic stellate cells
ALP	Alkaline phosphatase
ALT	Alanine-aminotransferase
ANOVA	Analysis of variance
APAP	Acetaminophen
APS	Ammonium Persulfate
ARPKD	Autosomal recessive polycystic kidney disease
αSMA	α-Smooth muscle actin
AST	Aspartate aminotransferase
BECs	Biliary epithelial cells
BSA	Bovine Serum Albumin
Caspase	Cysteine dependent aspartate directed protease
CCA	Cholangiocarcinoma
CCl_4	Carbon tetrachloride
CCK-8	Cell counting kit 8
CDK4	Cyclin-dependent kinase 4
cDNA	Complementary DNA
CHF	Congenital hepatic fibrosis
CK19	Cytokeratin 19
CLD	Chronic liver disease
CoH	Canals of Hering
CS	Caroli’s syndrome
CST	Cell Signaling Technology

DAB	3,3'-diaminobenzidine
DAPI	4,6-diamino-2-phenylindole
dCCA	distal cholangiocarcinoma
DEN	Diethylnitrosamine
Δhepa	Deleted in hepatocytes
DMEM:	Dulbecco´s modified Eagle´s medium
DNA	Deoxyribonucleic acid
dNTP	Deoxyribonucleotide triphosphate
DR	Ductular reaction
DTT	Dithiothreitol
ECL	Enhanced chemiluminescence
ECM	Extracellular matrix
EDTA	Ethylenediaminetetraacetic acid
EGF	Epidermal growth factor
eIF2α	Eukaryotic initiation factor-α
EMT	Epithelial mesenchymal transition
ER	Endoplasmic reticulum
ErbB2	Human epidermal growth factor receptor 2
ERK	Extracellular signal-regulated kinases
EtOH	Ethanol
^{18}FDG-PET	^{18}F-fluorodeoxyglucose positron emission tomography
GAPDH	Glyceraldehyde 3-phosphate dehydrogenase
GEF	Guanine nucleotide exchange factor
GLDH	Glutamate dehydrogenase.
GPCR	G protein-coupled receptor
GRP78	Glucose-regulated protein 78
GS	Glutamine Synthetase
HCC	Hepatocellular carcinoma
H&E	Hematoxylin and eosin

HGF	Hepatocyte growth factor
HNFs	Hepatocyte nuclear factors
HPC	Hepatic progenitor cell
HRP	Horseradish peroxidase
HSCs	Hepatic stellate cells
iCCA	intrahepatic cholangiocarcinoma
IF	Immunofluorescence staining
IGF	Insulin like growth factor
IHC	Immunohistochemistry
IP	Intraperitoneal
JNK	c-Jun NH2-terminal kinase
Ki 67	Cell cycle specific protein encoded by the MKI 67 gene
KCs	Kupffer cells
KLF6	Krüppel-like factor 6
LSECs	Liver sinusoidal endothelial cells
LPS	lipopolysaccharide
MAPK	Mitogen-activated protein kinase
MF	Myofibroblast
$MgCl_2$	Magnesium chloride
mRNA	Messenger RNA
NK cells	Natural killer cells
NPCs	Non-parenchymal cells
OD	Optical density
PAS	Periodic Acid Schiff
PBC	primary biliary cholangitis
PBS	Phosphate buffered saline
PBS-T	Phosphate buffered saline supplemented with Tween 20
pCCA	perihilar cholangiocarcinoma
PCNA	Proliferating cell nuclear antigen

PDGF	Platelet-derived growth factor
PFA	Paraformaldehyde
pJNK1/2	Phospho-c-Jun N-terminal Kinases1/2
PKA	Protein kinase A
PLD	Polycystic liver disease
PSC	primary sclerosing cholangitis
qHSCs	Quiescence hepatic stellate cells
qRT-PCR	Quantitative polymerase chain reaction
RDCs	Reactive ductal cells
RIP	Receptor-interacting protein kinase
RNA	Ribonucleic acid
RT	Room temperature
SDS	Sodium dodecyl sulphate
SEM	standard error of the mean
SOS	Son of sevenless
SOX9	Sex-determining region Y-box (SRY-box) containing gene 9
SR	Sirius Red
TAA	Thioacetamide
TAE	Tris Acetate EDTA Buffer
TBS	Tris buffered saline
TBS-T	Tris buffered saline supplemented with Tween 20
TEMED	N´, N, N´, N´-Tetramethyl diamine
TGF-β	Transforming growth factor β
TGR5	G-protein coupled bile acid receptor-1
TNF-α	Tumor necrosis factor-α
Tris	2-Amino-2(hydroxymethyl)-1,3-propandiol
TUNEL	Terminal deoxynucleotidyl transferase dUTP nick end labeling
Tween 20	Polyoxyethylene (20) Sorbitan Monolaurate

VEGF	Vascular endothelial growth factor
VEGFR	Vascular endothelial growth factor receptor
WB	Western blot
YAP1	Yes-associated protein 1

3. Introduction

3.1 Liver anatomy and Function

3.1.1. Liver structure

The liver is the largest organ and gland in the human body and weighs on average 1200-1500 g, which makes up around 2% of the whole-body weight. However, the liver complies about 4.5% of the total bodyweight in mice. Most of the liver is located in the right quarter and upper ventral region, and a small part is located in the left quarter. A significant feature of the liver is its dual blood supply. The blood supply to the liver comes from the hepatic artery (20%-40%) and the portal vein (60%-80%). The blood flow of the liver is 1500-2000ml/min, accounting for about 30-40% of cardiac output. Blood flows out of the liver through the hepatic vein into the portal vein. The liver is highly vascularized and receives about a quarter of the cardiac output. The blood entering the liver is a mixture of 25% oxygen-rich blood from the hepatic artery and 75% oxygen-poor blood entering through the portal vein. The portal vein carries visceral nutrients and potentially or obviously harmful substances. These substances will be monitored and cleared by the liver when needed to ensure that the blood leaving the liver is compatible with normal homeostasis. The hepatic lobule is the most basic structural and functional unit of the liver. A complete hepatic lobule is composed of the central vein, hepatocytes, bile ducts, liver plate, hepatic sinusoids, peri-sinus space, and hepatic macrophages. The porta hepatis is a fissure structure that contains the entrance to the hepatic artery, portal vein, and common bile duct. Arterial, venous, and bile duct catheters follow the septum throughout the liver and correspondingly extend into multiple intralobular branches. In human, the Glisson system consists of the intrinsic arteries, portal vein and intrahepatic bile duct, and divides the liver into 4 lobes (including Right (largest), left, caudate, quadrate) and 8 segments[1, 2] (**Fig. 1**).

The right lobe and left lobe of the liver are further divided into 8 segments according to the distribution of portal scissure. At hilus, the right portal vein goes

through a short course (1-1.5 cm) before entering the liver. Once in the liver parenchyma, the portal vein divides into a right anterior branch, which arches vertically in the front of the liver, and a posterior branch moves along the posterolateral side. The right portal vein supplies the anterior (or anteromedial) and posterior (or posterolateral) portions of the right lobe. The branching pattern of these portal veins divides the right liver into 4 segments, the anterior segment is segment V (anterior and inferior) and segment VIII (front and upper), while segment VI (rear and inferior) and segment VII (rear and upper) form the posterior sector[3]. The portal vein is the main blood vessel of the portal system formed by the confluence of the spleen and superior mesenteric vein. It is excreted directly into the liver and accounts for about 75% of its blood flow[4]. Hemodynamic watersheds or cracks separate the incoming and outgoing large blood vessel segments, allowing the surgical removal of single or adjacent large blood vessel segments[5].

The liver is an active, bidirectional biological filter that participates in maintaining the body's homeostasis. Because it not only filters the portal blood that transports nutrients and toxic compounds from the environment through the gastrointestinal tract, but also filters the blood of the whole body (the body's own products, such as bilirubin which is produced when the liver breaks down old red blood cells), and it also provides the only channel of human bile transportation, the biliary system, which allows the bile to enter into the intestine and assist food digestion. It is classified as an active filter because it can quickly metabolize most nutrient compounds, and it can also neutralize and remove toxic exogenous (xenobiotics) and endogenous substances[6]. Although the liver is powerful, it also causes the liver to be constantly exposed to strong microbial and antigen stimuli. These stimuli require the functions of the innate immune system and the adaptive immune system. These different functions are completed by a complex structure, a multiple cellular tissue with unique vascular structure and the comprehensive activities of the participants.

The liver has not only two main cell types-hepatocytes and biliary cells (or cholangiocytes), but also liver sinusoidal cells (see chapter 3.1.2). Hepatocytes are parenchymal cells in liver tissue. They do not constitute a homogeneous cell population. They are highly polarized cells (e.g., molecular specializations of various surface membranes, such as receptors, pumps, transport channels, and carrier proteins). Their functions and morphology are opposite to a certain extent, and their position in parenchyma. This polarization allows them to perform the most complex metabolic tasks in the mammalian organism.

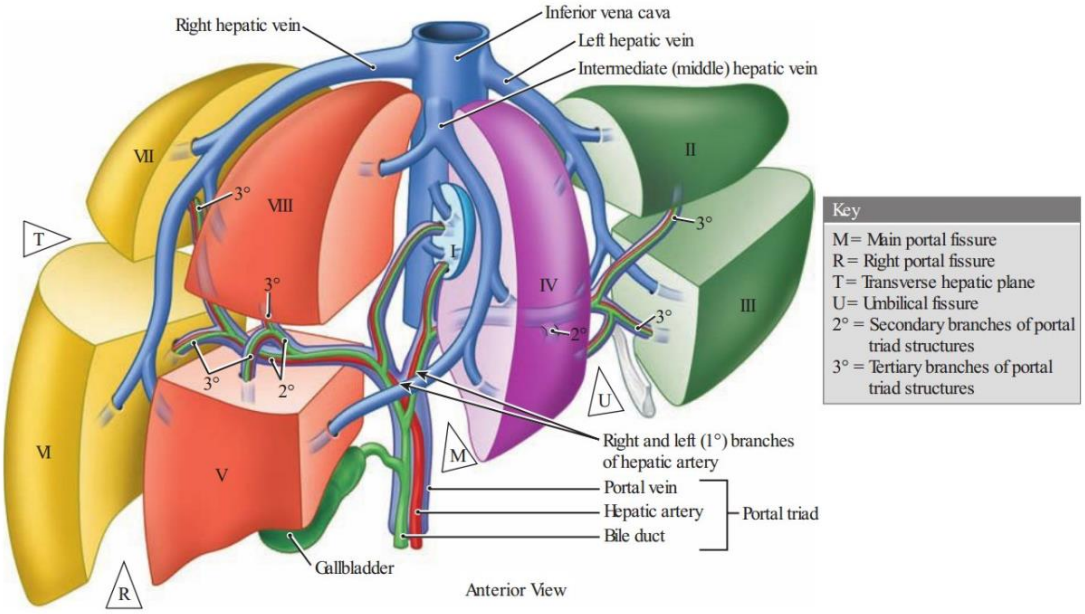

Figure 1. The segments and vascular structure of the liver. The right hepatic vein divides the right lobe into anterior and posterior lobes. The middle hepatic vein divides the liver into left and right lobes (or left and right hemiliver). This plane extends from the inferior vena cava to the fossa gallbladder. The falciform ligament divides the left lobe into medial segment IV and lateral segment II and III, and the portal vein divides the liver into upper and lower segments. The left and right portal veins branch up and down, extending into the center of each segment. Portal vein, Hepatic artery and Bile duct make up to the formation of Glisson system[2].

3.1.2. Function of liver cells

Hepatic parenchymal cells are arranged in a hexagon around the central vein, forming a single layer of thick epithelium, thereby generating hepatic lobule.

Then, the hepatic lobule is composed of the central terminal hepatic vein, surrounded by 4-6 terminal portal vein triads, forming a polygonal unit, which in turn forms the structural and functional unit of the liver. The liver has approximately 50,000-100,000 functional units, and each of them radiates around the central vein. Blood flows from the portal venous tract to the peripheral small veins of the liver to form a so-called "sinusoid". The sinusoidal cells, including hepatic stellate cells (HSCs), liver sinusoidal endothelial cells (LSECs), and liver Kupffer cells (KCs) and pit cells (or natural killer cells (NK cells)), together with the sinusoidal morphology of liver cells constitute a functional and histological unit (**Fig. 2**). These cells interact with other signaling mechanisms through cytokines. Whilst the liver cells around the portal vein closer to the portal vein are functionally different from the central hepatic cells near the central small vein of the liver[7].

Hepatocytes account for the vast majority of the total liver mass, approximately 80% of the liver cell volume, and liver non-parenchymal cells (NPCs) account for approximately 6.3%, including HSCs, LSECs and KCs, accounted for about 1.4%, 2.8% and 2.1% respectively[8]. The cytoplasm of hepatocyte is eosinophilic and the nucleus is round, including mitochondria and endoplasmic reticulum (ER) ribosomes. Hepatocytes can be regenerated and the average life span of them is 5 months. In addition to being responsible for their typical liver histology, these cells are the main functional cells and play a vital role in protein synthesis, detoxification, bile salt and phospholipid synthesis, lipid and carbohydrate metabolism as well as modification and excretion of bile formation and secretion[9].

HSCs, or liver myofibroblasts, also named Ito cells, store vitamin A, and produce extracellular matrix and collagen[10]. HSCs play a role in the complex mechanisms of liver fibrosis and cirrhosis. They are also distributed between endothelial cells, but it is difficult to observe through an optical microscope. Other pit cells or liver-related natural killer cells, whose main functions include

local host defense and maintenance of immune balance[11, 12]. In response to injury, quiescence HSCs (qHSCs) differentiate into activated HSCs (aHSCs), characterized by the expression of α-actin smooth muscle (αSMA), fibrogenic and mitogenic sensitive, and has the ability to actively secrete extracellular matrix (ECM) proteins (especially laminin, collagen I and III). This results in changes in the normal composition of the matrix, including cell-matrix interaction and the deposition of growth factors[13, 14].

LSECs form the sinusoidal endothelial layer, and play a key regulatory role in all aspects of intra-and transendothelial transport. In liver pathobiology, LSECs play central roles in liver fibrosis, cancer metastasis, and liver toxicology. Less than 20% of the ATP produced by LSECs and KCs from exogenous substrates comes from glucose metabolism, and the main energy source in these cells is the oxidation of glutamine and palmitate[15].

KCs or liver macrophages, which are mainly present on the sinus wall of the portal vein, are the first line of defense formed by removing foreign substances that enter the liver circulation. They are also part of the reticuloendothelial system and engulf aging red blood cells. They can also secrete cytokines, which may damage liver cells and take part in the remodeling of the ECM.

Cholangiocytes or biliary epithelial cells (BECs), account for much less than 1% of the total liver parenchymal cells, because most of them are located in the portal bile duct[16]. Only the smallest bile duct penetrates the parenchyma of the portal vein and connects to the bile duct in the liver plate. The connection point between the catheter and the liver plate is defined by a tubular structure called the Canals of Hering (CoH), which is composed of cholangiocytes and hepatocytes. Furthermore, the biliary tree was first generally recognized for its function of transporting and modifying primary bile secreted by hepatocytes, but now it is generally believed that the bile duct tree is actually a complex structure with many different biological functions, which is reflected in the morphological and functional specialization of BECs[17]. Changes in bile composition can trigger

a series of events, such as the formation of bile obstruction, the accumulation of toxicities, damage to BECs, causing focal cholangiocytes inflammation changes, which then may progress to sclerosing cholangitis, eventually cirrhosis[18].

Fibrosis is a reversible scar formation process caused by chronic liver injury, which is characterized by excessive deposition of ECM. HSCs are the main source of ECM in normal and fibrotic livers, while LSECs and KCs stimulate this process through activation of transforming growth factor β (TGF-β) signaling, and the production of pro-inflammatory molecules[19]. In liver fibrosis, TGF-β is a main factor mainly secreted by fibroblasts and macrophages, and has the function of activating HSCs, which is responsible for the deposition of most (about 80%) matrix proteins[20]. In addition to inflammatory cells, it is related to the crosstalk between cells of mesenchymal origin, especially KCs and portal vein fibroblasts. They are the main effector of fibrosis and the stimulus of ECM deposition. After the stimulation of toxicity carbon tetrachloride (CCl_4), the composition of ECM in the liver has changed greatly, similar to that detected in human liver diseases.

There is a complex interaction between KCs and endothelial cells, sinusoidal cells and hepatocytes (**Fig. 2**). These cells play an important role in the metabolic homeostasis of the whole organism by coordinating the absorption, reprocessing and distribution of nutrients and their subsequent energy products. The liver is the main filter of the human body, which can not only detoxify, but also remove many exogenous and endogenous compounds[21].

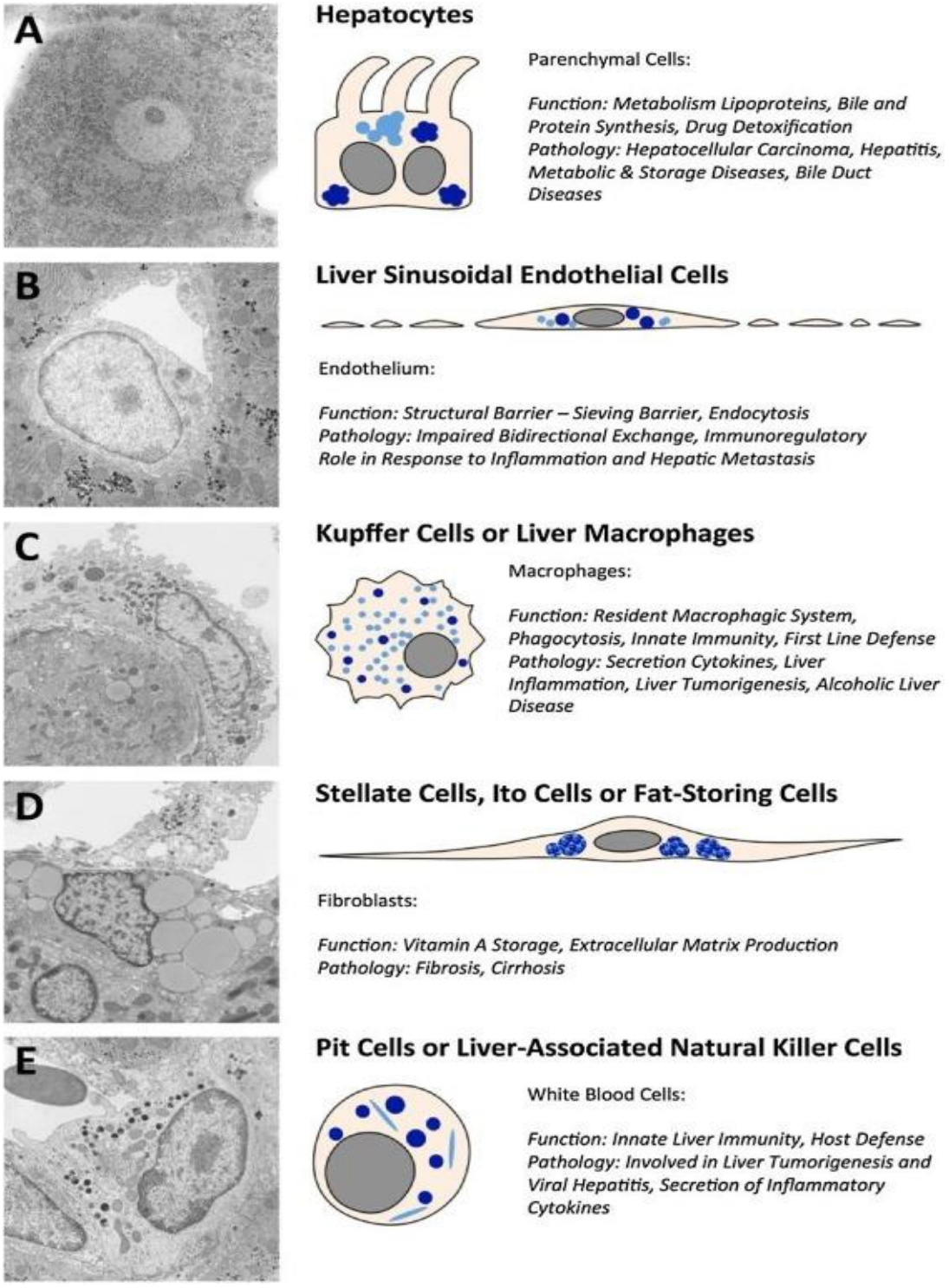

Figure 2. Function of the distinct parenchymal and non-parenchymal liver cells. The hepatocyte population can be divided into two families: (i) parenchymal cells or hepatocytes (**A**) and (ii) nonparenchymal cells or sinusoidal cells (**B-E**). **A)** Hepatocytes are the dominant cells, accounting for 80% of the volume of liver tissue. In addition to producing typical liver histological features, these cells are also the main functional cells, playing an important role in protein synthesis, detoxification, lipid- and carbohydrate metabolism. **B)** LSECs form the endothelial lining of the sinusoids, and play a key regulatory role in all aspects of intra- and trans-endothelial transport. **C)**

KCs or hepatic macrophages, which are mainly attached to the wall of the portal sinus, are the first line of defense to eliminate foreign bodies entering the hepatic circulation. **D)** Stellate cells or liver fibroblasts are the storage cells of vitamin A and play a role in the complex mechanisms of liver fibrosis and cirrhosis. **E)** Pit cells or liver-related natural killer cells, whose main functions include local host defense and maintaining immune balance. Courtesy of Filip Braet et al[11].

3.1.3. Cholangiocytes: Embryology and Function

Cholangiocytes are arranged in extrahepatic and intrahepatic bile ducts, and modify bile from hepatic cell tubules through the intrahepatic biliary tree. From the 12th week to the 16th week of gestation, the ductal plate replicated in the discrete region, inhibited the expression of hepatocyte markers, and began to express K7 and K19, biliary phenotype commitment markers[22].

The function of cholangiocytes has both of secretion and absorption, regulated to the volume, fluidity and basicity of primary bile secreted by hepatocytes. Thus, the bile duct epithelium can reabsorb water, glucose, glutathione, bile acids and electrolytes[23]. The biliary system is a complex network of small tubes surrounded by cholangiocyte. Cholangiocytes starts from the CoH in the hepatic lobule (intrahepatic bile duct tree), continues to the extrahepatic (extrahepatic bile duct tree), and terminates into the ampulla of hepatic Vater. In addition to its role in liver development, the biliary system is also at the center of discussions about liver regeneration and repair, partly due to the recognition that the biliary tree may hide hepatic progenitor cells (HPCs) in the terminal ductulus and CoH. The maintenance of a normal liver requires only occasional self-replication of existing adult epithelial cells (hepatocytes and cholangiocytes) via mitosis, rather than HPCs differentiation[24, 25] (**Fig. 3**).

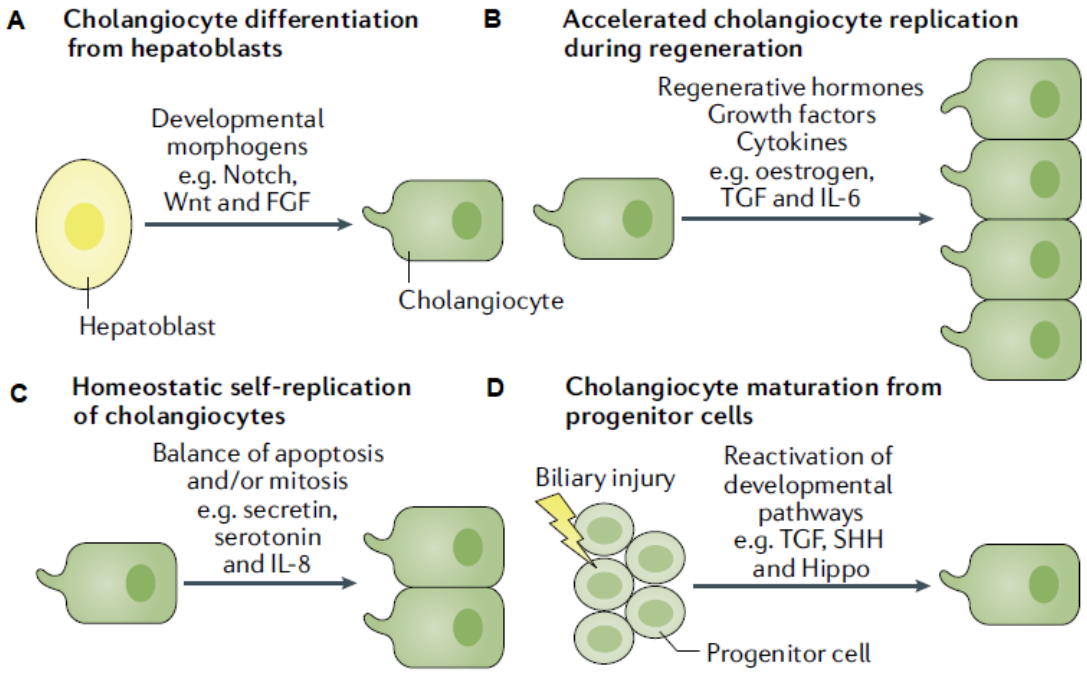

Figure 3. Potential sources of cholangiocytes in development and liver regeneration. A) Cholangiocytes develop by differentiating into hepatocytes in response to the developmental morphogen. **B)** The homeostasis of cholangiocytes is based on the self-replication of existing mature cholangiocytes. **C)** Cholangiocytes regeneration is achieved by accelerating the replication of regeneration hormones, growth factors and cytokines. **D)** The differentiation of cholangiocytes from HPCs can occur during biliary damage and repair after reactivation of developmental pathways[25].

Cholangiocytes can be activated by a variety of injuries, including infection, cholestasis, ischemia, and xenobiotics[26]. Activated cholangiocytes are also involved in the recruitment and crosstalk of immune cells, vascular and mesenchymal cells, as well as the development of bile duct fibrosis and cholangiocarcinoma (CCA) underwent chronic stimulus. In many cholangiopathies, including primary sclerosing cholangitis (PSC) and primary biliary cholangitis (PBC), but activation of liver injury is unknown. Features of activated BECs/cholangiocytes include increased proliferation, pro-fibrosis, and pro-inflammatory secretions[27]. Depending on the type of the injuries, a series of morphogenetic signals and transcription factors are also involved and/or activated, including Notch, IL-6 and Wnt/β-catenin pathways, TGF-β and

hepatocyte nuclear factors (HNFs)[28].

Reactive ductal cells (RDCs), the epithelial component of the catheter response, show a biliary phenotype and are organized into irregularly shaped structures[29]. RDCs are a completely different cell population from HPCs and have a repair function rather than a regeneration function. Some studies have shown that there is a strong correlation between RDCs and portal fibrosis[30]. RDCs may be partly derived from BECs/cholangiocyte, and this has been clearly shown in CCA[31]. The neonatal expression of epithelial to mesenchymal transition (EMT) markers was observed in RDCs, and the ability of RDCs to express EMT markers and increase mobility is necessary for wound repair[25, 32]. Most of the evidences show that during the repair of liver injury, cholangiocytes lose part of epithelial characteristics, thus obtaining some biological and immunophenotypic characteristics of mesenchymal cells, such as motility and collagen deposition ability. However, they do not completely transition to mesenchymal phenotype and BECs, only obtain some functional characteristics conducive to the repair of liver injury[25, 32, 33].

Recent studies have also shown that SOX4 and SOX9 are involved in development of primary cilia, and the normal formation, elongation, and branching of bile duct trees[34]. These two factors cooperatively control the expression of mediators of TGF-β, Notch, and Hippo/Yes-associated protein 1 (YAP1) signaling pathways, which are required for normal biliary development. They’re also related to the Wnt/β-catenin signaling pathway and involved in the liver cilia disease[35], such as polycystic liver disease(PLD) [36].

3.2 Polycystic liver disease (PLD)

PLD is a hereditary biliary disease characterized by multiple hepatic cysts of different shapes and sizes, which are filled with cystic fluid [37]. The pathogenesis of PLD is still unclear. Currently, it is believed that the mainly cystic changes caused by the loss of related gene functions due to the malformation of the duct

plate and the second mutation during the embryonic development of the liver[38], and the related genes to PLD, including *PKD1*, *PKD2*, *GANAB*, *PRKCSH*, *SEC63*, *SEC61B*, *LRP5*, *GANAB*, *ALG8* and *PKHD1* as published[39, 40]. The incidence of PLD varies from 1/1,000,000 to 1/400, according to different sub-classifications associated with or without polycystic kidney disease, divided into autosomal dominant polycystic liver disease (ADPLD, ~1:100,000), autosomal dominant polycystic kidney disease (ADPKD, ~1:400–1:1,000), and autosomal recessive polycystic kidney disease (ARPKD) as well as congenital hepatic fibrosis (CHF)/ Caroli's syndrome (CS, 1/1,000,000~1/20,000)[41]. These diseases that encode fibrocystin can cause severe portal hypertension and may be complicated by acute and/or chronic cholangitis, intra/extrahepatic bile duct stones, and eventually induced to CCA[42].

Proliferation of cystic duct epithelial cells is a sign of disease progression or regression, which is considered to be one of the main mechanisms of hepatic cystogenesis[43]. The proliferation of cholangiocytes is not only the basis for maintaining the normal internal environment balance of the bile duct tree, but also the response to liver injury. The development of cysts after birth is closely followed by proliferation-dependent cyst expansion. Basically, cholangiocytes show excessive proliferation during cyst expansion as shown by positive staining, such as proliferating cell nuclear antigen (PCNA). However, the proliferation of cholangiocytes decreased in the well-established disease. Different cytokines and growth factors, such as IL-6, tyrosine kinase receptors (EGF), vascular endothelial growth factor (VEGF) and insulin like growth factor (IGF), promote cholangiocytes proliferation through ERK/PI3K/AKT signaling pathway. These cytokines and growth factors are present the cystic fluid and/or secreted by the BECs[44, 45].

The overexpression of cAMP in PLD cholangiocytes is considered to be one of the main mechanisms driving the occurrence of liver cysts. Bile duct epithelial cell proliferation involves multiple cAMP downstream effectors, including

cAMP-activated exchange protein, protein kinase A (PKA), and the mitogen-activated protein kinase/extracellular signal-regulated kinase (MAPK / ERK1/2) [38, 46].

3.3 Cholangiocarcinoma (CCA)

In recent years, the incidence of liver tumors has been continuously rising, including two main common types of hepatic malignancies, Hepatocellular carcinoma (HCC) which is the fifth most common malignant tumor, and CCA the incidence of which is rising up to 2.1 cases per 100,000 people in Western countries. Recently, CCA, the cancer of gallbladder and biliary tract are matters of great concern.

Depending on the anatomical location, CCA is basically divided into three categories: intrahepatic (iCCA), perihilar (pCCA) and distal (dCCA) [47, 48]. It is noteworthy that although these three CCA subtypes share common features, they also have important inter-tumor and intra-tumoral differences that may affect the pathogenesis and outcomes[49-52]. The complexity of the pathogenesis and the apparent heterogeneity of CCA have hindered clinical therapeutic effect in their management [53-55].

Especially CCA, not only lack of specific biomarkers makes early diagnosis much more difficult in the early stage, but also patients would have a poor prognosis. Surgery seems to be the only effective treatment, but the vast majority of patients are found to be advanced and have a high rate of recurrence after surgery. At the same time, CCA lacks sensitivity of radiotherapy and chemotherapy. Despite the variety of treatment options, the 5-year survival rate of CCA has not been improved, still 5-10% during the past 30 years[56]. It is considered fortunately for patients diagnosed with CCA to have a 5-year survival after radical surgery, while unfortunately to patients in advanced stage usually less than 12 months[57, 58]. At present, the diagnosis and treatments of CCA has become a worldwide problem, especially in patients with recurrent and

unresectable CCA even treated with advanced medical methods[51].

Previously data showed that c-Jun N-terminal kinases (JNK)/ Cyclin-dependent kinase-4 (CDK4)-dependent pSmad3L signaling pathway was involved in the development of polycystic kidney disease in *cpk* mice which is a model of autosomal recessive PKD[59]. Interestingly, Cubero[60] group showed a novel function of JNK1/2 in cholangiocyte hyperproliferation in recent published paper. Loss function of JNK1/2 in hepatocytes triggers biliary hyperproliferation and ductular dilation in chronic liver disease animal models, eventually inducing the formation of CCA after sustained treatment of toxicity. At the same time, $Jnk^{\Delta hepa}$ mice progressed into CCA with continuous stimulation[60]. Furthermore, recent studies also suggest that the formation of liver cancer is associated with the dysfunction of JNK signaling pathway, including both HCC[61] and CCA[60, 62]. Based on previously studies, we believe that JNK1/2 play an important role in triggering the formation of CCA.

3.4 EMT Transition in CCA

In 1968, Hay[63] pointed out that during the development of chicken embryos, epithelial cells underwent through several stages of differentiation and de-differentiation, and migrated a considerable distance in the body. All these processes require the mutual transformation between epithelial cells and mesenchymal cell phenotypes (including "multipotent", mesenchymal stem cells), called EMT, and the opposite process is mesenchymal epithelial transformation (MET). EMT is a special physiological process in which epithelial cells lose their polarity and show a mesenchymal phenotype. Subsequently, multiple in vivo studies were reported. EMT is essential for embryonic development, wound healing, stem cell biology and plays a key role in tumorigenesis[64, 65].

Previously, it was generally believed that HCC originated from hepatocytes and that CCA originates from BECs[66]. Moreover, cholangiocytes may be involved in liver fibrosis[67]. In CCA, developmental changes seen in cholangiocytes may be due to the activation of hepatic stem/progenitor cells,

the proliferation of bile duct cells, or through ductal metaplasia of mature hepatocytes [29, 68]. However, alongside the progress seen in histopathological studies, there is now a better understanding of the origins of BECs. Both HPCs [69] and CCA stem cells [66] seem to be capable of differentiating into BECs, whilst CCA stem cells can also originate from HPCs [66, 70, 71]. These indicate that CCA can be derived from common HPCs, which can differentiate into both hepatocytes and cholangiocytes [72, 73].

At the biochemical level, various morphogenetic and environmental signals including TGF-β, Wnt, EGFR, Notch and platelet-derived growth factor (PDGF), inflammatory cytokines and integrin receptor ligands promote EMT [74, 75]. TGF-β is also involved in several steps of cancer progression, from tumorigenesis to metastasis, which promotes cancer cell invasion and metastasis through an EMT process, although at later stages [76-80]. Similarly, the TGF-β-induced ERK/MAPKs pathway contributes to EMT induction, as ERK is required to remove cell adhesion junctions, which leads to increased cell migration [74, 81, 82]. In other words, EMT plays an important role in CCA progression[83].

3.5 JNK/MAPKs and liver cancer

In normal liver, the JNK family is minimally or transiently activated, the latter usually physiological, whereas sustained activation is pathological. In addition to playing an important role in liver physiological reactions (such as cell death, apoptosis and cell cycle regulation) [84, 85], JNK also plays a carcinogenic role by promoting inflammation, proliferation, invasion and angiogenesis, depending on the specific situation and duration of JNK signaling pathway activation[86, 87]. Previous studies have reported that the JNK signaling pathway plays a vital role in hepatocarcinogenesis[88, 89]. Das et al[90] showed that JNK play a dual role in the development of HCC. Another study suggested that lack of JNK1 and JNK2 in hepatocytes may increase the tumor development, and the pro-tumor effect of JNK on HCC is related to inflammation[91]. While the other data indicated that the JNKs, particularly JNK1, contribute to malignant transformation and tumor growth [92]. Possibly, JNK1 has a larger role than JNK2 in development of liver

tumor [93]. In human HCC tissue samples, JNK1 activation was associated with tumor size. In fact, by knockdown of JNK1 rather than JNK2, the proliferation of human HCC occurs through the upregulation of c-MYC and downregulation of p21 [90, 94].

The JNK signaling pathway is also involved in the development of CCA according to the recent studies. JNKs play a key role in regulating the interaction between different pro-apoptotic proteins and anti-apoptotic proteins[95].

Feng et al[96]. reported that JNK exerted its carcinogenic effect in human CCA cells. In human CCA, high expression of TNF-α was found in the cells near the lesion of CCA, and the overexpression of JNKs in phosphorylated cholangiocytes (80% related the patients with CCA) as well as the accumulation of ROS around hepatocytes been observed. ROS accumulation leads to Caspase-3-dependent apoptosis through JNK signaling pathway. Yuan's group[55] suggested that mitochondrial dysfunction and oxidative stress promote the excessive growth of CCA and tumorigenesis. While, Sabio[62] group found that liver JNK deficiency can alter cholesterol metabolism and bile acid synthesis, binding and transport, leading to cholestasis, increased BECs proliferation and formation of CCA. Nishikawa[97] group have demonstrated that, within collagen-rich matrix, TNF-α specifically stimulated branching morphogenesis associated with the expression of bile duct/ductular markers, including cytokeratin 19 (CK 19). Meanwhile, the phosphorylation of JNKs and c-Jun increased during collagen gel culture, and TNF-α strongly enhanced bile duct transdifferentiation of hepatocytes, especially by inhibiting hepatocyte differentiation and enhancing ductular morphogenesis. These results also suggest that activation of JNK/c-Jun signaling pathway may occur during “ductular reaction” (DR) which is closely related to the formation of CCA.

As mentioned above, the JNK/MAPKs signaling pathway may be a key target for the treatment of CCA. However, more research is needed to test this

possibility. Therefore, new mice model links to JNK signaling pathway seems a useful method for detecting the molecular mechanism of CCA.

4. Objectives

In the present work, we hypothesize that the synergistic function of *Jnk1* and *Jnk2* in hepatocytes drives the development of cholangiocarcinogenesis. The main Objectives are as follow:

1) To understand the role of JNK in undifferentiated hepatocytes and its differentiation into hepatocytes and cholangiocytes.

2) To evaluate the molecular mechanisms driving the early stages of cholangiocyte pathology in a $Jnk^{\Delta hepa}$ knockout mice.

3) To evaluate the potential therapeutic value of JNK-deletion in hepatocytes during cholangiocarcinogenesis.

5. Materials and Methods

5.1 Materials

Table 5.1.1 Chemicals

Reagent	Manufacturer	Catalog
Acetic Acid Reagent plus (R),>=99%	Sigma-Aldrich, Darmstadt, Germany	A6283
Agarose Electrophoresis Grade	Sigma-Aldrich, Darmstadt, Germany	A9539
BSA (Bovine Serum Albumin, lyophilized powder, ≥96%)	Sigma-Aldrich, Darmstadt, Germany	A2153
Calcium chloride	Sigma-Aldrich, Darmstadt, Germany	C5670
Cell Counting Kit – 8	Sigma-Aldrich, Darmstadt, Germany	96992
Cell incubator clean reagent	Panreac AppliChem, München, Germany	A5230,1000
Chloroform	AppliChem, Munich, Germany	A3691.1000
DEPC Water (Water for molecular biology)	AppliChem, Munich, Germany	A7398, 0500
DJNKI1	MedChem Express, Monmouth Junction, USA	HY-P0069
DMEM with High Glucose, without L-Glutamine, with Sodium Pyruvate	GE Healthcare, Munich, Germany	SH30285.01
DNA Ladder (50 bp)	Thermo Fisher Scientific, Massachusetts, USA	10416014
Direct Red 80	Sigma-Aldrich, Darmstadt, Germany	365548

di-Sodium Hydrogen Phosphate 7-hydrate for analysis	AppliChem (Dismalab), Barcelona, Spain	132656.1211
DMSO (Dimethyl sulfoxide)	Sigma-Aldrich, Darmstadt, Germany	D4540
DTT (Dithiothreitol)	Thermo Fisher Scientific, Massachusetts, USA	20291
Eosin Y	Sigma-Aldrich, Darmstadt, Germany	E4009
Ethanol absolute for analysis	AppliChem (Dismalab), Barcelona, Spain	131086.1214
FBS (Fetal Bovine Serum)	Thermo Fisher Scientific, Massachusetts, USA	10270106
Formaldehyde stabilized with methanol for clinical diagnosis	AppliChem (Dismalab), Barcelona, Spain	252931.1214
Gelatin from bovine skin, Type B	Sigma-Aldrich, Darmstadt, Germany	G6650-500G
Glycine for molecular biology	AppliChem, München, Germany	A1067,5000
Glycerol, for molecular biology, ≥99%	Sigma-Aldrich, Darmstadt, Germany	G5516-500ML
Gibco™ Goat Serum, New Zealand origin, Standard (Sterile-Filtered)	Thermo Fisher Scientific, Massachusetts, USA	11530526
Gibco™ MEM Non-Essential Amino Acids Solution (100X)	Thermo Fisher Scientific, Massachusetts, USA	11350912
Gibco™ Penicillin-Streptomycin-Glutamine (100X)	Thermo Fisher Scientific, Massachusetts, USA	12090216
HepaRG Maintenance and Metabolism Medium Supplement	Sigma-Aldrich, Darmstadt, Germany	ADD620C

with Antibiotics		
HyClone L Glutamine	Thermo Fisher Scientific, Massachusetts, USA	SH3003401
HyClone Trypsin Protease	Thermo Fisher Scientific, Massachusetts, USA	SH3023602
37% Hydrochloric Acid technical grade	AppliChem (Dismalab), Barcelona, Spain	211020.1611
30%Hydrogen Peroxide	AppliChem (Dismalab), Barcelona, Spain	121076.1211
Isopropanol	AppliChem (Dismalab), Barcelona, Spain	131090.1612
Isoflutek	Karizoo, Barcelona, Spain	586259.0
Mayer's Hematoxylin	AppliChem (Dismalab), Barcelona, Spain	254766.1611
Methanol BioChemica	AppliChem, Munich, Germany	A3493.5000
Nonfat dried milk powder	AppliChem, Munich, Germany	A0830,0500
Nonidet P-40	AppliChem, Munich, Germany	A1694,0250
Ponceau S solution	Sigma-Aldrich, Darmstadt, Germany	P7170
Potassium chloride> 99.0%(KCL)	Sigma-Aldrich, Darmstadt, Germany	P9541-500G
Restore Western Blot Stripping Buffer 500ml	Thermo Fisher Scientific, Massachusetts, USA	21059
Sodium Chloride for molecular biology	AppliChem, Munich, Germany	A2942,5000

Sodium fluoride	Sigma-Aldrich, Darmstadt, Germany	215309
SDS (Sodium dodecyl sulfate)	AppliChem, Munich, Germany	A2572,0500
Trizol Reagent	Thermo Fisher Scientific, Massachusetts, USA	5596018
Triton X-100	AppliChem, Munich, Germany	A4975,0100
Xylene	Carl Roth, Karlsruhe, Germany	9713.5

Table 5.1.2 Primer sequences used for genotyping PCR

Reagent	Forward	Reverse
JNK1	GGATTTATGCCCTCTGCTTGTC	GAACCACTGTTCCAATTTCCATCC
JNK2	GTTTTGTAAAGGGAGCCGAC	CCTGACTACTGAGCCTGGTTTCTC
Total-Cre01	AAATTTGCCTGCATTACCG	AATCGCGAACATCTTCAGGT
Total-Cre02	CTAGGCCACAGAATTGAAAGATCT	GTAGGTGGAAATTCTAGCATCATCC

Table 5.1.3 Primer sequences used for qRT-PCR

Gene	Forward	Reverse
AFP	AGTTTCCAGAACCTGCCGAG	ACCTTGTCGTACTGAGCAGC
Albumin	GCAGATGACAGGGCGGAACTTG	CAGCAGCAATGGCAGGCAGAT
αSMA	CCCCTGAAGAGCATCGGACA	TGGCGGGGACATTGAAGGT
CD133	TCTGTTCAGCATTTCCTCAC	TCAGTATCGAGACGGGTC
CK19	GGGGGTTCAGTACGCATTGG	GAGGACGAGGTCACGAAGC

c-Myc	AGTGCTGCATGAGGAGACAC	GGTTTGCCTCTTCTCCACAG
Cyclin A2	AACTGTAAGGTTGAAAGCTTAGC	TCTGTTGTGCCAATGACTCAGG
Cyclin D1	AAGCATGCACAGACCTTTGTGG	TTCAGGCCTTGCATCGCAGC
Cyclin E1	TCCACGCATGCTGAATTATC	TTGCAAGACCCAGATGAAGA
DMBT1	GCCACATCCCAATGACTTCT	GCACCGTGAGGAGGTATCAT
ErbB2	ACAGCTCGGAGACCTGCTA	GTAGTGGGCACAAGCCTCA
GAPDH	TGTTGAAGTCACAGGAGACAACCT	AACCTGCCAAGTATGATGACATCA
GABRP	GCGCCTTGCTCAGTACACAA	ACGTTCCTCCGAAGCTCAAAT
Hes1	CCCCAGCCAGTGTCAACAC	TGTGCTCAGAGGCCGTCTT
Hey1	GGGAGGGTCAGCAAAGCA	GCTGCGCATCTGATTTGTCA
HeyL	GTCTTGCAGATGACCGTGGA	CTCGGGCATCAAAGAACCCT
IGF2BP3	GGGAGGTGCTGGATAGTTTAC	CTAGCTTGGTCCTTACTGGAATAG
IL-6	GCTACCAAACTGGATATAATCAGGA	CCAGGTAGCTATGGTACTCCAGAA
Jag1	ACACAGGGATTGCCCACTTC	AGCCAAAGCCATAGTAGTGGTCAT
Klf6	CGGACGCACACAGGAGAAAA	CGGTGTGCTTTCGGAAGTG
MUC1	CTGTTCACCACCACCATGAC	CTTGGAAGGGCAAGAAAACC
Notch1	CCAGCAGATGATCTTCCCGTAC	TAGACAATGGAGCCACGGATGT
Notch3	ACACTGGGAGTTCTCTGT	GTCTGCTGGCATGGGATA
PDGFα	GAGGAAGCCGAGATACC	TGCTGTGGATCTGACTTCGAG
TNFα	CCTCTTCTCATTCCTGCTTGTGG	GAGAAGATGATCTGAGTGTGAGG
TGFβ1	GCTCGCTTTGTACAACAGCACC	GCGGTCCACCATTAGCACG

YAP1	AGCAGCAGCAATACAGCAG	AGCATTTGCTGTGCTGGGATT GT

Table 5.1.4 Primary Antibodies used for Immunostaining (IHC/IF) and/or Western blot

Product	Manufacturer	Catalog	Concentration
αSMA	Sigma-Aldrich, Darmstadt, Germany	A2547	1:100 (IHC/IF) 1:1000 (WB)
pAKT	CST, Massachusetts, USA	9271s	1:1000 (WB)
AKT	CST, Massachusetts, USA	9272s	1:1000 (WB)
BiP	CST, Massachusetts, USA)	3177S	1:1000 (WB)
Phospho-β-Catenin	CST, Massachusetts, USA	9561	1:1000 (WB)
β-Catenin	CST, Massachusetts, USA	9562	1:1000 (WB)
Chop	CST, Massachusetts, USA	2895S	1:1000 (WB)
CK19	Abcam, Cambridge, UK	ab15463	1:100 (IHC/IF) 1:1000 (WB)
Cleaved Caspase3	CST, Massachusetts, USA	9661S	1:1000 (WB)
Cleaved Caspase8	CST, Massachusetts, USA	8592S	1:1000 (WB)
c-MYC	Abcam, Cambridge, UK	ab32072	1:100 (IHC) 1:1000 (WB)
peIF2α	CST, Massachusetts,	3398S	1:1000 (WB)

	USA		
pERK1/2	CST, Massachusetts, USA	9101S	1:1000 (WB)
ERK1/2	CST, Massachusetts, USA	4696S	1:1000 (WB)
GAPDH	Bio-Rad, Kentucky, USA	MCA4739	1:5000 (WB)
GS	Abcam, Cambridge, UK	ab73593	1:100 (IHC)
pIRE1α	BIONOVA (Novus Biologicals), Colorado, USA	NB100-2323	1:1000 (WB)
IRE1α	CST, Massachusetts, USA	3294S	1:1000 (WB)
Ki 67	Abcam, Cambridge, UK	ab16667	1:100 (IHC/IF)
pJNK	CST, Massachusetts, USA	9251S	1:1000 (WB)
JNK	CST, Massachusetts, USA	9252S	1:1000 (WB)
pJNK1	BIONOVA (Novus Biologicals), Colorado, USA	NB100-82009	1:1000 (WB)
JNK1	CST, Massachusetts, USA	3708S	1:1000 (WB)
pJNK2	BIONOVA (Novus Biologicals), Colorado, USA	NBP1-45787	1:1000 (WB)
JNK2	CST, Massachusetts,	4572s	1:1000 (WB)

	USA		
pMLKL	Abcam, Cambridge, UK	ab196436	1:1000 (WB)
MUCIN 2 (F-2)	Santa Cruz, Heidelberg, Germany	sc-515032	1:100 (IHC)
Notch1(A6)	Abcam, Cambridge, UK	ab44986	1:100 (IHC)
PCNA	Thermo Fisher Scientific, Massachusetts, USA	13-3900	1:100 (IHC)
pRIP	CST, Massachusetts, USA	31122S	1:1000 (WB)
RIP	Biosciences, San Diego, USA	610459	1:1000 (WB)
pRIP3	CST, Massachusetts, USA	57220S	1:1000 (WB)
RIP3	ProSci, California, USA	2283	1:1000 (WB)
SOX9	Abcam, Cambridge, UK	ab185966	1:1000 (IHC) 1:100 (IF)

Table 5.1.5 Secondary antibodies used for Immunostaining (IHC/IF) and/or Western blot

Product	**Manufacturer**	**Catalog**	**Concentration**
Anti-rabbit-HRP	CST, Massachusetts, USA	7074S	1:3000 (WB)
Anti-Mouse-HRP	Bio-Rad, Kentucky, USA	STAR207P	1:5000 (WB)

Anti-Rabbit-HRP IgG	Vector Laboratories, California, USA	MP-7401	ready-to-use (IHC)
Anti-Mouse-HRP IgG	Vector Laboratories, California, USA	MP-7402	ready-to-use (IHC)
Goat-Anti-Rat (IF, 488)	Thermo Fisher Scientific, Massachusetts, USA	A-11006	1:400 (IF)
Goat-Anti-Mouse (IF, 488)	Thermo Fisher Scientific, Massachusetts, USA	A-11001	1:400 (IF)
Donkey-Anti-Rabbit (IF, 488)	Thermo Fisher Scientific, Massachusetts, USA	A-21206	1:500 (IF)

Table 5.1.6 Analytical chemicals, reagents, enzymes and kits

Product	**Manufacturer**	**Catalog**
30% Acrylamide/Bis Solution, 29:1	Bio-Rad, Kentucky, USA	1610156
AEBSF Hydrochloride (White to Off white Crystals)	Thermo Fisher Scientific, Massachusetts, USA	BP635-100
Ammonium Persulfate (APS)	Bio-Rad, Kentucky, USA	1610700
BIO-RAD Protein Assay Dye Reagent	Bio-Rad, Kentucky, USA	5000006
Blasticidin S HCl	Thermo Fisher Scientific, Massachusetts, USA	A1113903
CCL4 (Carbon tetrachloride)	Sigma-Aldrich, Darmstadt,	289116

	Germany	
Clariom™ S Assay, mouse	Thermo Fisher Scientific, Massachusetts, USA	902930
Complete Mini (protease inhibitors)	Sigma-Aldrich, Darmstadt, Germany	11836153001
DAB (ImmPACT® DAB Peroxidase (HRP) Substrate)	Vector Laboratories, California, USA	SK-4105
DAKO PEN	Agilent, California, USA	S200230-2
DAPI (VECTASHIELD® Antifade Mounting Medium with DAPI)	Vector Laboratories, California, USA	H-1200
N-Nitrosodiethylamine	Sigma-Aldrich, Darmstadt, Germany	N0756
ECL™ Prime Western Blotting System	GE Healthcare, München, Germany	RPN2232
Eppendorf tubes 1.5ml	Sigma-Aldrich, Darmstadt, Germany	Z606316-1000EA
Eppendorf tubes 2.0ml	Sigma-Aldrich, Darmstadt, Germany	Z606324-1000EA
High Capacity cDNA Reverse Transcription Kit	Thermo Fisher Scientific, Massachusetts, USA	43-688-13
In Situ Cell Death Detection Kit, AP	Sigma-Aldrich, Darmstadt, Germany	11684809910
4x Laemmli Sample Buffer	Bio-Rad, Kentucky, USA	1610747
Leica Microsystems Surgipath Paraplast Tissue Embedding Medium	Leica, Illinois, USA	39602004
Midori Green Advance	Nippongenetics, Düren, Germany	MG04

Mounting medium (Roti®-Histokitt II)	Carl Roth, Karlsruhe, Germany	Art. No. T160.1
Periodic acid solution	Sigma-Aldrich, Darmstadt, Germany	3951
phosSTOP (phosphatase inhibitor)	Sigma-Aldrich, Darmstadt, Germany	4906837001
Precision Plus Protein™ Dual Color Standards, 500 µl	Bio-Rad, Kentucky, USA	1610374
Proteinase K – Solution	AppliChem, München, Germany	A4392,0010
Powerup SYBR Green Master Mix (50 ml)	Thermo Fisher Scientific, Massachusetts, USA	15360929
Puromycin Dihydrochloride	Thermo Fisher Scientific, Massachusetts, USA	A1113803
REDTaq(R) ReadyMix(TM) PCR Reaction Mix	Sigma-Aldrich, Darmstadt, Germany	R2523-100RXN
Schiff's reagent	Sigma-Aldrich, Darmstadt, Germany	3952016-500ML
TAA(Thioacetamide)	Sigma-Aldrich, Darmstadt, Germany	163678
Tissue-Tek	Sakura, Heppenheim, Germany	4583
Tris Buffer grade	AppliChem, München, Germany	A2264,5000
Tri-Sodium Citrate 2-hydrate for analysis, ACS	AppliChem (Dismalab), Barcelona, Spain	131655.1210
TUNEL Label Mix	Sigma-Aldrich, Darmstadt, Germany	11767291910

Tween 20	Sigma-Aldrich, Darmstadt, Germany	P1379-500ML

Table 5.1.7 Instruments and Equipment

Product	**Manufacturer**
Adobe Photoshop CS6 13.0*32	Adobe Systems, California, USA
AxioVision SE64. Rel.4.9	Carl Zeiss Microscopy GmbH, Munich, Germany
Centrifuge 5415 D	Eppendorf AG, Hamburg, Germany
Centrifuge 5804/5804R	Eppendorf AG, Hamburg, Germany
Centrifuge 5920 R	Eppendorf AG, Hamburg, Germany
Centrifuge 4K15 10740	Sigma, DJB Labcare Ltd, UK
Centrifuge Z233M-2 and Refrigerated Z233MK-2	Hermle LaborTechnik GmbH, Wehingen, Germany
Class II Bio II Advance Plus Microbiological Safety Cabinet	Azbil Telstar Technologies Slu, Barcelona, Spain
Digital microscope camera Moticam 2500	Ryf AG, Bettlachstrasse, Switzerland
Gel Doc 2000 System	Bio-Rad, Kentucky, USA
GraphPad Prism 8.0 software	GraphPad Software, California, USA
ImageJ Version 1.52u	LOCI, University of Wisconsin, Wisconsin, USA
LAS mini 4000 Chemiluminescence scanner	FUJIFILM, super CCD, Marlborough, USA

Leica EG1160 Embedding Center, Dispenser + hot Plate (HistoCore Arcadia)	Leica Biosystems Nussloch GmbH, Nußloch, Germany
Leica MZ16 Stereomicroscope with Leica DFC480 Digital Camera	Leica Microsystems, Cambridge, UK
Microsoft Excel	Microsoft Corp., Redmond, Washington, USA
Microtome (Model HI1210 RM2125RTS)	Leica Biosystems Nussloch GmbH, Nußloch, Germany
Nanodrop (A30221)	Thermo Fisher Scientific, Massachusetts, USA
7300 Real Time PCR System AND Sequence Detection Software Version 1.3.1	Applied Biosystems, Massachusetts, USA
2100-Retriever	Aptum Biologics, Kassel, Germany
Thermo Scientific Forma Steri-Cycle i250 C02 incubator	Thermo Fisher Scientific, Massachusetts, USA
UV-transilluminator (Gel Doc 2000 System)	Bio-Rad, Kentucky, USA
Vertical laminar flow workbench, Mini-V/PCR	Azbil Telstar Technologies Slu, Barcelona, Spain
Water bath (STANDARD of 12877)	DILABO, London, UK

Table 5.1.8 Other Equipment

Plastic and Glassware	**Manufacturer**	**Catalog**
Big flacon 50ml	Dismalab, Madrid, Spain	PTGP-E050-500
Blue tips 1ml	Dismalab, Madrid, Spain	740290
Cell culture plate sterile, 96 Well, F-bottom with lid	Dismalab, Madrid, Spain	655180
CellStar® Cell Culture Multiwell Plates, Wells=6	Greiner Bio-One, Frickenhausen, Germany	657160

CELLSTAR® Cell Culture Multiwell Plates, Wells=12	Greiner Bio-One, Frickenhausen, Germany	665180
Centrifuge tube 50ml （falcon）	Labbox, Madrid, Spain	PTGP-E50-025
Coverslips	Dismalab, Madrid, Spain	8000120
Cryogenic tubes	Thermo Fisher Scientific, Massachusetts, USA	375353PK
Easypet 3 electronic pipetting	Eppendorf, Madrid, Spain	4430000018
Eppendorf® Reference® 2 G single-channel, fixed, volume (10 µl)	Eppendorf, Madrid, Spain	EP4925000049
Eppendorf® Reference® 2 G single-channel, fixed, volume (100 µl)	Eppendorf, Madrid, Spain	EP4925000103
Micro tube 1.1 ml	Sarstedt, Carolina, USA	41.1500.005
Eppendorf® Reference® 2 G single-channel, fixed, volume (1000 µl)	Eppendorf, Madrid, Spain	EP4925000154
Eppendorf™ Tubes (1.5ml)	Thermo Fisher Scientific, Massachusetts, USA	10398031
Falcon Tissue Culture Treated Flasks(50ml)	Thermo Fisher Scientific, Massachusetts, USA	10634501
Falcon Tissue Culture Treated Flasks(250ml)	Thermo Fisher Scientific, Massachusetts, USA	10537161
Graduated Filter Tip (Sterile) 10 µl	STARLAB, Hamburg, Germany	S1120-3810
MicroAmp Fast Optical 96 Well Reaction Plate, 0.1ml	Thermo Fisher Scientific, Massachusetts, USA	43-469-06
MicroAmp Optical Adhesive	Thermo Fisher Scientific,	43-119-71

Film	Massachusetts, USA	
MicroAmp Optical 8-Tube Strip with attached optical caps	Thermo Fisher Scientific, Massachusetts, USA	A30588
Mini Trans-Blot® Electrophoretic Transfer Cell	Bio-Rad, Kentucky, USA	170-3930
Pipettes 5 ml	Dismalab, Madrid, Spain	606107
Pipettes 10ml	Dismalab, Madrid, Spain	607180
Polyvinylidene difluoride (PVDF) membrane	Bio-Rad, Kentucky, USA	1620264
Sarstedt Inc PC MTUBE 1.1ML SER-GEL/PK100	Thermo Fisher Scientific, Massachusetts, USA	NC9436363
Slides	Klinipath, Darmstadt, Germany	PR-S-100
Syringes 1 mL Luer (BD Plastipak)	Dismalab, Madrid, Spain	303172
Small falcon 15ml	Dismalab, Madrid, Spain	PTGP-E15-500
Syringe 1 ml with 27 × 13 needle	Dismalab, Madrid, Spain	300635
Whatman® paper(Thick Blot Filter Paper, For WB)	Bio-Rad, Kentucky, USA	1704085
Yellow tips 200µl	Dismalab, Madrid, Spain	739290

5.2 Methods

5.2.1 Animal experiments

All animal experiments in the project are designed and carried out under appropriate supervision and in accordance with Spanish animal protection laws and regulations. All procedures have been approved by the Consejería de

Medio Ambiente, Administración Local y Ordenación del Territorio (PROEX-125.1/20).

5.2.1.2 Housing, breeding and generation of mice

All mouse strains were raised in cages with filters and bred in pathogen-free, temperature and humidity-free facilities of the Institute of Biology Animal Sciences (ILAS), University of Complutense, for a 12-hour cycle of light and shade and free access to standard food and water. All the procedures have been approved by the relevant Spanish authorities. Animals experiments followed the guidelines of the animal health institution of Complutense University School of Medicine, and with the standard humanitarian care outlined in the "Guide for the Care and Use of Laboratory Animals" prepared and published by National Research Council (US) Committee[98].

5.2.1.3 Mice strain

The generation of hepatocyte specific *Jnk1/2* knock-out mice ($Jnk^{\Delta hepa}$) was described in published paper in a C57BL/6 background[99], as well as described in Chapter 6.1. Cre negative $Jnk^{f/f}$ mice were used as controls. All male mice were housed for experiments. All studies were performed using C57BL/6J background, age matched, male mice. Alb Cre transgenic mice (expressing Cre recombinase under the control of Albumin promotor) in a C57BL/6 background were purchased from the Jackson Laboratory (Bar Harbor, ME). Moreover, $Jnk1/2^{\Delta hepa}$ (double mutants with ubiquitous deficiency of JNK2 and ablation of JNK1 only in hepatocytes) were generated by crossing Alb Cre mice with $Jnk1/2^{LoxP/LoxP}$ mice. This approach enabled the simultaneous genetic inactivation of JNK1 and JNK2 in hepatocytes.

5.2.1.4 Genotyping of transgenic mice

First, all of the tails were freshly cut from the mice when they were separated

from their mother aging 4 weeks old. The correct genotype was confirmed by PCR analysis. The tail was digested in the NID buffer (**Table 5.2.1**) 200µl mixed with 2µl Proteinase K (AppliChem, Munich, Germany) inside the thermomixer and shaken overnight at 56°C. The second day, enzyme activity was stopped by heating at 95°C for 10min. Subsequently, the tubes containing digested tails were centrifuged via 12000 rpm for 10 min at room temperature (RT). Each 2 µl supernatant of the samples was used for PCR reaction (**Table 5.2.2**, **Table 5.2.3**). Program procedures of PCR reaction and preparation of genotyping Gel for Jnk1, Jnk2, Total-Cre are listed in **Table 5.2.4**, **Table 5.2.5**, and **Table 5.2.6**, separately.

After PCR reaction, the procedure was started. Total 100ml Tris Acetate EDTA Buffer (TAE) Buffer/PCR-running Buffer with Agarose 2g were prepared to be mixed in a final (w/v) concentration of 2% in the beaker. Then the solution inside the microwave was boiled for 4 min. Later, Midori Green Advance buffer 10µl (Nippon genetics, Düren, Germany) was added, and the solution completely mixed before poured into an electrophoresis chamber/tank, until a solid gel was formed. The PCR products were added into each well, 1kbp DNA markers were used to determine the specific size of fragments, and the electrophoresis completed with 110 V for 35 min. Finally, the gel was placed under the UV-transilluminator (Gel Doc 2000 System, BIO-RAD, Kentucky, USA) and the PCR products were visualized and recorded by using BioDoc Analyze software (Biometra, Jena, Germany).

Table 5.2.1 NID buffer mixture was prepared as follows:

Reagent	**Final Concentration**	**PH value**
KCl	0.05 M	pH=8.3
Tris	0.01 M	
$MgCl_2$	2 mM	
Gelatine Type B	0.1 mg/ml	

NP-40	0.45 %	
Tween-20	0.45 %	

Table 5.2.2 Mixture for genotyping PCR *Jnk1* and *Jnk2*:

Reagent	**Volume**
DNA	2µl
Primer1	1µl
Primer2	1µl
Red taq	12.5µl
DEPC H_2O	8.5µl
TOTAL	25µl

Table 5.2.3 Mixture for genotyping PCR Total-Cre:

Reagent	**Volume**
DNA	2µl
Primer CRE Forward 01	1µl
Primer CRE Reverse 01	1µl
Primer CRE Forward 02	1µl
Primer CRE Reverse 02	1µl
RedTaq	12.5µl
DEPC H_2O	6.5µl
TOTAL	25µl

Table 5.2.4 PCR *Jnk1$^{\Delta hepa}$* program procedure:

***Jnk1$^{\Delta hepa}$* program**					
Procedure	**Temperature (°C)**	**Time**	**Cycles**	**Gel**	
1	94	3 min		Agarose	2%
2	93	30 sec		Size	100ML

3	58	45 sec	Total 35X	Midori	10µL
4	72	1 min			
5	Step Circulation	2→4			
6	72	10 min			
7	4	∞	Pause		

Table 5.2.5 PCR *Jnk2$^{\Delta hepa}$* program procedure:

***Jnk2$^{\Delta hepa}$* program**					
Procedure	**Temperature (°C)**	**Time**	**Cycles**	**Gel**	
1	96	15 min		Agarose	2%
2	96	30 sec	Total 35X	Size	100ML
3	60	30 sec		Midori	10µL
4	72	45 sec			
5	Step Circulation	2→4			
6	72	10 min			
7	4	∞	Pause		

Table 5.2.6 PCR *Cre* program procedure:

***Cre* program**					
Procedure	**Temperature (°C)**	**Time**	**Cycles**	**Gel**	
1	95	3 min		Agarose	2%
2	95	5 sec	Total 35X	Size	100ML
3	60	10 sec		Midori	10µL
4	72	20 sec			
5	Step Circulation	2→4			
6	72	1 min			
7	4	∞	Pause		

5.2.1.5 Diethylnitrosamine (DEN) injection

DEN liquid solution (Sigma-Aldrich, Darmstadt, Germany, N0756) was diluted in sterile 0.9% sodium chloride solution with a fixed working concentration. Mice were received a fixed dosage of 25mg/Kg via intraperitoneal injection (IP) according to the body weight at the 14th day postpartum (n=5-8 per group). The vehicle groups received the same IP injection with a volume of sterile 0.9% sodium chloride solution. Mice were carefully observed in the following days until sacrificed.

5.2.1.6 Thioacetamide (TAA) drinking water preparation

TAA was dissolved in sterilized water completely before the usage, and 8-week-old male mice were administrated with a fixed dose of TAA (300 mg/L) by oral-drinking over a period around 24 weeks according to the experimental models (n=5-8 per group). TAA oral-drinking water was refreshed per week with the same dosage. The vehicle groups received the same volume of vehicle sterilized water. Mice were carefully observed in the following days until sacrificed.

5.2.1.7 Carbon tetrachloride (CCl_4) injection

CCl_4 was diluted in corn oil and vortexed completely for usage. 8-week-old male mice were received a fixed concentration of 0.5ml/Kg via IP injection with continuing 14 weeks (n=5-8 per group). CCl_4 working solution was prepared freshly before IP injection every week. The vehicle groups received the same volume of vehicle corn oil. Mice were carefully observed in the following days until sacrificed.

5.2.1.8 Blood and liver sampling

In order to collect blood and liver tissue, mice were sacrificed using isoflurane

under brief anesthesia. Total body weights were recorded. First, the abdominal cavity was cut along the linea alba. Subsequently, the two sidewall incisions along the abdominal wall were relaxed. Blood samples were collected from the portal vein with a 1 ml syringe (27G needle), the blood samples were collected in serum tubes and centrifuged at 12000 rpm for 10 min. The supernatant was serum, and transferred to a new cryotube stored at -80°C for further experiments.

The whole liver was carefully taken out after the ligament was cut, and immediately immersed in ice-cold PBS buffer. Liver weight of each mouse was measured and recorded. The whole liver was sliced on ice with a scalpel. The liver lobes were separated and cut into small pieces for further analysis. Take two slices of different liver lobes of similar size, fixed them in 4% paraformaldehyde (PFA) for 24-48 hours, and embedded them in paraffin cassettes. The other two slices were placed in Tissue-Tek O.C.T. compound (Sakura, Heppenheim, Germany) and stored at minus 80°C for frozen sectioning. The remaining liver samples are cut into small pieces, transferred to cryotubes, quickly frozen in liquid nitrogen, and stored at - 80°C for other studies such as RNA and protein isolation. Blood samples were analyzed at the Hepatology and Gastroenterology Research Laboratory of the Hospital Gregorio Marañón by using automated standard procedures. Serum parameters determined in this study were alanine Aminotransferase (ALT), Aspartate Aminotransferase (AST), alkaline phosphatase (ALP) and Lactate Dehydrogenase (LDH), which are markers for general liver injury.

5.2.2 Cell culture and molecular methods

5.2.2.1 Cell culture

$HepG_2$ cells, as previously described[100], were cultured in Dulbecco's modified Eagle medium (DMEM, GE Healthcare, Munich, Germany) containing 10% fetal

bovine serum (Thermo Fisher Scientific, Massachusetts, USA), 1% L-Glutamine, 1% Non-Essential Amino Acids Solution and 1% Penicillin/Streptomycin at 37°C in a moist atmosphere containing 5% CO_2. HepaRG cells, as previously described[101]. Undifferentiated HepaRG cells were cultured in HepaRG Maintenance and Metabolism Medium Supplement with Antibiotics. Working medium was prepared by adding 15 ml/75 ml HepaRG™ Supplement to 100 ml/500 ml of Williams' Medium E. Working medium should be stored at 4°C for a maximum of one month. Medium was changed every 2-3 days. Cells were differentiated after changed into differentiated medium incubation at 37°C for at least 14 days within 21% O_2 and 5% CO_2 in a moist atmosphere.

The number and viability of cells was determined by Neubauer counting chamber and trypan blue staining method. Cells were passed and cultivated in 6 or 12 wells plates with or without coverslips in each well. After proper cell adhesion, TAA with or without DJNKI1 (MedChem Express, Monmouth Junction, USA) were added into the culture medium with a final concentration of 0mM, 10mM, 20mM, 30mM, 40mM, separately, and the treatment groups of $HepG_2$ and undifferentiated/differentiated HepaRG cells for 18 to 24 h. Cell RNA was isolated and protein was extracted for further experiments (see below RNA and protein experiments).

5.2.2.2 Cell viability assay

Cell viability was measured by a cell counting kit 8 assay (CCK-8) that was purchased from Sigma-Aldrich according to the instructions of the manufacture. Briefly, both $HepG_2$ and undifferentiated HepaRG cells were seeded in 96 well plates at 5×10^3 cells per well in 0.1 mL medium and cultured for 24 h. The cells were treated with different concentrations of TAA (0, 10mM, 20mM, 30mM, 40mM) for 18h and 24h, separately. In parallel, the kit reagent CCK-8 was added to the wells with the final concentration of 10%, and the cells were

protected from light and incubated for 1 h at 37°C. Then the optical density (OD) at 450 nm was measured using a microplate reader, results were sent to Excel and calculated by mathematics according to the instruction of manufacturer.

5.2.3 Molecular mRNA methods

5.2.3.1 RNA isolation

RNA isolation (cells and liver tissues) was first done before quantitative polymerase chain reaction (qRT-PCR) procedure program. At the beginning of the experiment, sterilized tubes and 70% ethanol (EtOH) (prepared with MiliQ water, EtOH: MiliQ water = 7:3) for cleaning homogenizer were prepared. The hood, homogenizer and the bench used for isolation procedure were disinfected with 70% EtOH.

Lysis of both cells and tissues was performed using Trizol reagent. For cells, an appropriate volume of Trizol reagent was added into 6-well or 12-well plate and incubated for 30 min at RT. While for liver tissues, 50-80mg liver tissues were homogenized completely in 1ml Trizol reagent using an electronic homogenizer. After the cells or liver tissues were homogenized completely, each eppendorf was kept still under RT 30 mins. Then 200µl chloroform was added into the each eppendorf and vortexed completely. After incubation on the bench for at another 20 mins at RT, eppendorfs were centrifuged for 10 min, 12000 rcf at 4°C. Then, 400µl supernatant of each eppendorf was transferred into a new sterilized eppendorf, following with another 400µl of isopropanol (AppliChem, Dismalab, Barcelona, Spain) was added into each eppendorf and mixed completely one by one. This step was followed by keeping eppendorfs 15 min at RT. The tubes were centrifuged 10 min, 12000 rcf at 4°C, the supernatant discarded and the pellet would be underneath. 70% Ethanol was used to clean the pellet inside the eppendorf, via vortex and centrifuged 3x 10 min, 12000 rcf at 4°C. Then, the supernatant was discarded and the pellet dried

completely at RT. The pellet was diluted with DEPC water and vortexed 20 to 30 seconds at 65°C max RPM in the Thermomixer. Each sample was measured by Nanodrop at an OD of 260 nm combined with using DEPC water as blank. The concentration is calculated spectrophotometry at an OD of 260nm and the purity of the sample is determined according to the E260/E280 ratio. Therefore, the purity of the mRNA ranges from 1.8 to 2.0 is relatively high. RNA samples were stored at -80°C.

5.2.3.2 Real time PCR: Reverse transcription

Single stranded mRNA is reverse transcribed into complementary DNA (cDNA). Reverse transcription was performed using an Applied Biosystems™ High-Capacity cDNA Reverse Transcription Kit according to the manufacturer's recommendations (**Table 5.2.7**, **Table 5.2.8**). Afterwards, cDNA was diluted with a comfortable concentration (85 µl DEPC+ cDNA). cDNA samples were stored at -20°C or directly used for qRT-PCR.

Table 5.2.7 Reverse transcription system

Reagents	**Volume (µl)**
RNA sample with DEPC WATER	Total 10
DEPC WATER	4.2
10x buffer RT	2
25x dNTPs	0.8
10X random PRIMER	2
Enzyme Reverse transcriptase	1
Total volume	20

Table 5.2.8 Reverse transcription procedure:

Program: RT-applied Bio-Rad machine

25°C	10 min
37°C	120 min
8°C	5 min
4°C	∞

5.2.3.3 Quantitative real-time PCR

SYBR Green Master Mix was used to analyze under the 7300 Real Time PCR System and Sequence Detection Software Version 1.3.1(Applied Biosystems, Massachusetts, USA). RT-PCR was repeated with a volume of 20µl reaction mixture according to the instruction of manufacturer (**Table 5.2.9**). After reaction, the Ct values were exported to Microsoft Excel (Microsoft Corp., Redmond, Washington, USA) for analysis. The Sequence Detection Software Version 1.3.1 was used for calculating the CT value for each reaction. Relative mRNA expressions were calculated according to the ΔΔCT method[102]. Each CT value of the reaction was compared with the untreated control group and compared with GAPDH gene expression serving as an internal reference.

Table 5.2.9 Details for RT-PCR reaction mixture are given as follows:

Reagents	**Volume (µl)**
cDNA	5
Forward primer	1
Reverse primer	1
SYBR green master mix	10
DEPC water	3
Total reaction volume	20

5.2.4 Molecular protein extraction and analysis

5.2.4.1 Extraction of whole-cell proteins from the cells or the liver tissue

For cell extraction, 100-200µl freshly complete NP40 lysis buffer (**Table 5.2.10, Table 5.2.11**) was added into each well in the cell culture plates (6-well or 12-well). For liver tissue protein extraction, approximately 50 mg frozen liver tissue was homogenized by homogenizer on the ice within 500 µl freshly complete NP40 lysis buffer holding in 2 ml eppendorf tube. Samples of protein were homogenized on the ice. After incubated on the ice for 30 min and centrifuged 10 min 12000 rpm at 4°C. The supernatant was transferred into a new tube and the concentration was determined (see below protein quantification), or store at -80°C for future use.

Table 5.2.10 NP40 buffer shown as follows:

NP40-Buffer	Volume	Final concentration
Tris/HCl 7.5 pH (1 M)	25 ml	50 mM
NaCl (5 M)	15 ml	150 mM
Nonidet P-40	2.5 ml	0.5%
Sodium Fluoride	1.05 g	50 mM
dH_2O added to	500 ml	

Table 5.2.11 Freshly complete NP40 lysis buffer as follows:

Freshly added components	Volume
AEBSF Hydrochloride (100mM)	100 µl
Complete Mini (protease inhibitors)	1 tablet
DTT (1M)	20 µl
PhosSTOP	1 tablet
NP40 buffer added to	10 ml

5.2.4.2 Protein quantification

According to Bradford's method, protein concentrations in the whole liver tissue lysate, cytoplasm and mitochondria were measured using Bio-Rad protein analysis reagent following with the manufacturer's instructions[103]. For the purpose of determination, 2 µl of each liver protein sample was mixed with 998 µl Bio-Rad protein reagent, which had been diluted in DEPC water with the final concentration of 20%. To generate the standard curve, BSA was diluted into 0.5 mg/ml, 1 mg/ml, 1.5 mg/ml, 2 mg/ml, 4 mg/ml, 6 mg/ml, 8 mg/ml, 10 mg/ml, separately in the same way as the samples. NP40 buffer was used as blank control. BSA standards of pre-adjusted concentrations together with protein samples were measured at the same time approach to use a spectrophotometer at OD_{630}. The concentration of the sample was calculated by comparing with the standard curve from the OD_{630} value of BSA standard protein. Before Western blot (WB) analysis, the final concentration of the protein solution was adjusted to 4 µg/µl for liver and 1-2 µg/µl for cells with complete NP40 lysis buffer.

5.2.4.3 Western blot (WB)

Proteins samples were denatured for 5 min 300 rpm at 95°C in the thermomixer after adding loading buffer (1/4 total volume), following with proteins centrifuged for another 5 min, 300 rpm at RT. Samples were loaded on a handmade gel which containing 5% polyacrylamide stacking gel (**Table 5.2.12**) and separating gel that range from 8% to 15% (**Table 5.2.13**) according to the molecular weight of the target proteins. Quantity of the uploading protein, for cells range from 30 to 80 µg and for liver tissue range from 80 to 150 µg separately (according to the different target proteins). Protein samples were separated at 80-120 V for approximately two hours in one-fold SDS-Running buffer (**Table 5.2.14**).

After electrophoresis, the separated proteins were transferred from the

polyacrylamide gel onto a PVDF membrane in the wet blotting chamber for 2 hours at 300 mA (Current) and 4°C (ice around). Whatman® paper, PVDF membrane and polyacrylamide gel were made as a sandwich then immersed in 1-fold transfer buffer (**Table 5.2.15**). The transfer was carried out in accordance with standard procedures[104]. Ponceau S solution was used for confirming proteins successfully transferred. After rinsing out the Ponceau S solution with 1% TBS-Tween 20 (TBST) buffer, the membrane was incubated in 5% BSA/1% TBST or 5% non-fat dry milk/1% TBST for 1 h at RT to block the unspecific binding sites. Subsequently, the membrane was shortly washed and incubated in the primary antibody diluted with an appropriate concentration in 1% BSA/TBST or 2.5% nonfat dry milk/TBST solution shaken overnight at 4°C. The primary antibodies and concentrations of working dilutions are listed in **Table 5.1.4**.

On the following day, the membrane was washed 3x 10 min in 1%TBST solution. Then the membrane was incubated in secondary antibody with the fixed concentration diluted in 5% BSA/1%TBST or 5% non-fat dry milk/1%TBST for 1 hour at RT, the concentrations of working dilution are listed in **Table 5.1.5**. Subsequently, the membrane was washed 3x 10 min in 1%TBST solution. Target signals were visualized using ECL™ Prime Western Blotting System. After incubation for 3-5 min, the membrane was developed in a LAS mini 4000 Chemiluminescence scanner (FUJIFILM, super CCD, Marlborough, USA).

Table 5.2.12 Handmade stacking gel as follows:

Stacking Gel	**Volume**
dH_2O	4.5ml
30% Acrylamide/Bis Solution	1.3ml
APS 10 %	80µl
SDS 10%	80µl
Tris/HCL PH=6.8	2ml

TEMED	8 µl
Total volume	8ml

Table 5.2.13 Handmade separating gel as follows:

Separating Gel	**8%**	**10 %**	**12 %**	**15 %**
dH_2O	9.3ml	7.9ml	6.6ml	4.6ml
30% Acrylamide/Bis Solution	5.3ml	6.7ml	8.0ml	10.0ml
APS 10 %	200µl	200µl	200µl	200µl
SDS 10%	200µl	200µl	200µl	200µl
Tris/HCL PH=8.8	5.0ml	5.0ml	5.0ml	5.0ml
TEMED	12ul	8ul	8ul	8ul
Total volume	20ml	20ml	20ml	20ml

Table 5.2.14 SDS-Running buffer mixture as follows:

10x SDS-Running Buffer	**Volume/Quality**
Tris	30.3g
Glycine	144.13g
SDS	10g
dH_2O add to	1L

Table 5.2.15 10x Transfer Buffer mixture as follows:

10x Transfer Buffer	**Volume/Quality**
Tris	30.3g
Glycine	144.13g
dH_2O add to	1L
1x Transfer Buffer	**Volume/Quality**
10x Transfer Buffer	100 ml
Methanol	200ml

dH_2O add to	1L

5.2.5 Histological analysis

5.2.5.1 Terminal deoxynucleotidyl transferase dUTP nick end labeling (TUNEL) Staining

Terminal deoxynucleotidyl transferase-mediated dUTP nick end labelling (TUNEL) staining is an established method for *in situ* labelling of DNA strand breaks that occur early during apoptosis. First, cryopreserved liver samples were cut into 5 µm thick, cells were cultured on the surface of the coverslips with an approximately concentration of $10^5/cm^2$. The slides/coverslips were then dried for 30 min at RT and then slides/coverslips were fixed in 4% PFA for 20 min at RT. After fixation, the slides/coverslips were washed 3x 10 min in PBS. During this period, 10% hydrogen peroxide (H_2O_2) was prepared by mixing 30% H_2O with methanol (1:9). The slides/coverslips were incubated in 10% H_2O in dark condition for 10 min. This step was followed by incubation for another 10 min PBS solution. In order to have access to the DNA, the nuclei were permeabilized in 150mM Na-Citrate (**Table 5.2.16**) in PBS solution for 2 min at 4ºC in the fridge. The permeabilization solution was removed by washing the slides/coverslips 2x 10 min in PBS solution. Subsequently, 100µl of labelling mixture reaction (**Table 5.2.17**) was spread on each section/coverslip and incubated overnight at 4ºC in the fridge. The second day, the slides/coverslips were washed 4x 10 min in PBS solution. Then, the slides/coverslips were mounted with DAPI for nuclear counterstaining with coverslips covering the sample, and keep them in dark at 4ºC in the fridge 15 minutes. Observe the samples under the microscope and calculate the positive cells by using the AxioVision© software and photographs saved in the format ". zvi". Photographs were analyzed by software ImageJ Version 1.52u (LOCI, University of Wisconsin, Wisconsin, USA).

Table 5.2.16 Precool the mixture together with glass tank as follows:

Reagent	Volume(ml)/Quality(g)
150mM Na-Citrate	8.8g
PBS solution	200ml
10-fold Triton-100	0.2ml
PH value	pH= 6.0

Table 5.2.17 The labelling mixture solution was composed as follows:

Reagent	Volume(µL) for 1 section
Enzyme Solution (blue cap)	1
10X TUNEL Diluent Buffer (20ml bottle)	10
TUNEL Labeling Solution (violet cap)	89
Total	100

5.2.5.2 Immunofluorescence staining (IF)

Freshly 5µm thickness of the cryosections made from the liver of the mice (cells coverslips) were used for IF staining. First, liver tissue sections or cells coverslips were incubated in 4% PFA 15 min at RT. This step was followed by washing slides 3x 10 min in PBS. Non-specific binding sites of the tissue were incubated in blocking solution (10%Goat serum, 0.3%Triton-100, 1-fold PBS buffer) 1 h at RT. Subsequently, incubate the tissue overnight at 4 ºC (in the fridge) with the primary antibody mixed with blocking solution which was prepared according to the instruction of the manufacturer (**Table 5.1.4**). The second day, samples were washed 3x 10 min in PBS solution. Then, tissues were incubated with the secondary antibody prepared with blocking solution 1 h at RT (**Table 5.1.5**). After washing the samples 3x 10 min in PBS solution, DAPI was used not only as mounting medium for mounting the samples, but also to visualize the nuclei. Pictures were taken using AxioVision© software

after incubating the stained sections at 4 ºC in the fridge 15 min, photographs were analyzed by software ImageJ Version 1.52u, subsequently.

5.2.5.3 Paraffin Embedding

After fixation in 4% PFA for 24-48 h, mice liver specimens were kept in PBS solution at 4 ºC in the fridge before embedding. We first washed the specimens/cassettes under running tap-water for 30 min. Then tissues were dehydrated sequentially by waxing cassettes in 50%, 70%, 85% and 95% EtOH for 0.5-h, 1 h, 1 h and 1 h, separately. Then, cassettes were incubated in 95% EtOH overnight. On the following day, the specimens were continued to be dehydrated via waxing cassettes in 100% EtOH for 2x 0.5 h. Clearing the tissues sequentially by waxing cassettes in the mixture buffer (EtOH absolute: Xylene=1:1) for 0.5 h, combined with waxing cassettes in xylene 2x 0.5 h at RT. Subsequently, waxing cassettes were put in liquid paraffin 3x 1 h at 70 ºC. Finally, tissue embedding was completed with paraffin by using the system Leica EG1160 Embedding Center Dispenser plus hot Plate (Leica Biosystems Nussloch GmbH, Nußloch, Germany) and paraffin blocks were kept at RT for future experiments.

5.2.5.4 Hematoxylin and eosin (H&E) staining

Paraffin embedded liver samples were cut 5 µm thick and slides were baked in the oven at 60 ºC for 1 h. Then, sections were incubated 2x 5 mins in xylene. This step was followed by incubating sections 2x 5 min in 100% ethanol. Then the sections were incubated into 96%, 90%, 85% EtOH for 3 min, 3 min, 3 min, consecutively. Later, sections were rinse under flowing tap-water for another 2 min. Then, the sections were incubated in hematoxylin 2 min followed by rinsing the sections under flowing warm tap-water for 10 min. Sections were turned into 1% hydrochloric acid alcohol incubated 2 seconds. Next, the sections were rinsed under flowing warm tap-water 15 min. After that, the sections were

incubated in 70%, 85%, 90% EtOH for 3 min, 3 min, 2 min, consecutively. Subsequently, sections were incubated in eosin 2 min in a dark environment. Sections were rinsed with 95% EtOH 3 sec to make sure the eosin was removed. This step was followed by waxing the sections 2x 3 min in 100% EtOH. Then, the sections were cleaned 2x 10 min in xylene. Finally, slides were mounted by mounting medium and dried in a fume hood. Photographs were taken using microscopy.

5.2.5.5 Sirius Red Staining

Sirius Red (SR) is one of the best techniques for detecting collagen deposition. Paraffin liver samples were cut 5 µm thick made into sections, and immersed in the respective solutions 2x 5 min xylene, 2x 5 min 100% ethanol, 2x 5 min 95% ethanol, 2x 5 min 80% ethanol, 2x 5 min distilled water, separately. This step was followed by waxing the sections in Picro-Sirius Red solution (**Table 5.2.18**) for 60 min at RT. Then, sections were followed by rinsing in acidified Water (**Table 5.2.19**) for 4 min at RT. The sections were rinsed 2x 30 seconds in 100% EtOH, 2x min in xylene, separately. Finally, the sections were mounted by mounting medium and dried in a fume hood. Photographs were taken by using microscopy and analyzed by software ImageJ Version 1.52u.

Table 5.2.18 Picro-Sirius Red solution was prepared as follows:

Reagent	**Volume/Quality**
Sirius Red OR Direct Red 80	0.25 g
Picric acid saturated aqueous solution	250 ml

Table 5.2.19 Acidified Water was prepared freshly as follows:

Reagent	**Volume(ml)**
Acetic Acid	1.5
Distilled water	300

5.2.5.6 Immunohistochemistry (IHC)

Paraffin liver samples were cut 5 µm thick made into slides/sections. The sections were preheating at 60°C for 30-40 min in the oven. The paraffin-embedded sections were deparaffinized and rehydrated with a reduced concentration of xylene and a series of ethanol solutions, immersed 2x 10 min in xylene, followed by incubated 2x 5 min in 100%, 96%, 70% ethanol, and dH_2O, consecutively. In order to improve the utilization of antigens, antigen retrieval was performed by cooking the sections in 10mM sodium citrate buffer (Citrate/PBST, PH = 6.0) using a pressure-cooker 2100-Retriever (Aptum Biologics, Kassel, Germany), with the slides kept wet. After one complete cycle (2 h) according to the instruction of the Retriever manufacturer, including cool the sections completely, the slides were taken outside of the pressure cooker and rinsed 3x 5 min in dH_2O. The sections were treated with 3% H_2O_2 for 10 min to quench endogenous peroxidases. The next step consisted of rinsing the sections 2x 5 min in dH_2O and 5 min in PBS. After blocking each section with 100 µl 2.5% normal horse serum (Vector Laboratories, California, USA) for 30 min at RT, 100 µl primary antibody solution (concentration listed in **Table 5.1.4**) was added to each section and incubated overnight at 4ºC. The following day, the primary antibody solution was removed and sections were washed in PBS 3x 5 min, then 100µl secondary antibody was added (concentration listed in **Table 5.1.5**) to each section incubating for 1 h at RT. Secondary antibody was removed and sections washed 3x 5 min in PBS. Staining was developed by using DAB as the manufacturer suggested, accompanied by counterstaining cell nuclear with hematoxylin 2 min. Sections were washed under running tap-water for 15 mi and 2x 5 min in dH_2O.

After sections were dehydrated in an ascending ethanol series (2x 10 sec in 96%, 2x 10 sec in 100% EtOH), cleared 2x 5 min in xylene and mounted with the mounting medium. Photographs were taken by using microscopy after the sections dried.

5.2.5.7 Periodic Acid-Schiff (PAS) staining

Paraffin embedded liver samples were cut 5 µm thick. Before using Periodic Acid solution and Schiff's Reagent, they need to be pre-warmed at RT 10 min. Paraffin-embedded sections were deparaffinized in xylene (2x 5 min) and rehydrated with a reduced concentration of EtOH (2x 5 min in 100%, 96%, 70% ethanol, and dH_2O, consecutively). Then, sections were immersed in Periodic Acid solution for 5 min at RT and after rinsing slides 3x 5 min in dH_2O. After immersing in Schiff's Reagent for 15 min at RT, sections were rinsed under running tap water for 5 min. Counterstain slides in Hematoxylin Solution for 2 min followed by rinsing the sections in running warm tap water 15 min. Subsequently, sections were dehydrated performed in increasing percentages of EtOH (2x 5 min in 95%, 100%, separately), cleared 2x 5 min in xylene and mounted with the mounting medium. Photographs were taken by using microscopy after the sections dried completely.

5.3 Statistical analysis

All data were expressed as mean ± standard deviation of the mean. The standard error of the mean (SEM) was calculated from the average of at least 3 independent samples per condition. Statistical significance was determined via using GraphPad Prism 8.0 software (GraphPad Software, California, USA), followed by a Student's t-test (unpaired, two-tailed test) or via one-way analysis of variance (ANOVA) including Tukey's multiple comparisons test, P values less than 0.05 were considered significant.

6. Results

6.1 Construction and generation of the *Jnk$^{\Delta hepa}$* knockout mice

Alb (Albumin)-Cre and *Jnk2* deficient mice in the C57BL/6 background were purchased from the Jackson Laboratory (Bar Harbor, ME). By homologous recombination in embryonic stem (ES) cells, mice with a floxed allele of *Jnk1/2* were constructed *Jnk1/2$^{LoxP/LoxP}$* (Jnk$^{f/f}$) according to the previously published studies, Alb-Cre mice were crossed to *Jnk1/2$^{LoxP/LoxP}$* to generate mice Jnk1/2$^{\Delta hepa}$ (Jnk$^{\Delta hepa}$)[99, 105, 106]. Both of *Jnk$^{f/f}$* mice and *Jnk$^{\Delta hepa}$* mice were fed to keep old without any treatment, and raised in cages with filters and bred in pathogen-free, temperature and humidity-free facilities of the Animal Facility at School of Biology, UCM, for a 12-hour cycle of light and shade and free access to standard food and water. Compared with *Jnk$^{f/f}$* mice, *Jnk$^{\Delta hepa}$* mice were difficult to survive more than 72-week-old, the survival rate of these mice was approximately 43.75% (7/16, survival data not shown), Both of the strains were kept older with age, and sacrificed at two different time points (32-week-old and 52-week-old, separately (**Fig. 4A**). PCR amplimers (described in chapter **Table 5.1.2**) were used to examine the genomic DNA to distinguish the controlled and the deleted (Jnk1$^{\Delta hepa}$) alleles, so that with *Alb*-Cre (Total-Cre 01/02) detected though genotyping test making sure *Jnk$^{f/f}$* mice *Alb*-Cre positive, which means *Jnk$^{\Delta hepa}$* (**Fig. 4B**). In order to confirm the effectiveness of the *Jnk1/2* deletion in the hepatocytes, WB from total liver tissue extracts. The proteins of the livers from *Jnk$^{\Delta hepa}$* mice were extracted to be detected and probed with mouse-specific JNK1 and JNK2 antibodies, the results are clearly presented in **Fig. 4C**. Compared with the *Jnk$^{\Delta hepa}$* mice, *Jnk$^{f/f}$* mice were used as control group mice.

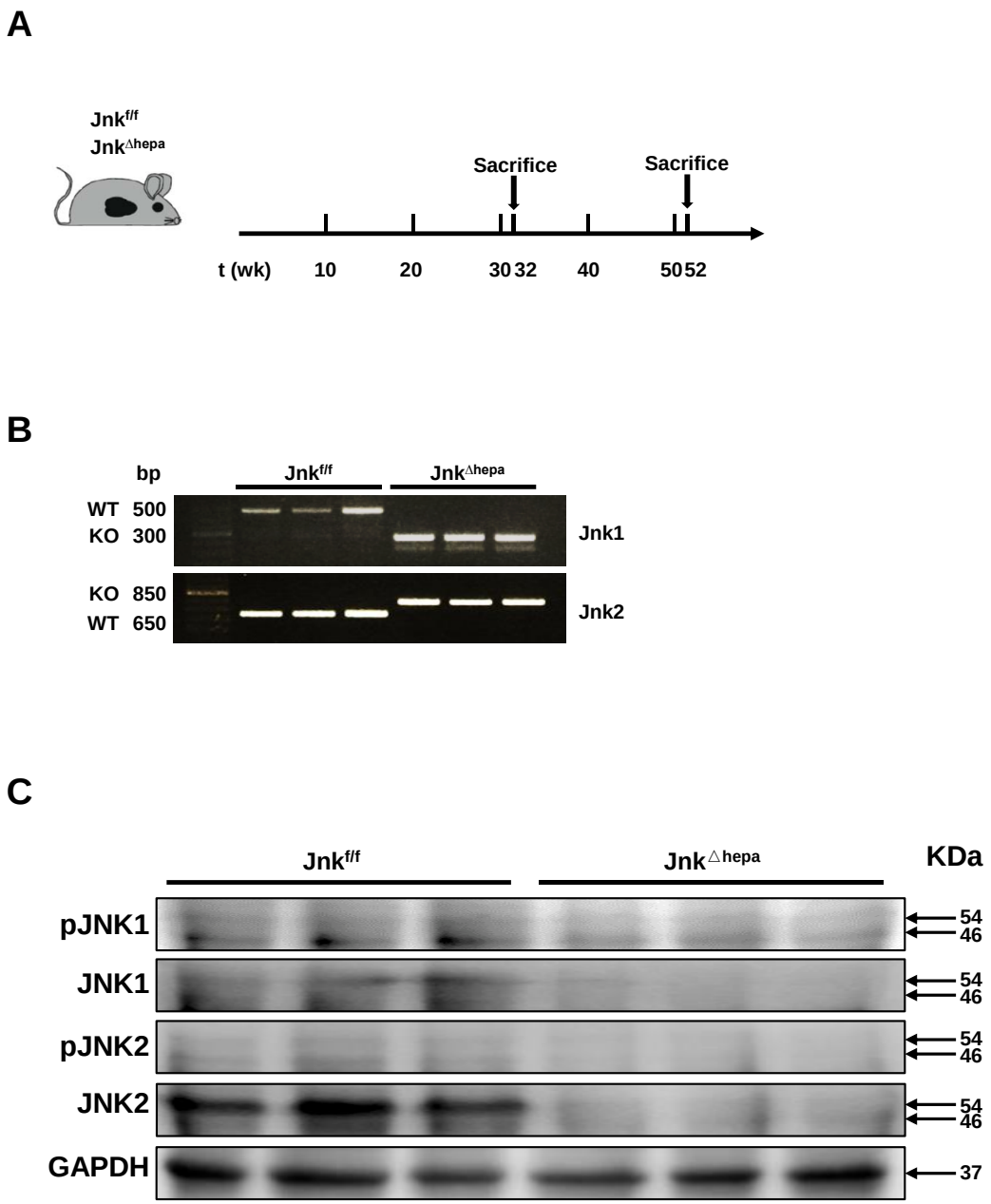

Figure 4. Efficient *Jnk1/2* deletion in hepatocytes *Jnk$^{f/f}$* mice. A) Compared with the *Jnk$^{\Delta hepa}$* mice, *Jnk$^{f/f}$* mice were used as control group mice. Mice were sacrificed at different time points, 32-week-old and 52-week-old, separately. **B)** Ethidium Bromide gel showed the respective PCR results from mice tails DNA derived from *Jnk1$^{\Delta hepa}$*/*Jnk2$^{\Delta hepa}$* mice. **C)** WB was presented to prove the deletion of *Jnk1/2* in hepatocytes of the liver. Expression of pJNK1, JNK1 and pJNK2 and JNK2 were assessed via WB. Numbers were denoted as the molecular weight (KDa) of proteins. GAPDH was used as a loading control.

6.2 Characterization of *Jnk$^{\Delta hepa}$* mice

We first focused on the phenotype of livers during the progression of liver disease starting at 32-week-old in both *Jnk$^{f/f}$* and *Jnk$^{\Delta hepa}$*. Previously, we had shown that livers of *Jnk$^{\Delta hepa}$* mice are characterized by small cyst-like structure at 32-week-old[60], and 33.7% mice showed the same results according to the frequency of cysts combined with ductular reaction (Arrows indicate positive areas) as observed by H&E staining (**Fig. 5A-B**). In our study, the altered phenotype of characteristic structures in the liver is consistent with the photographs of H&E staining (**Fig. 5B**). Compared with *Jnk$^{f/f}$* and *Jnk$^{\Delta hepa}$* mice, the difference between body weight (BW) and liver *vs* body weight (LW/BW) ratio were not significant in 32-week time point, but liver weight (LW) interestingly decreased (**Fig. 5C-E**). Serum markers of liver damage AST and ALT, as well as LDH were upregulated (**Fig. 5F-H**), but no difference in ALP (Data not shown). These results suggested that liver injury was induced after deletion of *Jnk1/2* in hepatocytes combined with phenotypic changes in liver structure. Altogether, target deletion of *Jnk1/2* in hepatocytes induces liver biliary hamartoma accompanied with liver dysfunction, related to hepatocellular vacuolation and exacerbated proliferation of biliary epithelial cells (BECs) triggering dilation of the ductular tracts (**Figure 5**).

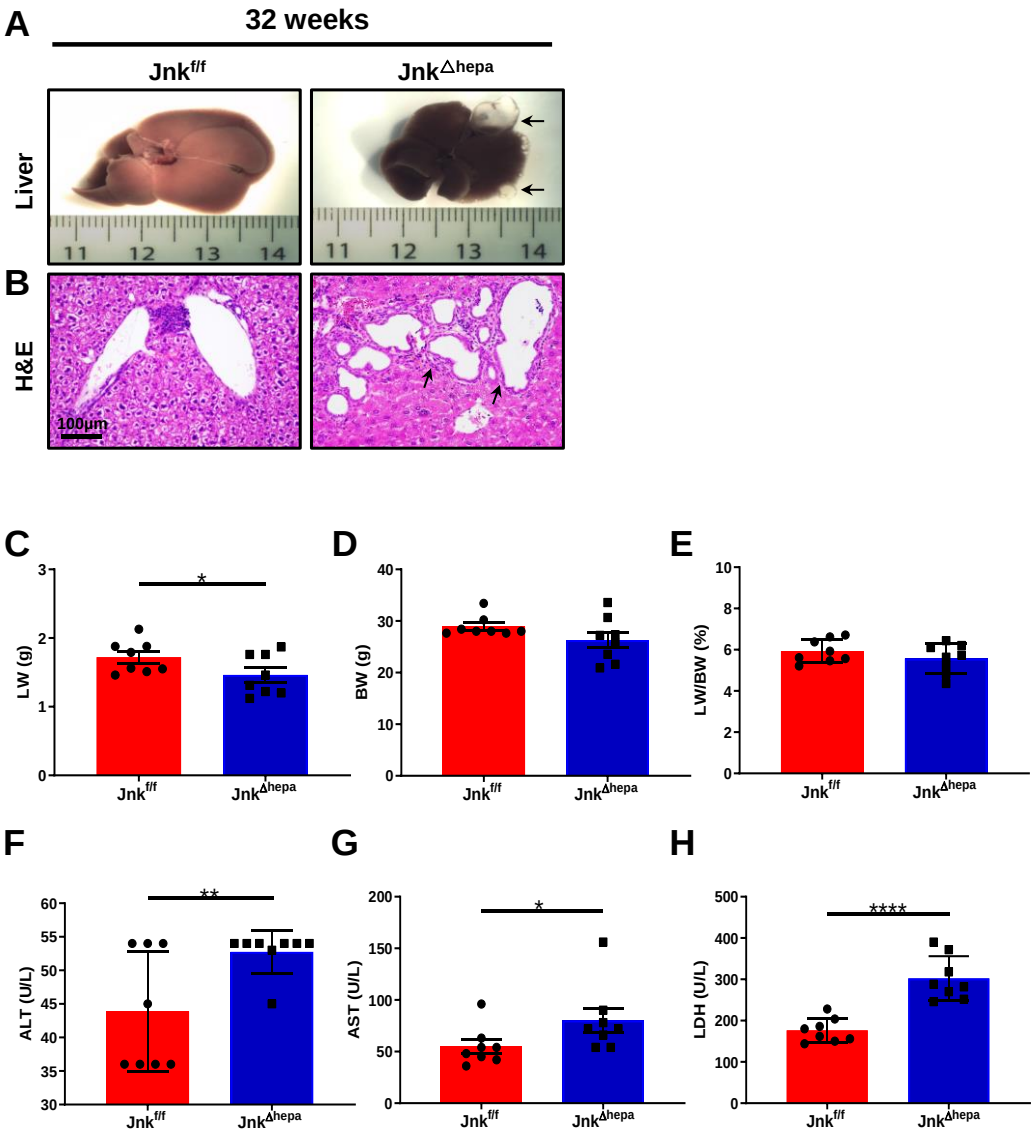

Figure 5. Presence of liver cysts and serum markers of hepatic damage in *Jnk$^{\Delta hepa}$* mice. A) 32-week-old male mice, both *Jnk$^{f/f}$* (n=8) and *Jnk$^{\Delta hepa}$* (n=8) mice in a C57BL/6 background were sacrificed, livers were harvested and photographed. **B)** Compared with *Jnk$^{f/f}$* mice, *Jnk$^{\Delta hepa}$* mice showed the phenotype of multiple liver cysts dilatations with varying sizes according to H&E staining. Scale bars, 100µm. **C)** LW of *Jnk$^{f/f}$* and *Jnk$^{\Delta hepa}$* mice were annotated in 32-week-old mice, and results were graphed as well as **D)** BW, and **E)** LW/BW ratio. Serum markers of liver damage in both groups were analyzed, **F)** ALT, **G)** AST, **H)** LDH were represented and graphed. Data were represented as the mean ± SEM and graphed (*p <0.05; **p<0.01; ****p <0.0001).

6.3 Cell death and fibrosis are increased in *Jnk$^{\Delta hepa}$* mice

In order detect hepatocyte damage in *Jnk$^{\Delta hepa}$* livers, TUNEL staining was accessed to detect cell death in both 32-week-old *Jnk$^{\Delta hepa}$* and *Jnk$^{\Delta hepa}$* mice, photographs were taken and results were calculated. Cell death was increased by calculating TUNEL-positive cells in *Jnk$^{\Delta hepa}$* mice group compared with *Jnk$^{f/f}$* animals, and with significant statistical difference (**Fig. 6A, C**). According to SR staining, these results were also in line with the progression of fibrogenesis in *Jnk$^{\Delta hepa}$* compared with *Jnk$^{\Delta hepa}$* at 32 weeks of age (**Fig. 6B**). SR staining showed fibrosis characterized with multiple cysts of ductular dilation in the liver, which suggested that fibrosis may promote the ductular reaction in *Jnk$^{\Delta hepa}$* livers. Positive stained areas were calculated by ImageJ (**Fig. 6D)**. These results suggested that cell death combined with fibrosis is increased by the progression of biliary hamartoma after the deletion of *Jnk1/2* in hepatocytes.

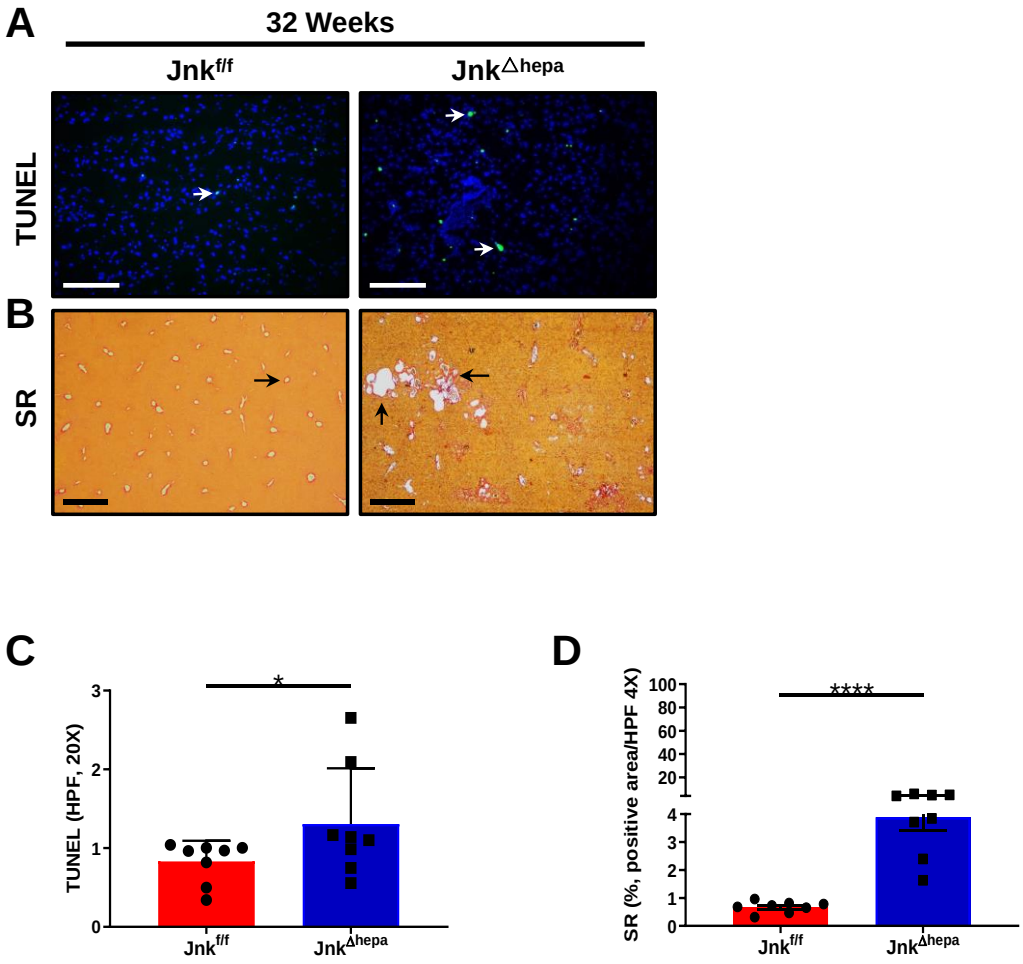

Figure 6. Cell death combined with fibrosis increased in *Jnk$^{\Delta hepa}$* mice. A) Cell death was performed using TUNEL staining in both *Jnk$^{f/f}$* and *Jnk$^{\Delta hepa}$* (n=8) mice at 32-week time point. Scale bars, 50μm. **B)** Fibrosis was also detected by SR staining in both *Jnk$^{f/f}$* and *Jnk$^{\Delta hepa}$* mice groups. Scale bars, 500μm. Data of **C)** TUNEL and **D)** SR staining, were represented as the mean ± SEM and graphed (*p <0.05; **** p <0.0001).

6.4 Presence of biliary hamartomas during the progression of liver disease in *Jnk$^{\Delta hepa}$* mice

Mesenchymal hamartoma is a rare, benign, developmental tumor of the liver, with occasional risk of malignancy. Histologically, it appears as a disordered arrangement of the mesenchyme, bile ducts, and hepatic parenchyma. The porous nature of the mesenchyme permits accumulation of fluid[107]. In order to

understand the progression of liver disease in older *Jnk$^{\Delta hepa}$* mice, 52-week-old mice were sacrificed. Livers were harvested and photographs taken. Hepatocyte-specific deletion of Jnk1/2 (*Jnk$^{\Delta hepa}$*) showed that the liver parenchyma is characterized by multiple cyst-like structures of different sizes ranging from 25um to 1560um according to the measurement of H&E staining, accompanied by fluid-filled in the cysts, when they grow up to 52-week-old (97.33%) according to the frequency of cysts in H&E staining (**Fig. 7A-B**). Histopathology of the liver was performed using H&E staining (**Fig. 7B**). Moreover, appearance of cysts was accompanied by proliferation of BECs. At the same time, LW and LW/BW ratio were obviously increased at the 52-week time point in *Jnk$^{\Delta hepa}$* mice (**Fig. 7C-E**). Serum markers of liver damage AST and ALT, as well as LDH were markedly elevated (**Fig. 7F-H**). These results are in line with the results of serum in 32-week-old mice. These results show that the *Jnk$^{\Delta hepa}$* mice are an interesting model of PLD[41] that could mimic the human situation.

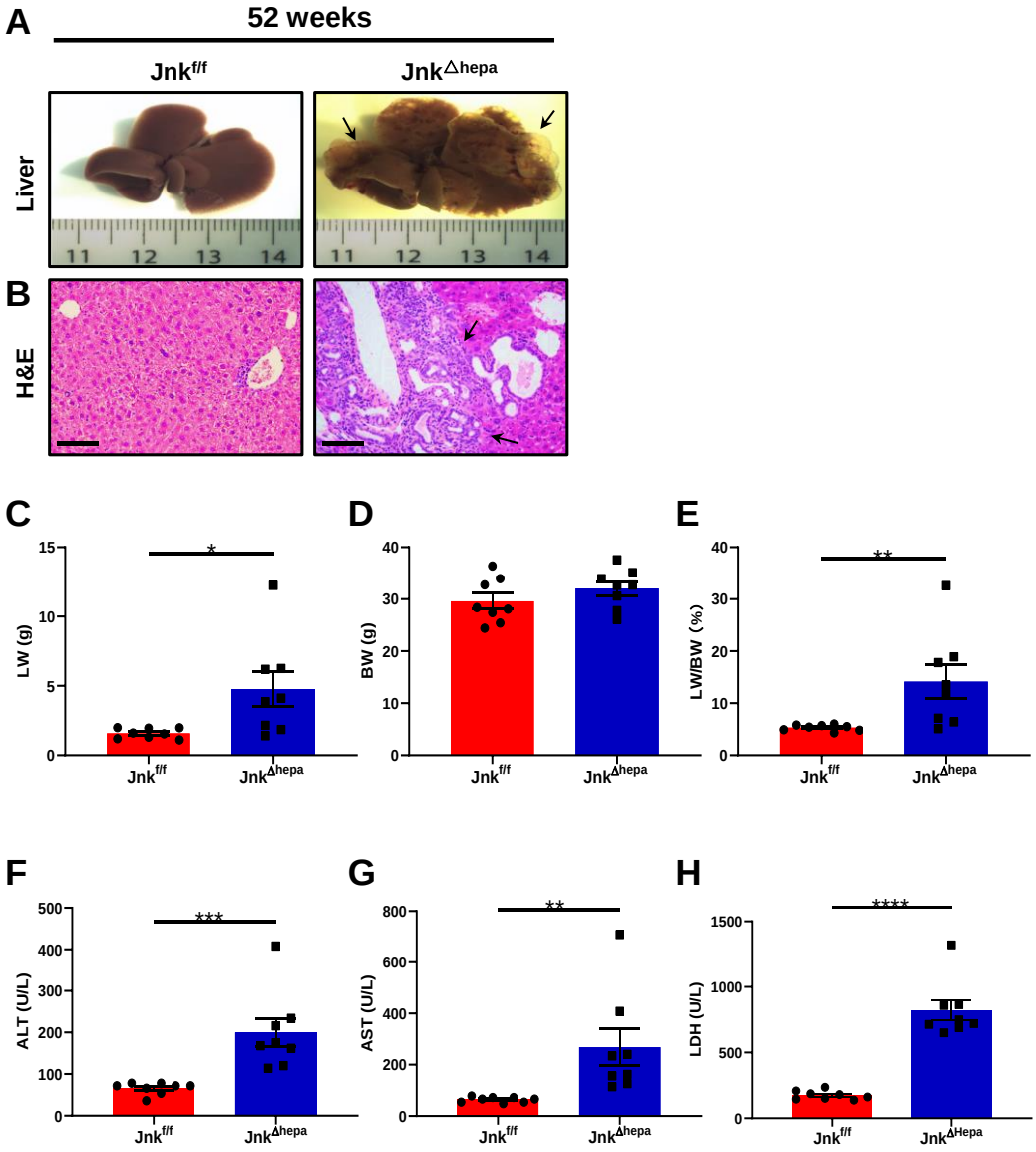

Figure 7. Liver biliary hamartoma progression in older *Jnk$^{\Delta hepa}$* mice. A) 52-week-old male mice, both *Jnk$^{f/f}$* and *Jnk$^{\Delta hepa}$* mice (n=8) with C57BL/6 background were sacrificed, livers were harvested and photographed. **B)** Compared with *Jnk$^{f/f}$* mice, *Jnk$^{\Delta hepa}$* mice showed the phenotype of multiple liver cysts dilatations with varying sizes according to H&E staining. Scale bars, 100µm. **C)** LW of *Jnk$^{f/f}$* and *Jnk$^{\Delta hepa}$* mice were annotated in 52-week-old mice, results were graphed as well as **D)** BW, and **E)** LW/BW. Results of serum in both groups were detected, **F)** ALT, **G)** AST, **H)** LDH were represented and graphed. Data were represented as the mean ± SEM and graphed. (*p <0.05; **p <0.01; ***p <0.001; ****p <0.0001).

6.5 Deletion of Jnk1/2 in hepatocytes does not trigger polycystic kidney disease (PKD)

Since PLD is associated with polycystic kidney disease (PKD)[40], we checked detected the anatomy and microscopy of kidneys at the same time points we sacrificed the mice during the progression of chronic liver disease (32 and 52 weeks) (**Fig.** 8). H&E staining showed normal anatomy and histology of kidneys of *Jnk*$^{f/f}$ and *Jnk*$^{\Delta hepa}$, accompanied by no cysts or biliary strictures at 32 and 52 weeks of age (**Fig. 8A**). Fibrous deposition measured by Sirius red (SR) staining was performed in kidneys of *Jnk*$^{f/f}$ and *Jnk*$^{\Delta hepa}$ mice. Concomitantly, no obvious fibrosis in the kidney of *Jnk*$^{f/f}$ and *Jnk*$^{\Delta hepa}$ was observed neither at 32 weeks or at 52 weeks (**Fig. 8B-C**). These results suggested that target deletion of *Jnk1/2* in hepatocytes did not cause PKD.

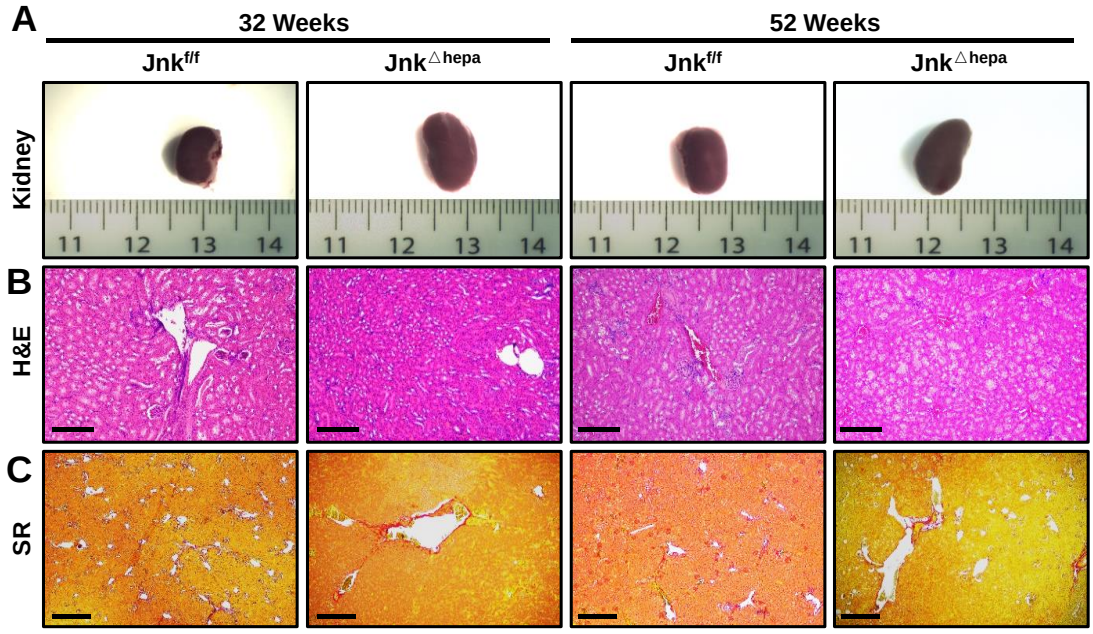

Figure 8. Anatomy and histopathology of kidneys in *Jnk*$^{f/f}$ and *Jnk*$^{\Delta hepa}$ mice. A) The phenotype of kidney was presented by both *Jnk*$^{f/f}$ and *Jnk*$^{\Delta hepa}$ mice at 32 and 52 weeks (n=8), separately. **B)** Kidneys of 32 and 52-week-old *Jnk*$^{f/f}$ and *Jnk*$^{\Delta hepa}$ mice were accessed through H&E staining (Scale bars, 100μm), as well as **C)** Sirius red (SR) staining. Scale bars, 500μm.

6.6 Cell death and fibrosis progression in older *Jnk$^{\Delta hepa}$* mice

Hepatocyte death and liver fibrogenesis are hallmarks of the progression of liver disease[108]. Cell death was obviously increased as age progressed with a statistically significant difference between *Jnk$^{f/f}$* and *Jnk$^{\Delta hepa}$* mice (**Fig. 9A**). According to SR staining, these results were also in line with the progression of fibrosis in the liver with age. SR staining displayed larger multiple cysts in the liver of *Jnk$^{\Delta hepa}$* mice at 52 weeks accompanied by fibrosis (**Fig. 9B-D**).

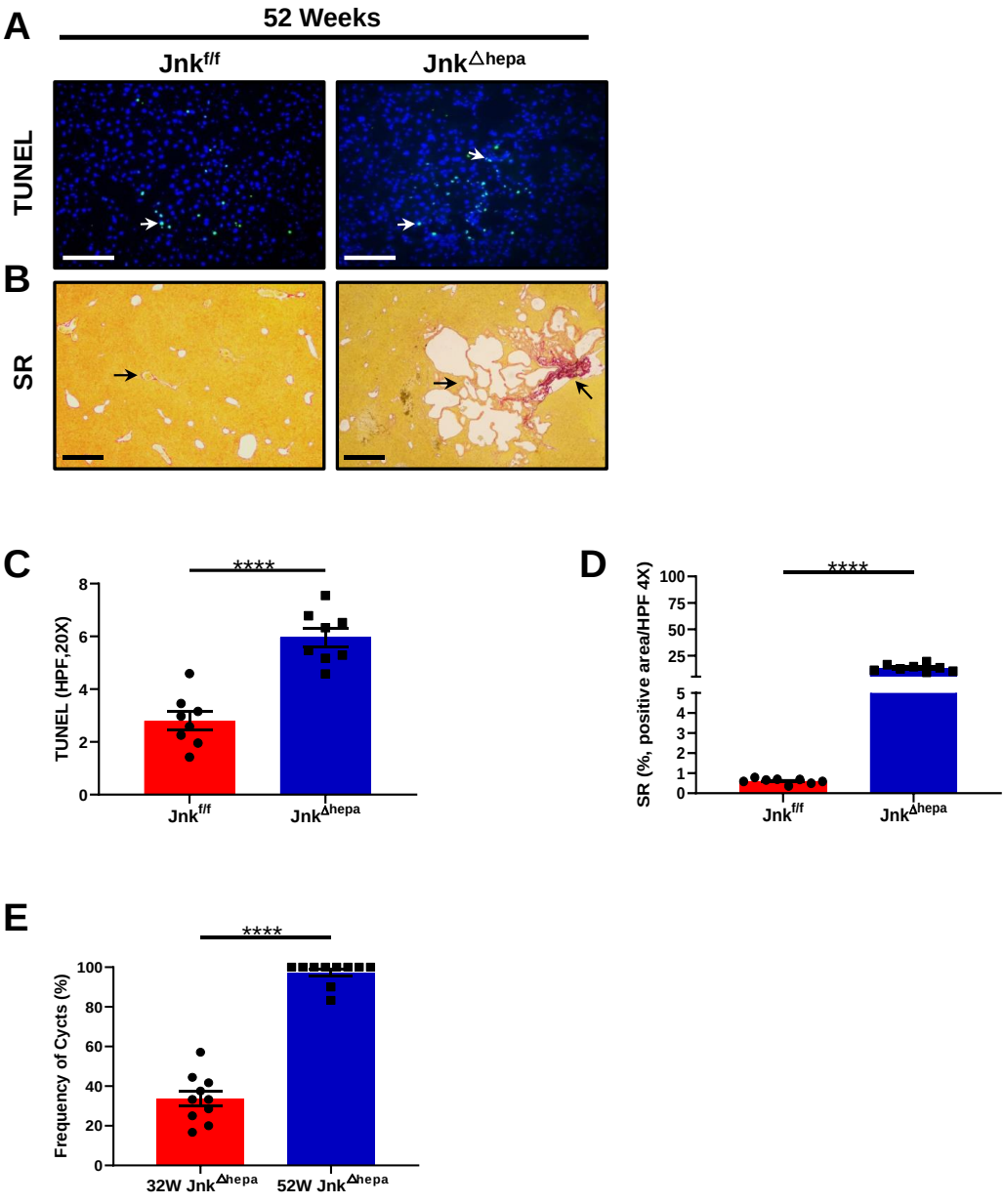

Figure 9. Cell death and liver fibrogenesis are increased in *Jnk$^{\Delta hepa}$* mice. A) Cell death was accessed via TUNEL staining in both *Jnk$^{f/f}$* and *Jnk$^{\Delta hepa}$* mice groups (n=8-10) at 32-week time point. Scale bars, 50μm. **B)** Fibrosis was also analyzed by SR staining in both *Jnk$^{f/f}$* and *Jnk$^{\Delta hepa}$* mice groups. Scale bars, 500μm. Data of **C)** TUNEL and **D)** SR staining, were represented as the mean ± SEM and graphed. **E)** The frequency of cysts was detected calculated by the photographs of H&E staining and represented as the mean ± SEM and graphed (***p <0.001; ****p <0.0001).

6.7 A pro-inflammatory environment is characteristic of disease progression in *Jnk$^{\Delta hepa}$* mice

Based on the fibrosis detected in *Jnk$^{\Delta hepa}$* mice as described above, we subsequently studied the expression of αSMA, a marker of hepatic stellate cell (HSC) activation[109], using immunoblotting. The results showed that overexpression of αSMA was significantly increased in the *Jnk$^{\Delta hepa}$* group compared to *Jnk$^{f/f}$* mice, at 32 weeks of age (**Fig. 10A**). Next, we evaluated the pro-inflammatory environment by examining the mRNA transcripts for pro-inflammatory cytokines (*Tnf-α*, *IL-6*, *Tgf-β1)* were analyzed using qRT-PCR. qRT-PCR results revealed that deletion of *Jnk1/2* in hepatocytes caused obviously upregulation of pro-inflammatory cytokines *Tnf-α and IL-6* in *Jnk$^{\Delta hepa}$* mice group compared to *Jnk$^{f/f}$* livers. *Tnf-α* was significantly increased 7-fold compared to *Jnk$^{f/f}$* mice, accompanied with increased 3-fold in *IL-6. Tgf-β1* showed increase of nearly 2-fold, while difference was not significant with expression of mRNA *pdgf-α* in *Jnk$^{\Delta hepa}$* mice (**Fig. 10B-E**). Therefore, the progression of hepatic cystogenesis is associated to a proinflammatory environment.

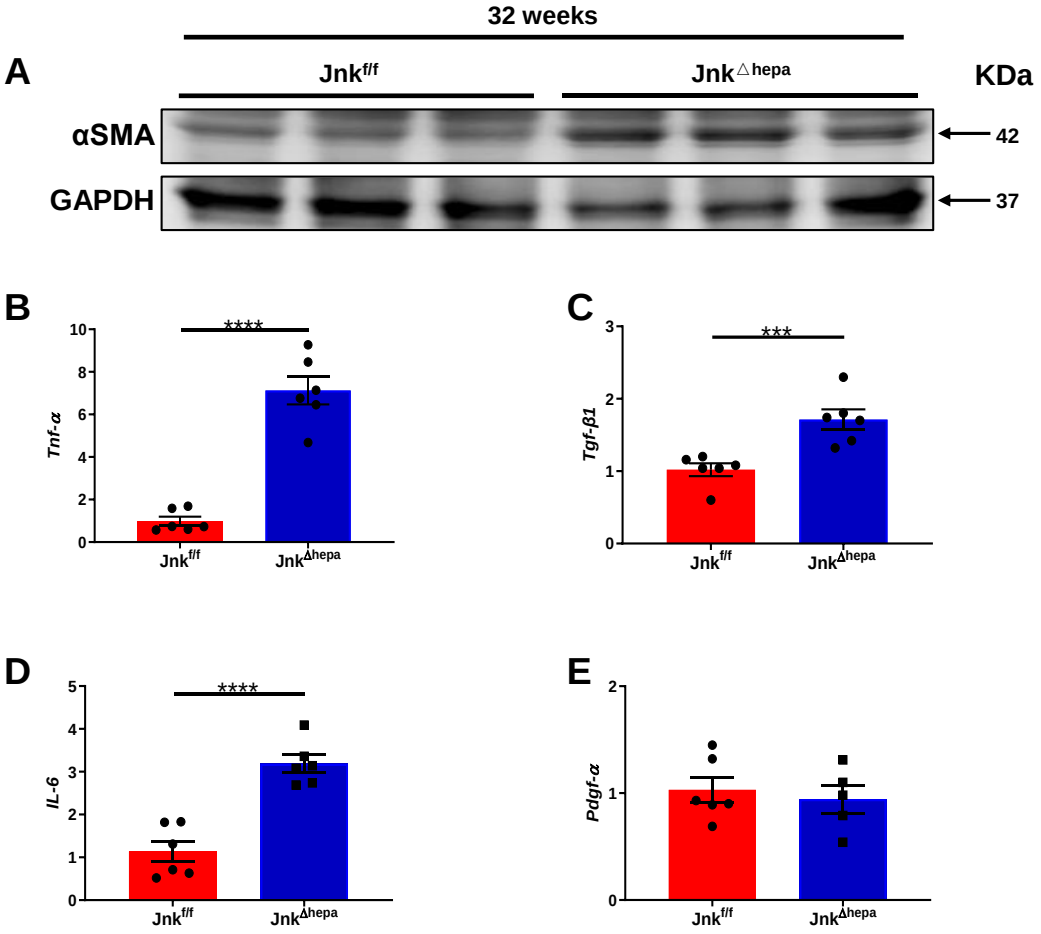

Figure 10. A proinflammatory environment favors the development of hepatic cystogenesis in *Jnk*$^{\Delta hepa}$ mice. A) Expression of protein αSMA was accessed via WB with 32-week-old *Jnk*$^{\Delta hepa}$ mice, compared to Jnk$^{f/f}$ mice. Numbers were denoted as the molecular weight (KDa) of proteins. GAPDH was used as a loading control. **B-E)** Expression of mRNA *Tnf-α, IL-6, Tgf-β1* and *pdgf-α* were accessed through qRT-PCR. The data were normalized for the amount of *Gapdh* mRNA in each sample. Data were represented as the mean ± SEM and graphed, separately. (***p <0.001; ****p <0.0001)

6.8 Hepatic oval cells are strongly activated in Jnk$^{\Delta hepa}$ livers

As presented above, we detected the multiple liver cysts were formatted coincide with ductular dilation in *Jnk*$^{\Delta hepa}$ mice with age, fibrosis was promoted as well. We hypothesized that oval cells are potentially activated and contribute to cholangiocellular hyperproliferation after deletion of *Jnk1/2* in hepatocytes.

Therefore, we examined the expression of oval cell related genes in 32-week-old mice. Oval cells are similar to fetal hepatoblasts in that they are bipotential. Therefore, biomarkers of hepatic oval cells and biliary epithelium were discriminated, such as CK19[110], SOX9[111], Notch1[112], IGF2BP3 and YAP1[113](**Fig. 11A-E**). Simultaneously, the ligand of Notch1 Jag1, as well as Hey1 which was also a downstream transcriptional target of Notch1, were also detected via qRT-PCR (**Fig. 11F-G**). Biomarkers of cholangiocytes CK19, SOX9, Notch1 were expressed via IHC staining, positive areas are obviously overexpression in $Jnk^{\Delta hepa}$ mice (**Fig. 11A**). Expression of mRNA *Ck19* were upregulated 1.85-fold which was in line with the overexpression of protein CK19 in $Jnk^{\Delta hepa}$ mice (**Fig. 11B**), while mRNA of *Notch1* was increased 1.25-fold but without statistical difference compared to $Jnk^{f/f}$ mice. Furthermore, expression of mRNA *Jag1* was upregulated to 1.58-fold. This was in line with the upregulation of the cytokine *Hey1* via qRT-PCR (2.5-fold) (**Fig. 11F-G**). Biomarker YAP1 was also associated with transdifferentiation of hepatoblasts, mRNA of *Yap1* was upregulated. However, *Igf2bp3* was decreased in $Jnk^{\Delta hepa}$ mice via qRT-PCR (**Fig. 11C-D**). All of these results suggested that loss function of JNK1/2 in hepatocytes might activate the oval cells and contribute to transdifferentiation of cholangiocytes, trigger the formation of fibrosis.

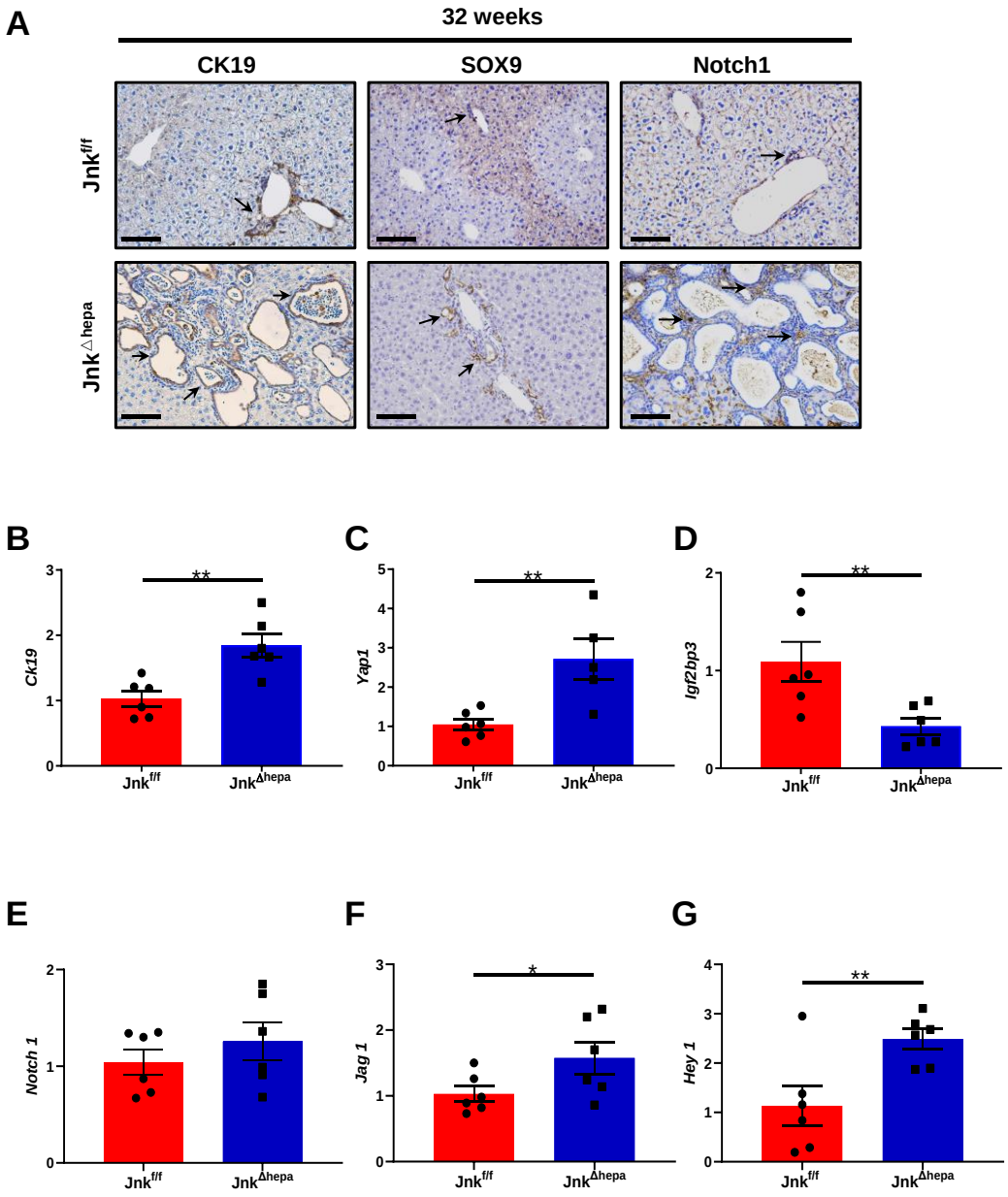

Figure 11. Biomarkers of hepatic oval cells were activated in Jnk$^{\Delta hepa}$ mice. A) Expression of CK19, SOX9 and Notch1 were accessed via IHC staining in *Jnk$^{f/f}$* (n=6) and *Jnk$^{\Delta hepa}$* (n=6) livers. Scale bars, 100µm. **B-G)** Biomarkers of oval cells and biliary epithelium, mRNA *Ck19*, *Yap1*, *Igf2bp3, Notch1, Jag1* and *Hey1* were accessed according to the results of qRT-PCR. The data were normalized for the amount of *Gapdh* mRNA in each sample. Data were represented as the mean ± SEM and graphed**,** separately (*p <0.05; **p <0.01).

6.9 Activation of ER-stress trigger cyst formation in $Jnk^{\Delta hepa}$ liver.

Furthermore, we need to know what happened to these mice which were significantly different from PCK rats[114], which is a typical PLD animal model as described before. We suspected that loss function of *Jnk1/2* in hepatocytes may activate a special signaling pathway so that trigger the formation of liver cysts when $Jnk^{\Delta hepa}$ mice grow old. According to the previous studies, hepatic cystogenesis may affect the hepatobiliary ducts by disfunction of encoded ER-resident proteins[115]. The abnormal deformation of the ER may subsequently activate the unfolded protein response signaling cascade, which consists of sensors (i.e., IRE1α, PERK and ATF6) and effector (i.e., CHOP, BiP/GRP78 and XBP1) proteins to promote protein folding, ER-associated protein degradation, and activation of pro-survival mechanisms[116, 117]. we focused on the 32-week-old mice. The investigation of ER-stress signaling pathway was detected. Overexpression of protein BiP/P62/peIF2α/Chop, and XBP1s, but not IRE1α, via WB (**Fig. 12**). The expression of these proteins showed us a new direction that ER-stress signaling pathway was activated in the formation of multiple liver cysts in $Jnk^{\Delta hepa}$ mice. These results suggested that overexpression of XBP1s showed interaction with upregulated BiP, and ER-stress may be activated after loss function of *Jnk1/2* in hepatocytes, and trigger the progression of liver cysts.

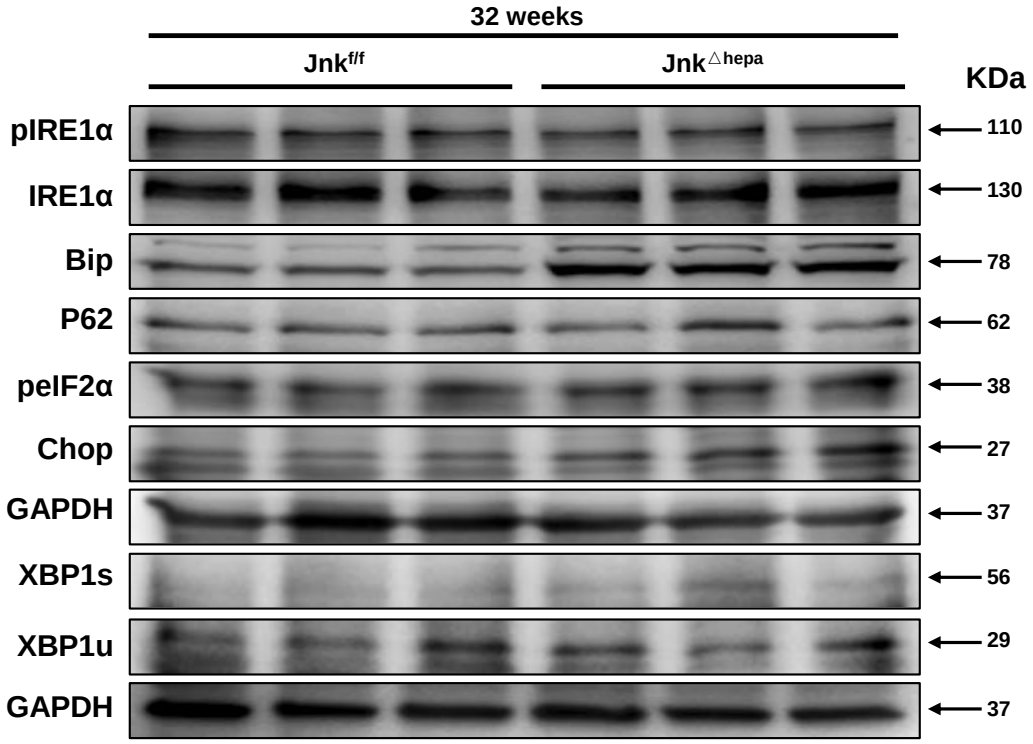

Figure 12. Activation of ER-stress associated with liver cystogenesis in Jnk$^{\Delta hepa}$ liver. Activation of ER-stress was evaluated by WB, expression of proteins BiP/P62/peIF2α/Chop, interaction with XBP1 and IRE1α, was analyzed. Numbers were denoted as the molecular weight (KDa) of proteins. GAPDH was used as a loading control.

6.10 The JNK signaling pathway is activated in HPR101 after TAA treatment

Based on the characteristic of Jnk$^{\Delta hepa}$ liver, we planned to promote the hepatic cells by external stress. Since TAA induces liver cirrhosis, and is a well-known model of induction of liver fibrosis, development of acute liver injury and liver failure[118]. In 1946, it was first declared hepatotoxic[119], and widely used for experiments both in vitro[120] and in vivo[118]. Similarly, we not only studied the profibrogenic action of TAA *in vitro* in cells, but also was challenged *in vivo* by using *Jnk$^{\Delta hepa}$* mice (The data is shown below). First our goal was to analyze *in vitro* using undifferentiated HepaRG cells (HPR 101) the mechanisms associated to biliary hyperproliferation in presence of TAA [0-40mM] for 18 h.

Cell death was increased in line with the increasing concentration of TAA according to the tests of CCK-8 as well as TUNEL staining (**Fig. 13A-B**). The median lethal dose (LD50) of TAA, approximately 36mM (36.11mM), was evaluated (**Fig. 13C**). In order to know what happened to these cells, we harvested the cells at the same time points and extracted the proteins of the cells. JNK signaling pathway was detected by WB in undifferentiated HepaRG cells ($10^5/cm^2$). Activation of pJNKs, specifically pJNK1 was observed (**Fig. 13D)**.

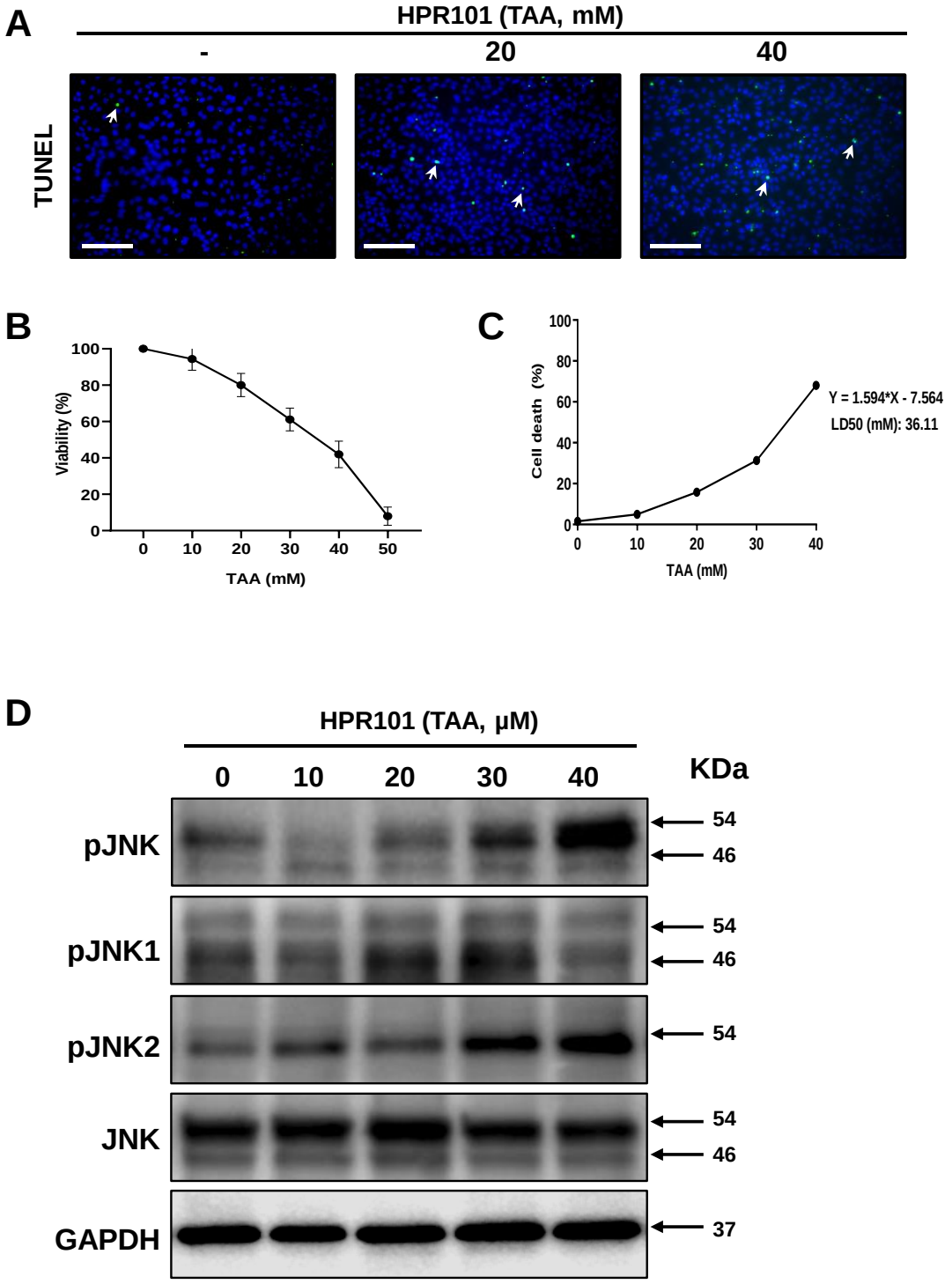

Figure 13. Cell viability and activation of the JNK in undifferentiated hepatocytes after TAA treatment. A) TUNEL staining was assessed in presence of different concentrations of TAA (0-40 mM) in HepaRG cells (HPR101). Scale bars, 50µm. **B)** The median lethal dose (LD50) and **C)** CCK-8 of cell death in TAA was assessed and calculated in HepaRG. **D)** Expression of proteins associated to MAPK8 (JNK1) and MAPK9 (JNK2) were performed using WB and GAPDH was used as a loading control in HPR101. pJNK, pJNK1/2 and JNK were assessed. Numbers were denoted as the

molecular weight (KDa) of proteins.

6.11 Activation of JNKs during hepatoblasts differentiation

Undifferentiated HepaRG cells, are hepatoblasts, normally have the ability of transdifferentiating into cholangiocytes and/or hepatocytes. We hypothesized that transdifferentiation of hepatoblasts to BECs might take place due to JNK signaling pathway. In order to inhibit JNK, the peptide inhibitor of JNK DJNKI-1 (also known as XG-102) was used in our experiment. A dose of TAA [0-40mM] was used to treat the undifferentiated HepaRG cells ($10^5/cm^2$) for 18 h, together in presence of DJNKI1 [2μM]. TUNEL staining showed that the increase in cell death was in line with the dose of TAA, but was suppressed with DJNKI1 (**Fig. 14A**). At the same time, cells were fixed with 4% PFA after the treatment, IF staining were completed with different biomarkers of transdifferentiation, such as Sex-determining region Y-box (SRY-box) containing gene 9 (SOX9) and hepatocyte nuclear factor-4α (HNF4α). SOX9 belongs to the SOX family of transcription factors[121]. HNF4α is a nuclear receptor rich in liver, which plays an important role in the early morphogenesis, fetal liver development, liver differentiation and metabolism[122]. Upregulation of SOX9 and HNF4α coincided with TUNEL staining under the treatment of TAA, but it was blocked by JNK inhibitor DJNKI1 (**Fig.14B-C**). Undifferentiated HepaRG cells, hepatoblasts, were induced to transdifferentiate into cholangiocytes via the toxicity of TAA which may be accompanied with the activation of JNK signaling pathway, but this was suppressed by JNK inhibitor. These results also suggested that inhibition of JNK signaling pathway via DJNKI1 could revert hepatoblasts transdifferentiation. Collectively, JNKs might play an important role in hepatic cell fatal of transdifferentiation.

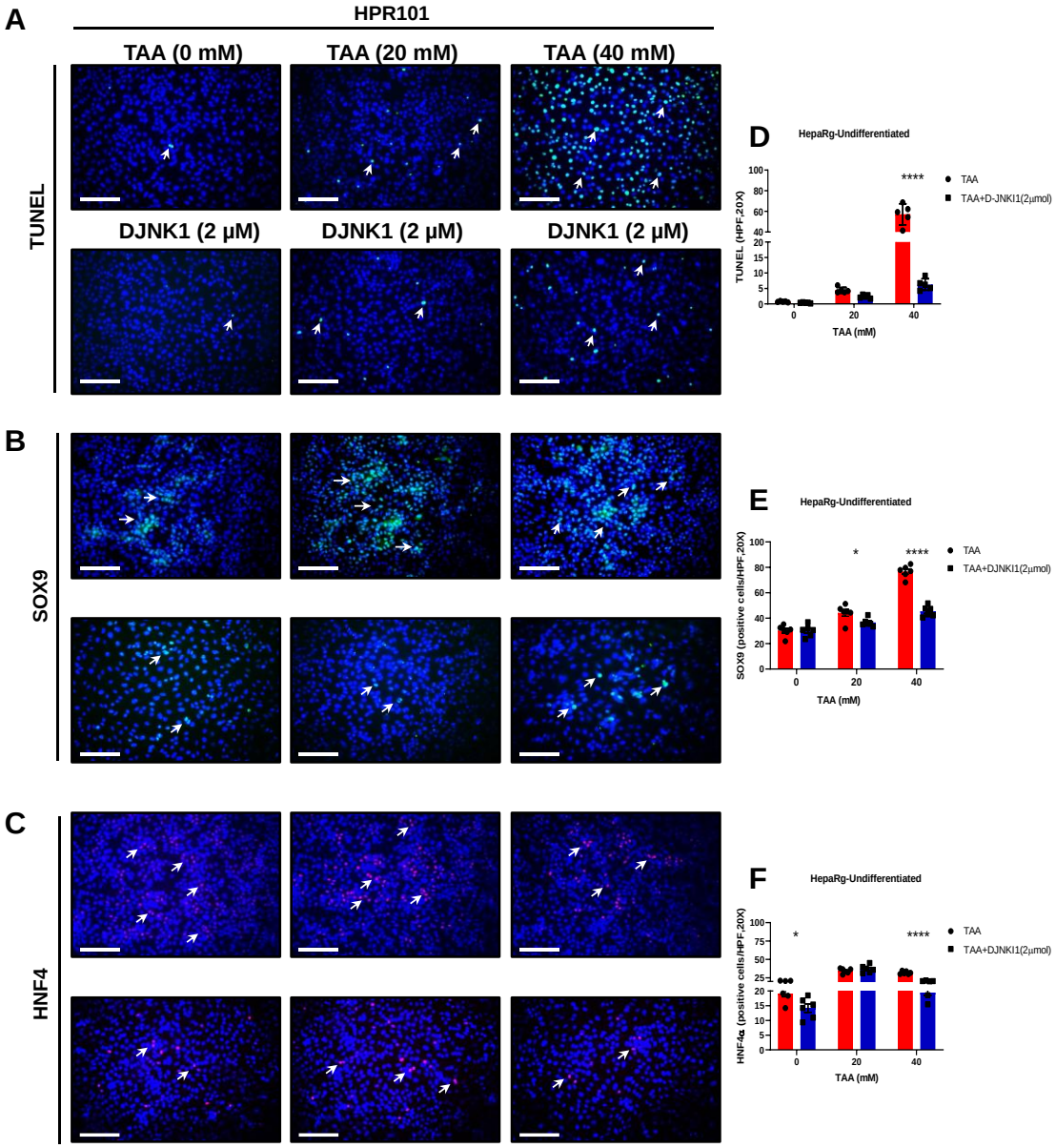

Figure 14. Transdifferentiation of hepatoblasts induced by the treatment of TAA was suppressed by JNK inhibitor, DJNKI1. A) TUNEL staining was shown the cell death of hepatoblasts under the treatment of TAA with or without JNK inhibitor DJNKI1. Representative IF staining for SOX9 and HNF4α was assessed. **B-C)** Expression of SOX9 and HNF4α upregulated after TAA treatment, but inhibited by JNK inhibitor, DJNKI1. Scale bars, 50μm. **D-F)** Positive cells of TUNEL, SOX9 and HNF4α were calculated, data were represented as the mean ± SEM and graphed (*p <0.05; ****p <0.0001).

6.12 Understanding fibrogenesis in Jnk$^{\Delta hepa}$ using TAA

Combined the study in vitro by using HPR101 cells, we also use TAA to treat

the mice. As discussed above, loss function of Jnk1/2 in hepatocytes gradually triggers the formation of biliary hamartomas in the liver, a condition known to be a precedent for the development of cholangiocarcinoma (CCA)[60]. TAA is a toxic drug that promotes the development of fibrosis and liver cancer as previously published[123]. Eight-week-old *Jnk*$^{f/f}$ and *Jnk*$^{\Delta hepa}$ mice were fed with a fixed concentration of TAA (300 mg/L) in the drinking water. All mice were sacrificed 24 weeks later, at the age of 32-week-old (**Fig. 15A**). Liver and blood were harvested, and nodules were calculated as well. Liver histology, serum parameters as well as LW/BW ratio were analyzed. LW/BW ratio was increased in TAA experimental groups compared to vehicle groups (**Fig. 15C-E**). TAA-treated *Jnk*$^{\Delta hepa}$ mice showed significant increased levels of AST, ALT, ALP, as well as LDH, compared to *Jnk*$^{f/f}$ mice (**Fig. 15F-I**). Overall, these results showed that liver injury might be worse in *Jnk*$^{\Delta hepa}$ mice, after TAA challenge.

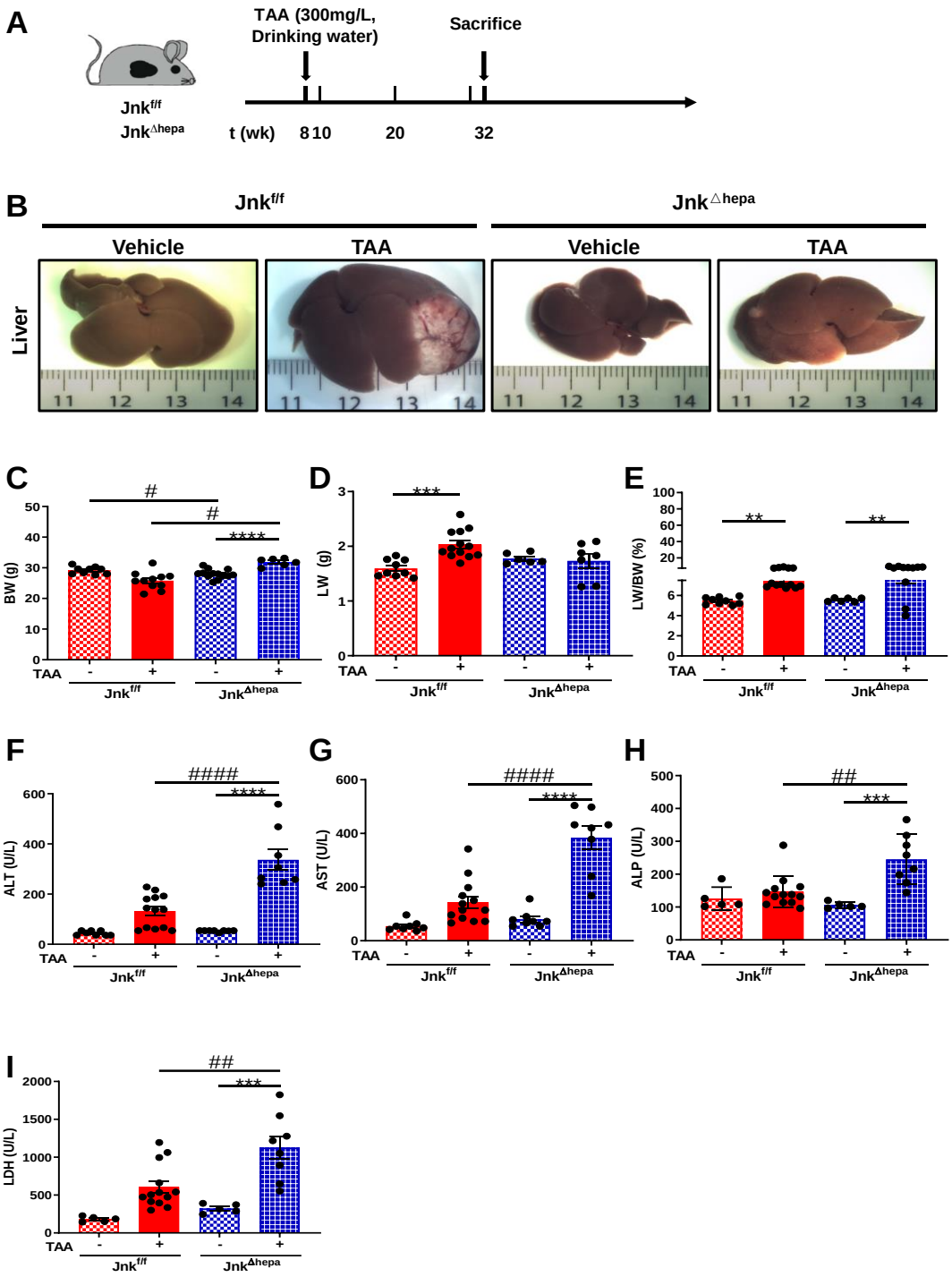

Figure 15. Markers of liver injury in Jnk$^{f/f}$ and Jnk$^{\Delta hepa}$ mice after 24 weeks of TAA. **A)** 8-week-old Jnk$^{f/f}$ and Jnk$^{\Delta hepa}$ male mice were used for the experiments with the administration of TAA in drinking water(300mg/L), Jnk$^{f/f}$ and Jnk$^{\Delta hepa}$ male mice treated as vehicle, all of the mice were sacrificed at 32-weeks (n=8-13). **B)** Phenotypes of the livers are shown. **C)** BW, **D)** LW, and **E)** LW/BW ratio of Jnk$^{f/f}$ and Jnk$^{\Delta hepa}$ mice were calculated as well as control littermates. **F-I)** Analysis of serum levels of were analyzed and graphed ALT, AST, ALP and LDH, separately. Data were represented as the mean ± SEM and graphed (#p <0.05; **/##p <0.01; ***p <0.001; ****/####p <0.0001).

6.13 Liver fibrogenesis in $Jnk^{f/f}$ and $Jnk^{\Delta hepa}$, 24 weeks after TAA

Based on cell damage presented above, we then focused on the detection of fibrosis, since TAA is a potential inducer of collagen deposit. Histologically, Sirius Red (SR) staining is used to detect the degree of fibrosis of inflammation caused by cancer, vascular or metabolic diseases[124]. It can be observed under a bright field microscope. The nucleus and the cytoplasm are shown as yellow, but collagen fibers displayed red color. Fibrosis was induced in both experiment mice group after the treatment of TAA as observed by SR staining. Compared with *Jnk$^{f/f}$* mice, *Jnk$^{\Delta hepa}$* mice developed more liver fibrosis. After treatment with TAA, SR showed a very interesting and different pattern of SR staining in livers of *Jnk$^{f/f}$* and *Jnk$^{\Delta hepa}$* mice. Whilst TAA-induced bridging fibrosis in $Jnk^{f/f}$ livers, the hepatic parenchyma of $Jnk^{\Delta hepa}$ livers displayed peribiliary-like fibrosis (**Fig. 16A**). The positive areas of SR were calculated and graphed, accordingly **(Fig. 16D)**. Simultaneously, αSMA, a marker of hepatic stellate cells (HSCs) activation[109], was detected via IHC and IF staining (**Fig. 16B-C**). Overexpression of αSMA was also detected via WB which was in line with IHC and IF staining (**Fig. 16E**). Compared with *Jnk$^{f/f}$* mice, activated fibrotic response area was upregulated in *Jnk$^{\Delta hepa}$* mice. This phenomenon was more significantly in both $Jnk^{f/f}$ and $Jnk^{\Delta hepa}$ livers after the treatment of TAA. While, TAA $Jnk^{\Delta hepa}$ liver showed especially significantly positive areas around biliary ducts compared with TAA-induced *Jnk$^{f/f}$* mice (**Fig. 16B-D**). These results suggest that loss function of *Jnk1/2* in hepatocytes promoted biliary tract proliferation and exacerbated liver fibrosis.

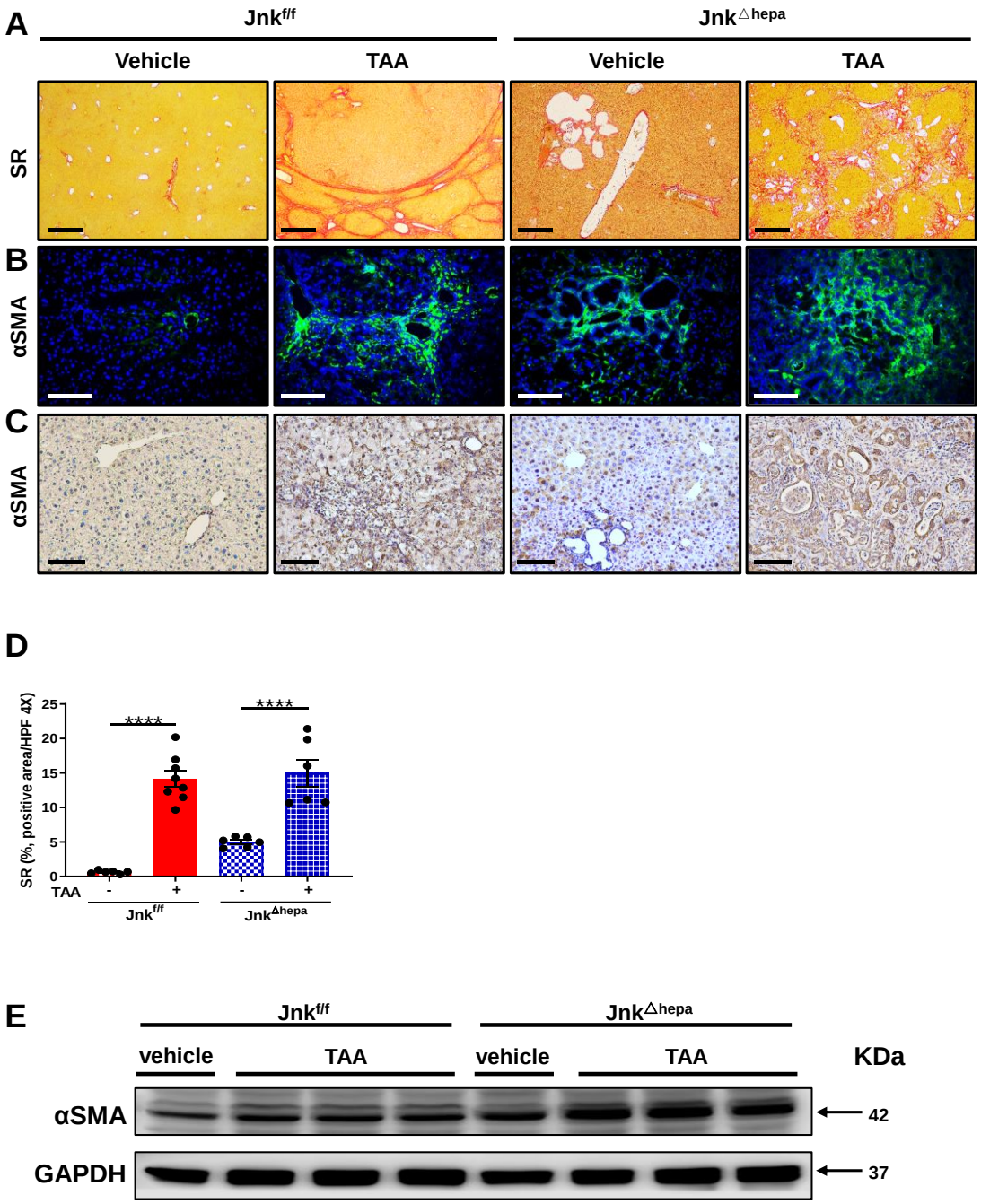

Figure 16. TAA induces significantly higher liver fibrogenesis in mice with *Jnk1/2* in hepatocytes. A) Representative Sirius Red staining of paraffin sections from the indicated livers after the treatment of TAA as well as vehicle group mice (n=6-8). Scale bars, 500μm. **B)** Expression of αSMA was accessed via IHC staining. Scale bars, 100μm. **C)** αSMA was detected by IF staining at the same time. Scale bars, 50μm. **D)** Positive area of fibrosis was calculated by ImageJ with photographs of SR staining, data were represented as the mean ± SEM and graphed (****p <0.0001). **E)** Expression of protein αSMA was also detected via WB. Numbers were denoted as the molecular weight (KDa) of proteins. GAPDH served as loading control.

6.14 Inflammation in Jnk$^{f/f}$ and Jnk$^{\Delta hepa}$ mice challenged with TAA

Based on the results we described above, such as cell death and fibrosis, we next detected inflammation in mice after the treatment with TAA. One biomarker of pro-inflammatory cytokines *Tnf-α,* as well as regulator of inflammatory processes *Tgf-β1* were detected via qRT-PCR. After the treatment of TAA, expression of mRNA *Tnf-α* was increased 7.1-fold in Jnk$^{\Delta hepa}$ liver, and obviously upregulated 10.4-fold in Jnk$^{f/f}$ liver. Compared with *Jnk$^{\Delta hepa}$* mice, mRNA *Tnf-α* expression increased only 3.4-fold in *Jnk$^{\Delta hepa}$* mice (**Fig. 17A**). However, mRNA *Tgf-β1* expression was significantly increased 3.6-fold in *Jnk$^{\Delta hepa}$* mice after treated by TAA, but only 1.6-fold in Jnk$^{f/f}$ liver (**Fig. 17B**). These results suggested that TAA induces a strong proinflammatory milieu in *Jnk$^{\Delta hepa}$* mice.

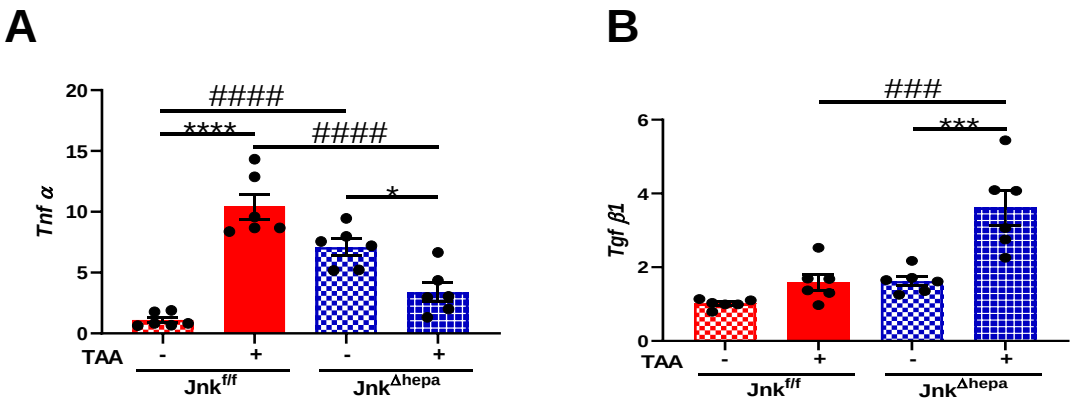

Figure 17. Inflammation was involved in Jnk$^{\Delta hepa}$ mice under the treatment of TAA. Expression of mRNA **A)** *Tnf-α* expression was accessed via qRT-PCR as well as **B)** *Tgf-β1* (n=6). Data were represented as the mean ± SEM and graphed (*p <0.05; ***/###p <0.001; ****/####p <0.0001).

6.15 Hepatocellular damage in Jnk$^{\Delta hepa}$ and Jnk$^{f/f}$ mice, after 24 weeks

TUNEL staining was first performed to detect cell death including necrosis,

apoptosis and necroptosis[125] in each group, photographs were taken and data calculated (**Fig. 18A-B)**. Expectedly, cell death increased in experimental group mice compared with the vehicle group. We further explored protein expression associated with cell death by WB. We focused on the proteins associated with JNK signaling pathway-induced cell death. Overexpression of both cleaved caspase-3 (CC3) and -8 (CC8) proteins was evident in $Jnk^{\Delta hepa}$ compared with $Jnk^{f/f}$ mice after 24 weeks of TAA(**Fig.18C**). Additionally, pRIP1, pRIP3 and pMLKL were clearly induced in $Jnk^{\Delta hepa}$ compared with $Jnk^{f/f}$ mice after 24 weeks of TAA (**Fig. 18C**). These results suggested that prominent activation of necroptosis occur in $Jnk^{\Delta hepa}$ mice, 24 weeks after TAA, and contribute to the liver phenotype of these mice.

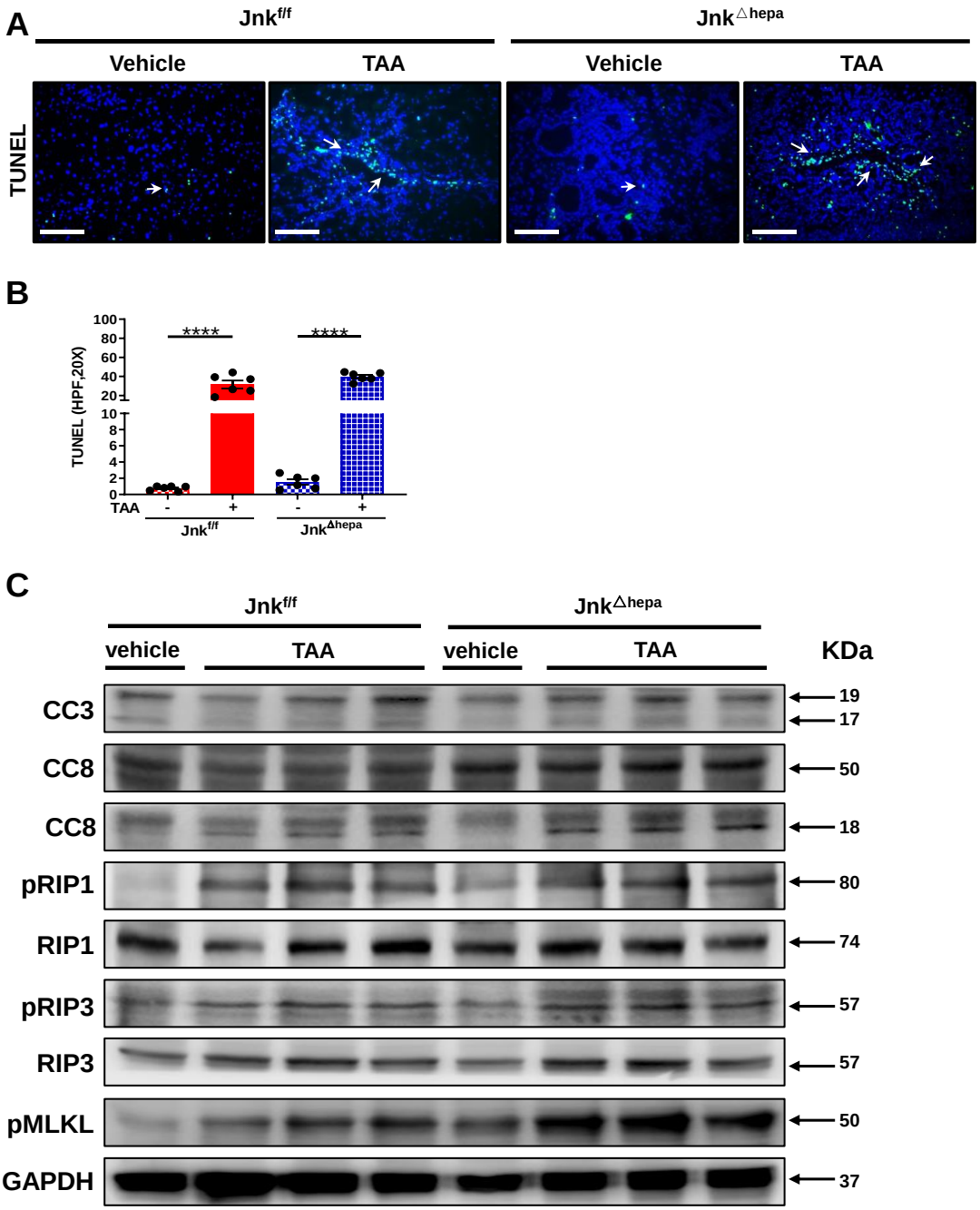

Figure 18. Hepatocellular injury in Jnk$^{f/f}$ and Jnk$^{\Delta hepa}$ mice, 24 weeks after TAA. **A)** Cell death was performed using TUNEL staining after the treatment of TAA in both Jnk$^{f/f}$ and Jnk$^{\Delta hepa}$ mice groups (n=6). Arrows (→) indicate positive cells. Scale bars, 50µm. **B)** Data were represented as the mean ± SEM and graphed (####p <0.0001). **C)** The expression of cleaved-Caspase 3 (CC3), cleaved-Caspase 8 (CC8), pRIP1/3 and pMLKL, were demonstrated via WB. Numbers were denoted as the molecular weight (KDa) of proteins. GAPDH served as loading control.

6.16 Hepatocellular proliferation in $Jnk^{f/f}$ and $Jnk^{\Delta hepa}$, 24 weeks after TAA

Compensatory proliferation is linked with increased cell death during liver injury[89, 126]. Proliferation was detected using IF and IHC staining for Ki 67 (**Fig. 19A-B**). Our data revealed that expression of positive Ki 67 cells was less than 1% in $Jnk^{f/f}$ vehicle group, but increased up to nearly 3% in $Jnk^{\Delta hepa}$ vehicle group. However, the number of positive Ki 67 cells increased compared in both *$Jnk^{f/f}$* and *$Jnk^{\Delta hepa}$* mice, after TAA treatment. We found positive Ki 67 cells increased to approximately 17.5% in TAA-treated $Jnk^{f/f}$ livers, and reached up to 20% of positive Ki 67 cells in TAA-challenged $Jnk^{\Delta hepa}$ animals. In $Jnk^{f/f}$ group, positive Ki 67 cells mainly expressed inside the nodule area by hepatocytes combined with less positive cholangiocytes, most of them maybe hepatocellular carcinoma stem cells. Statistically significant difference between vehicle group and experimental group was calculated and graphed with a p-value less than 0.0001 (**Fig. 19C**). These results suggest that *Jnk1/2* in hepatocytes promotes hepatocellular hyperproliferation in response to the liver damage by TAA.

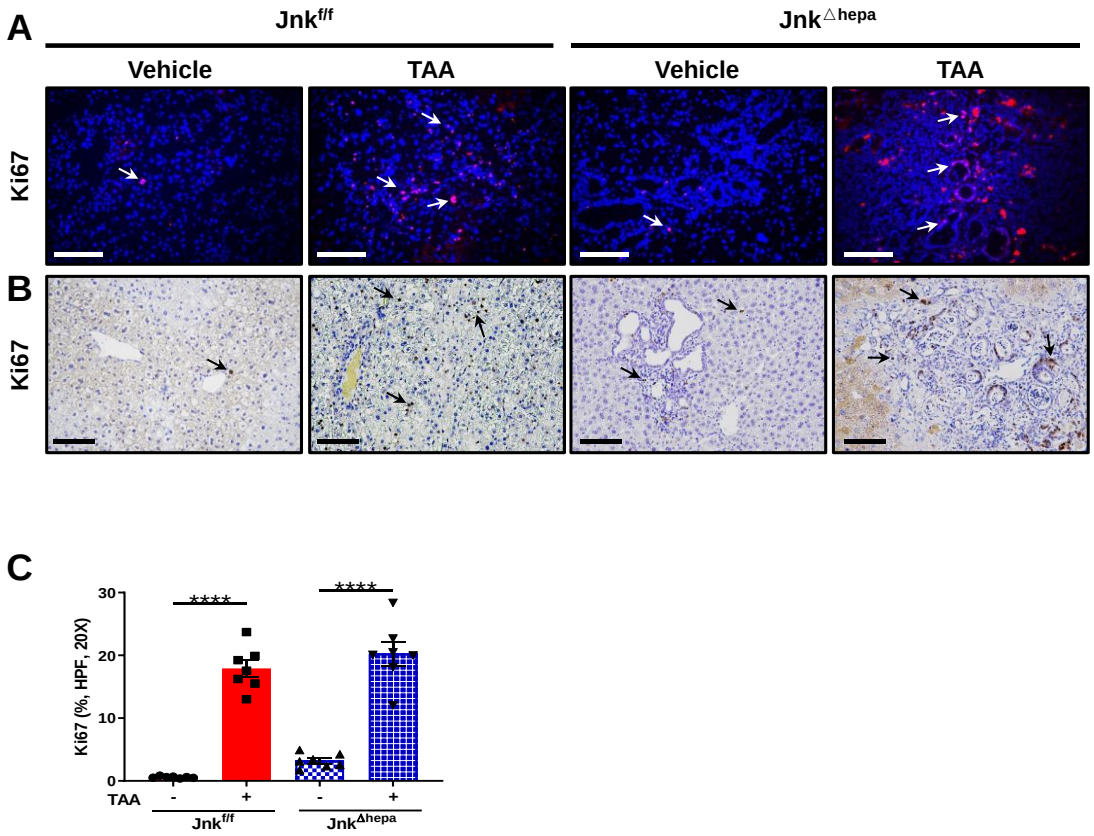

Figure 19. Hepatocellular proliferation of Jnk$^{f/f}$ and Jnk$^{\Delta hepa}$ livers, 24 weeks after TAA. A) Expression of Ki 67 was evaluated by IF staining (n=7). Scale bars, 50µm. **B)** Expression of Ki 67 was also accessed by IHC staining accompanied by expression of **C)** Positive Ki 67 cells were calculated by ImageJ. Data were represented as the mean ± SEM and graphed (****p <0.0001).

6.17 Cholangiocytes were strongly activated in Jnk$^{\Delta hepa}$ livers 24 weeks after TAA

We next investigated the cell type that was clearly differentiated between Jnk$^{f/f}$ and Jnk$^{\Delta hepa}$ livers. Typical markers of oval cells and biliary epithelium were evaluated including, CK19, SOX9, Notch1, AFP, YAP1 and MUCIN2 (**Fig. 20)**. First, CK19, SOX9, Notch1 and MUCIN2 were investigated by IHC staining. The results presented that these markers were upregulated in TAA groups, compared to vehicle groups. However, they were significantly upregulated in TAA-treated Jnk$^{\Delta hepa}$ liver compared with Jnk$^{f/f}$ livers (**Fig. 20A-D**). Expression of mRNA *Ck19* was also detected, mRNA *Ck19* was upregulated 1.9-fold in

Jnk$^{\Delta hepa}$ mice compared to 2.5-fold in TAA *Jnk*$^{f/f}$ mice, and increased more significantly 3.7-fold in TAA *Jnk*$^{\Delta hepa}$ mice, which was in line with IHC results (**Fig. 20E**). Additionally, the mRNA of *Afp* was upregulated 3.1-fold in Jnk$^{\Delta hepa}$ mice, and 2.9-fold in TAA *Jnk*$^{f/f}$ mice, while significantly upregulated 153.3-fold in TAA-treated *Jnk*$^{\Delta hepa}$ mice (**Fig. 20F**). Expression of mRNA of *Yap1* was upregulated 3.8-fold in *Jnk*$^{\Delta hepa}$ mice, and 1.2-fold in TAA *Jnk*$^{f/f}$ mice, while significantly upregulated 5.4-fold in TAA-treated *Jnk*$^{\Delta hepa}$ mice (**Fig. 20G**). At the same time, protein CK19 was analyzed by WB, and it was consistent with IHC (**Fig. 20H**). In short, biomarkers of cholangiocyte/BECs were strongly activated after treatment with TAA, and much more significantly in Jnk$^{\Delta hepa}$ liver. These results suggested that oval cell proliferation was characteristic of Jnk$^{\Delta hepa}$ liver livers, after TAA.

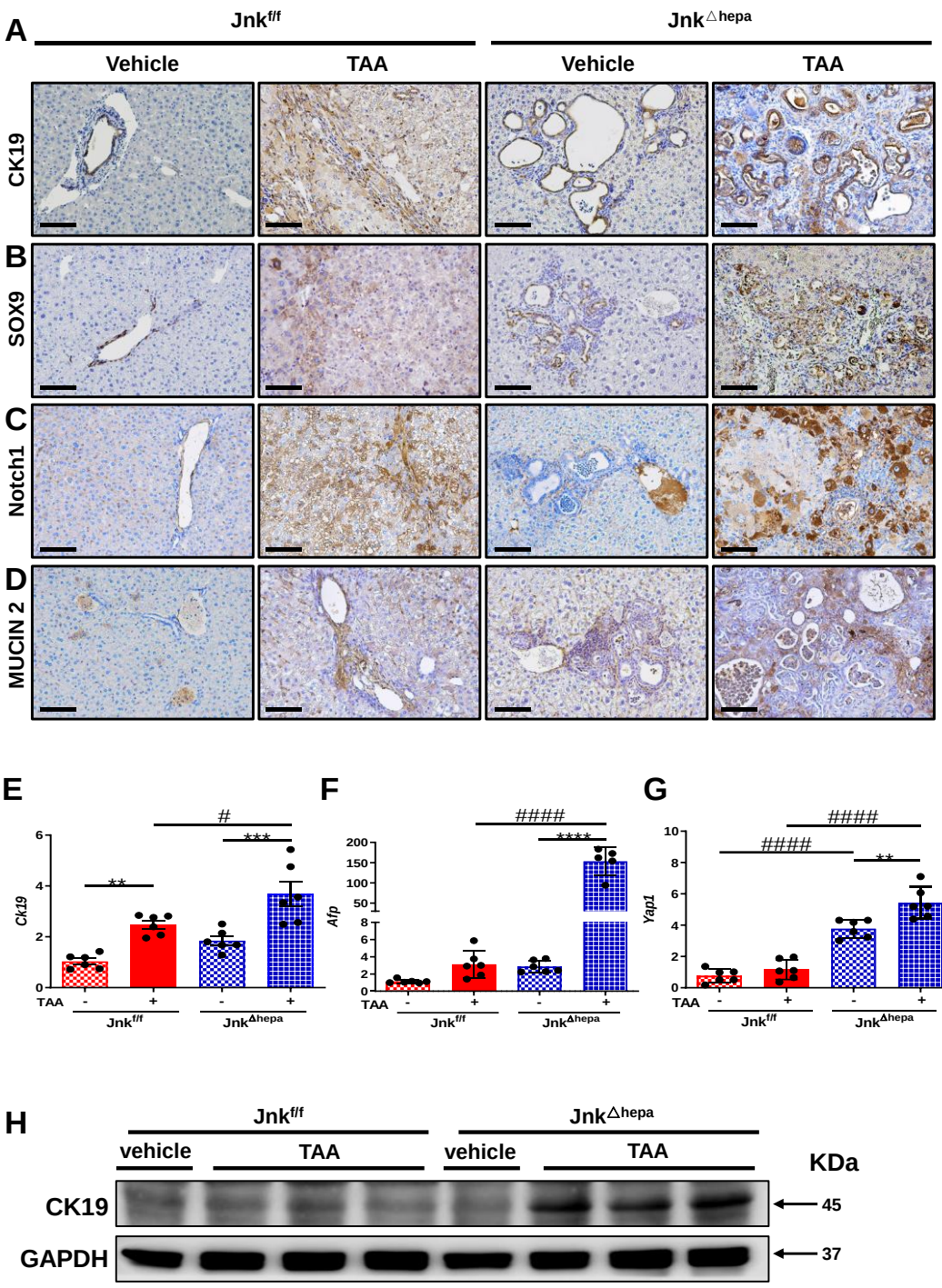

Figure 20. Cholangiocytes/BECs are activated in Jnk$^{\Delta hepa}$ liver, after TAA. A-D) Representative IHC staining for markers of cholangiocytes, CK19, SOX9, Notcch1 and MUCIN2 were evaluated. Scale bars, 100μm. **E-G)** Expression of mRNA *Ck19*, as well as *Afp* and *Yap1* were investigated by qRT-PCR (n=6) and graphed (#p <0.05; **/##p <0.01; ***p <0.001; ****/####p <0.0001). **H)** Expression of protein CK19 was accessed via WB. Numbers were denoted as the molecular weight (KDa) of proteins. GAPDH served as loading control.

6.18 Liver carcinogenesis in $Jnk^{\Delta hepa}$ vs $Jnk^{f/f}$ mice, after TAA

Histological examination of the livers by H&E staining after TAA treatment was performed in *Jnk$^{\Delta hepa}$* mice and *Jnk$^{f/f}$* mice. Whilst hepatocellular damage and an infiltration of inflammatory cells was obvious in *Jnk$^{f/f}$* mice, compared to vehicle-treated animals. Moreover, the cells in the lesion area of *Jnk$^{f/f}$* mice presented as prominent acinar pattern, small cell changes, combined with cytologic atypia under the treatment of TAA (**Fig. 21A**). However, in *Jnk$^{\Delta hepa}$* mice, nuclear of the cells in the lesion area were abnormally presented accompanied with multiple ductular dilations. At the same time, the ductular dilations and cell nuclei mitosis in the lesion area of the liver in TAA *Jnk$^{\Delta hepa}$* mice were significantly different, compared with the structural characteristics of spontaneous cystic dilatation of the ductular tracts in vehicle group (**Fig. 21A**). Additionally, periodic-acid Schiff stain (PAS) is a method used for the staining of structures containing high proportion of carbohydrate macromolecules, such as glycogen, glycoprotein, proteoglycans, and mucins in tissue[127]. It is widely believed that that HCC does not produce mucins, whereas CCA may produce glycoproteins[128], PAS staining areas are characteristic. Normally, positive routine stains for hepatocytes (PAS without diastase) as show in $Jnk^{f/f}$ vehicle group, but glycogen was rich produced combined with positive mucin in $Jnk^{f/f}$ experimental group. In the $Jnk^{\Delta hepa}$ experimental group, positive PAS stain was presented accompanied by positive mucins secreted around the hyperplastic cholangiocellular and ductular dilation (**Fig. 21B**). Collectively, these results suggested that, whilst 24 weeks of TAA treatment triggered HCC formation in $Jnk^{f/f}$ livers, malignancy of biliary hamartomas compatible with CCA was observed in animals with deletion of *Jnk1/2* in hepatocytes.

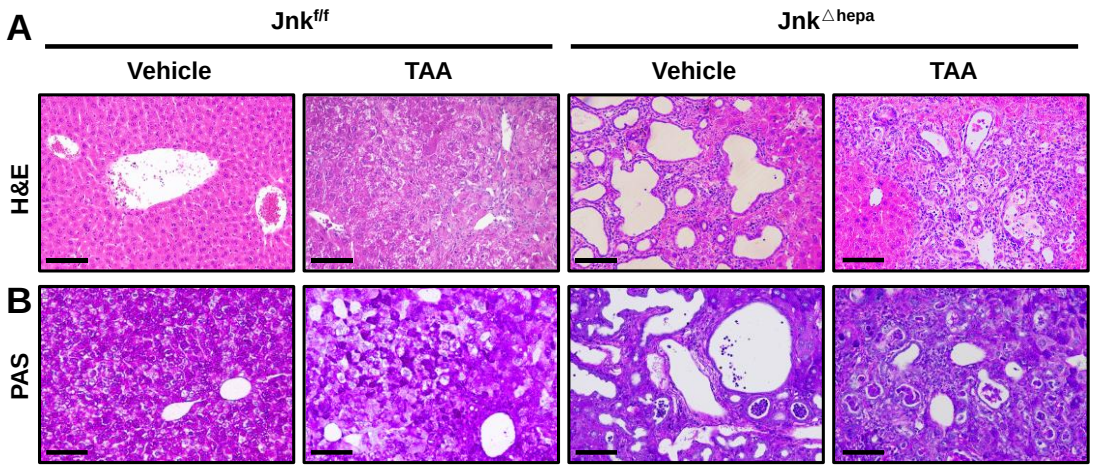

Figure 21. Liver carcinogenesis associated to TAA challenge in Jnk$^{\Delta hepa}$ animals
A) Pathology of the liver were analyzed using H&E staining in each experimental group. **B)** PAS staining was use to describe structures containing high proportion of carbohydrate macromolecules. Scale bars, 100μm.

6.19 Overexpression of c-MYC is involved in TAA-induced phenotype in *Jnk$^{\Delta hepa}$* mice

Overexpression of c-MYC might trigger tumorigenesis, especially in the formation of CCA as described recently[129]. Similarly, c-MYC is one of the most frequently mutated genes in tumors and an important regulator of cell cycle and apoptosis, its dysregulated expression could be associated with many malignancies[130]. In TAA experiment group, expression of protein c-MYC was demonstrated in IHC staining together with mRNA *c-Myc* (**Fig. 22A-B**). The expression of mRNA *c-Myc* was upregulated in TAA-treated animals compared with vehicle groups, and more significantly (5.3-fold) in *Jnk$^{\Delta hepa}$* mice (**Fig. 22B**). Simultaneously, the mRNA transcripts of Krüppel-like factor 6 (Klf6), a transcription factor involved in the regulation of several cellular processes, considered as a tumor suppressor[131]. Was significantly upregulated with an approximately 12.7-fold increase in *Jnk$^{f/f}$* mice, while exhibited an around 1.1-fold expression in *Jnk$^{\Delta hepa}$* mice (**Fig. 22C**). P21, functions as a regulator of cell cycle progression and acting as tumor suppressor[132, 133]. Expression of *p21* was increased 1.6-fold in Jnk$^{\Delta hepa}$ vehicle mice, exhibited upregulation 2.8-fold in

Jnk$^{\Delta hepa}$ experimental group. However, *p21* was strongly increased 13.7-fold in *Jnk$^{f/f}$* mice challenged with TAA (**Fig. 22D**). Therefore, deletion of *Jnk1/2* in hepatocytes promoted the formation of CCA in chronic liver injury via the activation of c-MYC. Furthermore, results of *p21* were in line with *Klf6*, indicating these two gene maybe expressed as tumor suppressors in the formation of CCA.

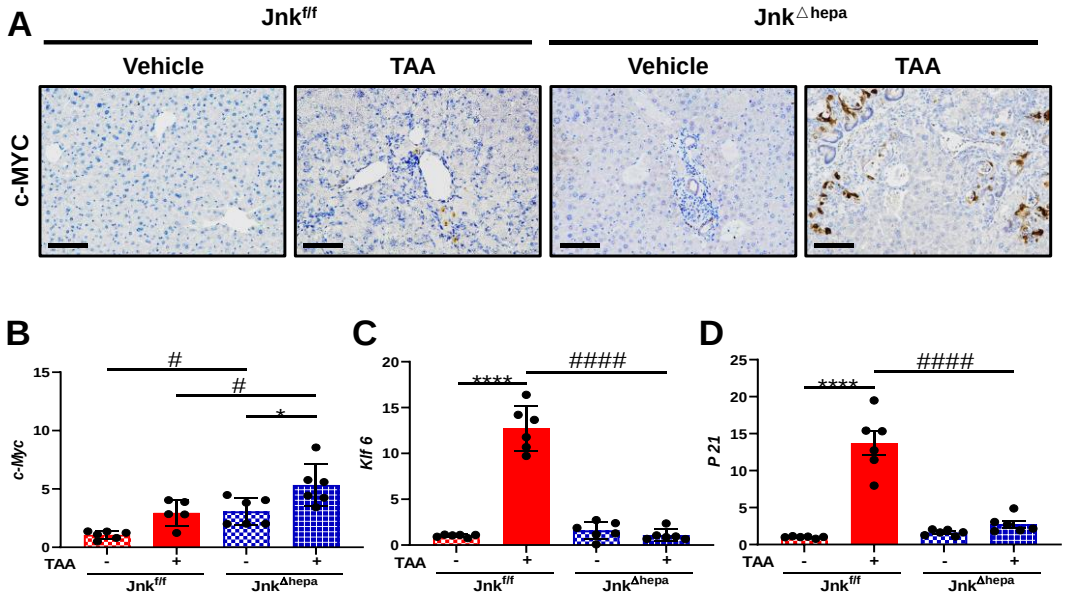

Figure 22. Overexpression of c-MYC involved in CCA. A) Representative IHC staining for c-MYC was analyzed. Scale bars, 100μm. **B)** Expression of mRNA c-*Myc* was detected by qRT-PCR, as well as **C)** *Klf6 and* **D)** p21. Data were represented as the mean ± SEM and graphed (*/#p <0.05; ****/####p <0.0001).

6.20 Liver tumorigenesis in Jnk$^{\Delta hepa}$ mice challenged with DEN/TAA

Since loss function of JNK1/2 in hepatocytes gradually triggers the progression of hepatic cystogenesis to CCA development in a model of spontaneous carcinogenesis, the NEMO mice, we next sought to understand if in a chemical model of HCC- the DEN model- in a setting of a profibrotic milieu triggered by TAA would alter the formation of liver tumorigenesis[60]. After the administration of DEN, Jnk$^{\Delta hepa}$ mice develop hepatic ducto/cystogenesis but

without hepatocarcinogenesis[60]. At the same time, deletion of *Jnk1/2* in hepatocytes contributed to peribiliary fibrosis under TAA treatment. Therefore, $Jnk^{f/f}$ and $Jnk^{\Delta hepa}$ mice were challenged with the carcinogen DEN combined with TAA. Controls were treated with vehicle. A fixed dosage of 25mg/Kg was used to treat the mice via intraperitoneal injection (IP) according to the body weight at the 14th day postpartum. Later, mice were fed with a fixed concentration of TAA (300 mg/L) from 8-week-old in drinking water, water was changed every week. All mice were sacrificed at 26 weeks, liver and blood were harvested, and number of nodules was annotated (**Fig. 23A)**. Liver morphology, combined with LW, BW, as well as LW/BW ratio were examined. Macroscopically, $Jnk^{\Delta hepa}$ livers were yellowish albeit decreased visible nodules compared with $Jnk^{f/f}$ mice after DEN/TAA treatment (**Fig. 23B, F-G**). LW was increased in both mice after the treatment of DEN/TAA, and LW of $Jnk^{f/f}$ mice was significantly increased compared with $Jnk^{\Delta hepa}$ liver, after DEN/TAA treatment. Interestingly, BW of $Jnk^{f/f}$ mice increased but significantly decreased in $Jnk^{\Delta hepa}$ mice (**Fig. 23C-E**). LW/BW ratio increased in both $Jnk^{f/f}$ and $Jnk^{\Delta hepa}$ animals. However, no statistical differences were found in the LW/BW ratio between both mice strains.

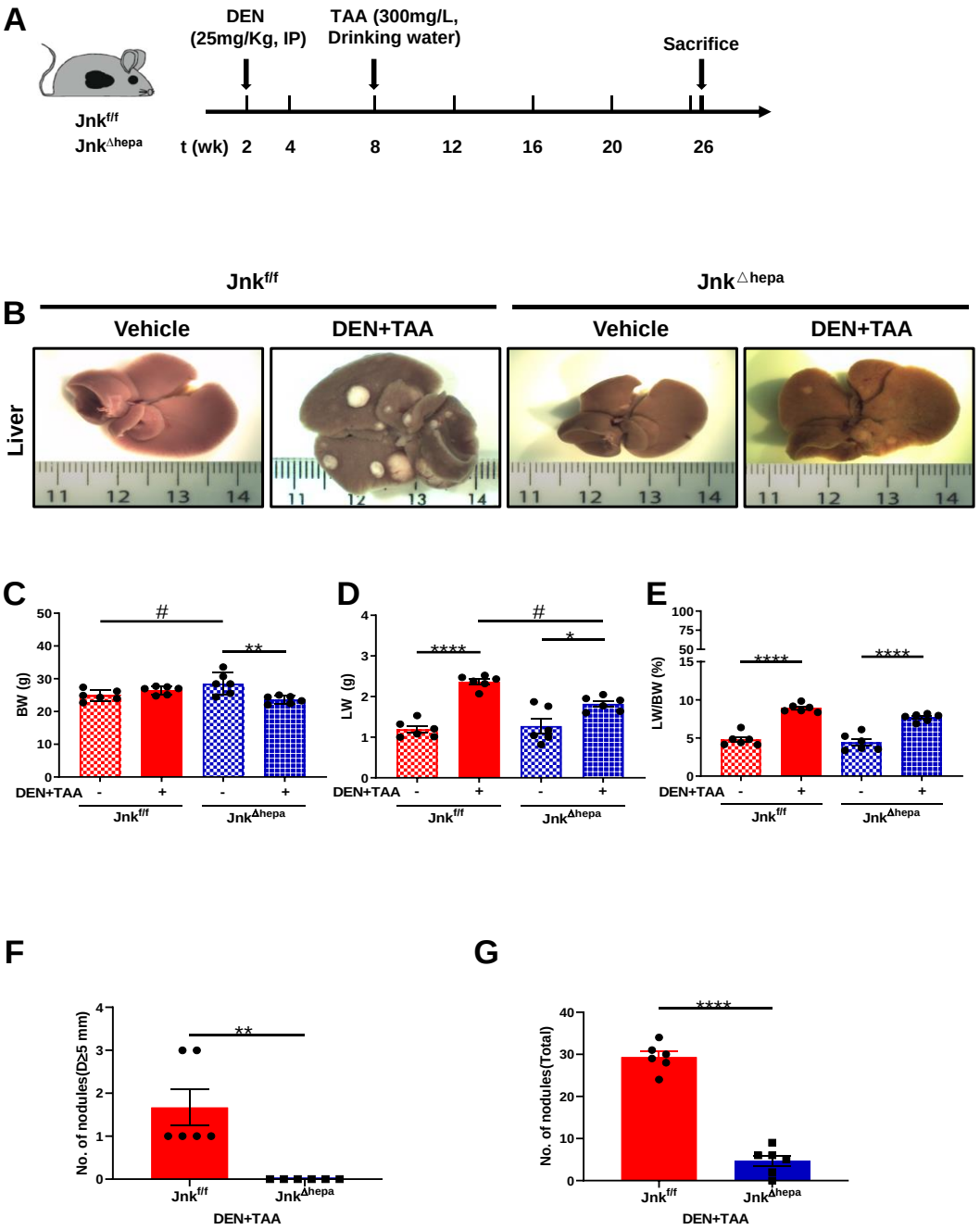

Figure 23. Liver weight and reduced tumorigenesis in Jnk$^{\Delta hepa}$ mice treated with DEN/TAA. A) Mice received a fixed dosage of 25mg/Kg via intraperitoneal injection (IP) according to the body weight at the 14th day postpartum, followed by administration of TAA in drinking water (300mg/L) since 8-week-old. Both Jnk$^{f/f}$ and Jnk$^{\Delta hepa}$ male mice treated as vehicle, all of the mice were sacrificed at 26-week-old (n=6). **B)** Phenotypes of the livers were accessed via taking photographs combined with the ruler. **C)** BW, **D)** LW, and **E)** LW/BW ratio of Jnk$^{f/f}$ and Jnk$^{\Delta hepa}$ mice were calculated as well as control littermates. **F)** Tumor burden for each individual mouse was characterized by calculating total number of visible tumors ≥ 5 mm in diameter per mouse, together with **G)** Total number of liver nodules formatted in each mouse. Data were represented as

the mean ± SEM and graphed (*/#p <0.05; **p <0.01; ****p <0.0001).

6.21 DEN/TAA promote the formation of CCA in $Jnk^{\Delta hepa}$ mice

Histological examination revealed that $Jnk^{\Delta hepa}$ mice livers exhibited small cysts formation but without any significant changes in the serological parameters compared to $Jnk^{f/f}$ vehicle group by H&E staining, the same as described earlier. After treatment with DEN/TAA, H&E staining showed that cells nuclei in the lesion area of $Jnk^{\Delta hepa}$ mice were abnormally divided, cholangioma-like structures were detected in $Jnk^{\Delta hepa}$ liver parenchyma accompanied with ductular dilation as well as strong infiltration of immune cells, which was different with TAA single treatment (**Fig. 24A**). It is widely believed that that HCC does not produce mucins, whereas CCA may produce glycoproteins[128], PAS staining areas are characteristic. PAS staining is used for detecting structures where is containing high proportion of carbohydrate macromolecules. Positive routine stain for hepatocytes (PAS without diastase) as show in $Jnk^{f/f}$ mice, but glycogen was rich produced combined with positive mucin after DEN/TAA. After treatment with DEN/TAA, positive PAS stain was observed, accompanied by positive mucins secreted around the hyperplastic cholangiocellular and ductular dilation in $Jnk^{\Delta hepa}$ livers (**Fig. 24B**). Serum markers of liver damage ALT, AST, ALP, LDH were also analyzed. Interestingly, DEN/TAA treated-$Jnk^{\Delta hepa}$ mice, manifested exacerbated levels of AST, ALT, ALP, as well as LDH, compared to $Jnk^{f/f}$ mice after the treatment of DEN/TAA (**Fig. 24C-F**). These results suggested that loss function of Jnk1/2 in hepatocytes is sensitive to DEN/TAA-induced liver damage.

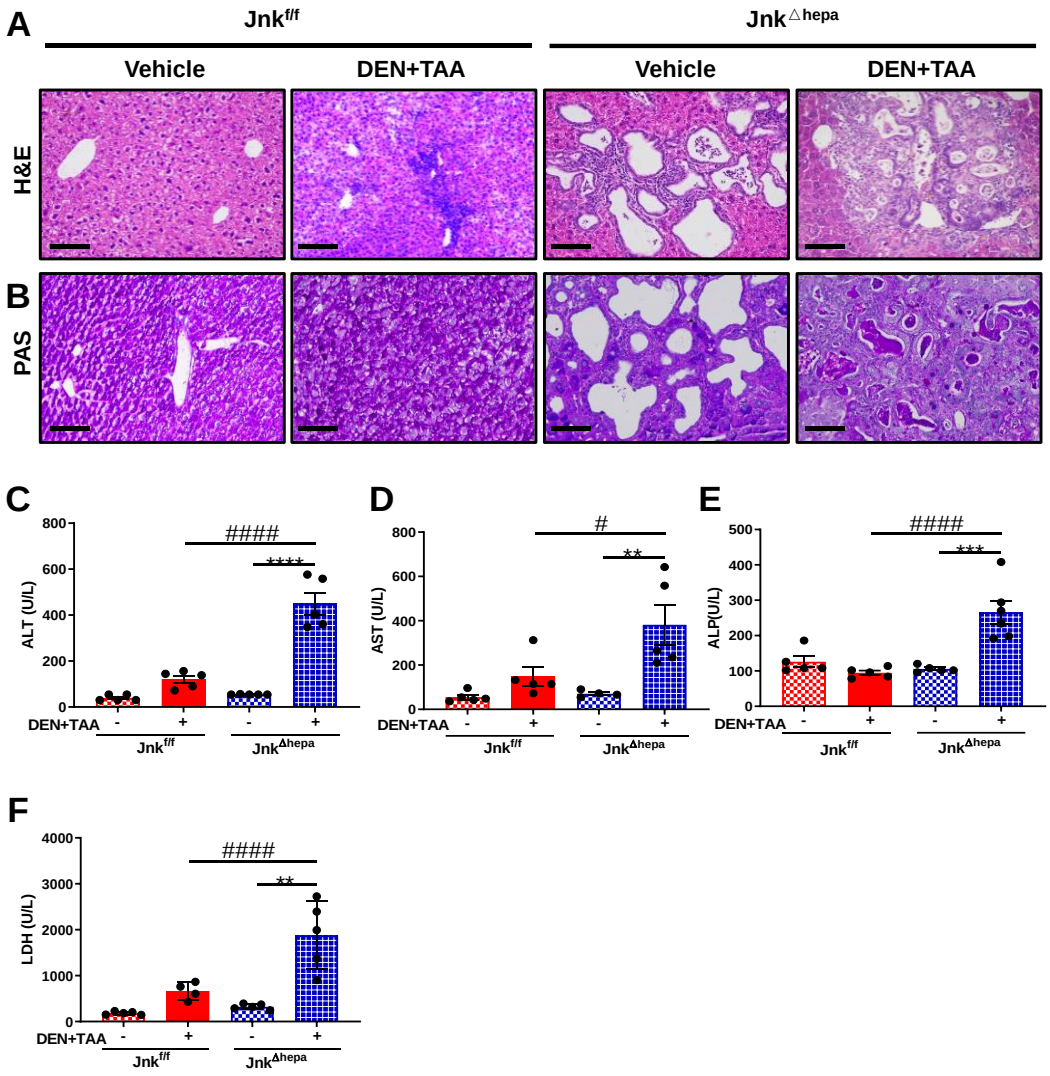

Figure 24. DEN/TAA exacerbate liver damage in *Jnk$^{\Delta hepa}$* mice. A) Pathology of the livers was evaluated using H&E staining. Scale bars, 100μm. **B**) PAS staining was presented, positive PAS stain was presented after diastase predigestion, accompanied by positive mucins secreted around the hyperplastic cholangiocellular and ductular dilation in Jnk$^{\Delta hepa}$ liver. Scale bars, 100μm**. C-F)** Serum levels of AST, ALT, ALP and LDH were from 26-week-old mice. Data were represented as the mean ± SEM and graphed. (#p <0.05; **p <0.01; ***p <0.001; ****/####p <0.0001).

6.22 Modes of cell death due to DEN/TAA related liver damage in Jnk$^{\Delta hepa}$ mice

TUNEL staining was accessed to detect cell death in each group including necrosis, apoptosis and necroptosis, photographs were taken and results were

calculated by ImageJ (**Fig. 25A-B**). Simultaneously, Caspase-independent apoptotic proteins, including CC3 and CC8, were detected via WB. Overexpression of both CC3 and CC8 occurred both in $Jnk^{f/f}$ and $Jnk^{\Delta hepa}$ mice, suggesting that apoptosis occurred after DEN/TAA treatment. Therefore, we next examined necrosis-associated proteins, including pRIP1/RIP1, pRIP3/RIP3, and pMLKL. Interestingly, increased protein expression of pRIP1/pRIP3/pMLKL was demonstrated in $Jnk^{\Delta hepa}$ group, compared to $Jnk^{f/f}$ mice after DEN/TAA treatment (**Fig. 25C)**. These results suggested that *Jnk1/2* in hepatocytes protect from DEN/TAA-induced necroptosis.

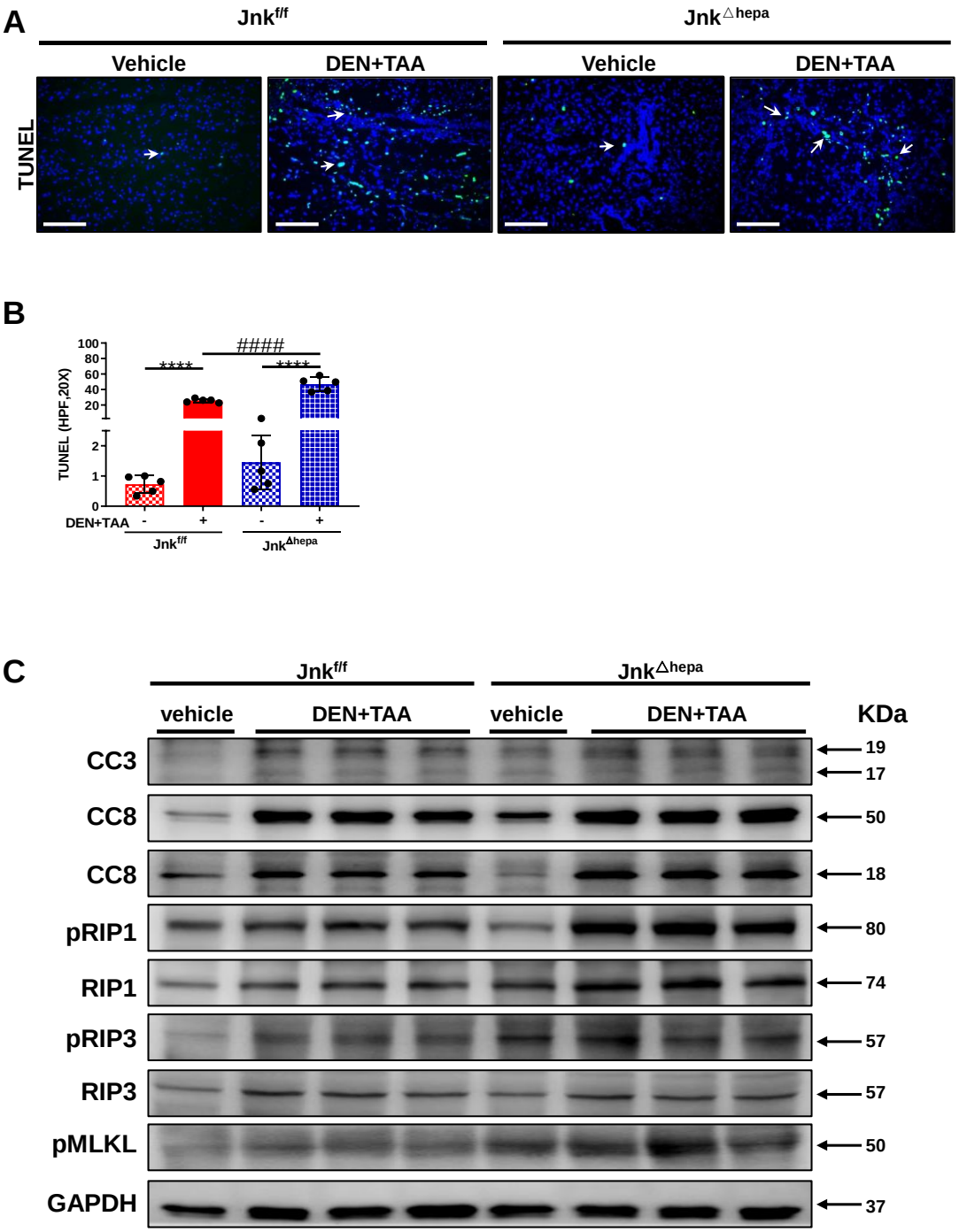

Figure 25. Necroptosis is induced in Jnk$^{\Delta hepa}$ mice after DEN/TAA treatment. A) Cell death was accessed via TUNEL staining after the treatment of DEN/TAA in both Jnk$^{f/f}$ and Jnk$^{\Delta hepa}$ mice groups (n=6). **B)** Data were represented as the mean ± SEM and graphed (****/####p <0.0001). **C)** Biomarkers of apoptosis proteins cleaved-Caspase 3 (CC3) and cleaved-Caspase 8 (CC8) were analyzed, combined with biomarkers of necroptosis pRIP1/RIP1, pRIP3/RIP3, and pMLKL, that were demonstrated via WB. Numbers were denoted as the molecular weight (KDa) of proteins. GAPDH served as loading control.

6.23 Compensatory proliferation in $Jnk^{f/f}$ and $Jnk^{\Delta hepa}$ mice after DEN/TAA

Markers of proliferation were evaluated by IHC staining. Ki 67 was evaluated by IF and IHC staining, and statistical analysis of the Ki 67 was represented and graphed (**Fig. 26A-B**). Data showed that expression of positive Ki 67 cells, was less than 3% in $Jnk^{f/f}$ vehicle group, but increased up to nearly 3% in $Jnk^{\Delta hepa}$ vehicle group. However, after DEN/TAA treatment, positive Ki 67 cells increased to approximately 25% in $Jnk^{f/f}$ liver, and nearly 50% positive Ki 67 cells were detected in $Jnk^{\Delta hepa}$ liver (**Fig. 26C**). In $Jnk^{f/f}$ group, positive Ki 67 cells mainly expressed inside the nodule area by hepatocytes combined with less positive cholangiocyte (**Fig. 26B**). Moreover, expression of protein PCNA was evaluated by WB. Overexpression of PCNA was characteristic of both $Jnk^{f/f}$ and $Jnk^{\Delta hepa}$ groups after the DEN/TAA treatment, but more pronounced in $Jnk^{\Delta hepa}$ livers (**Fig. 26G**). Furthermore, expression of mRNA *Cyclin E1* increased 2.7-fold in $Jnk^{f/f}$ mice and 4.2-fold $Jnk^{\Delta hepa}$ mice after DEN/TAA. *Cyclin A2* expression was upregulated 11.5-fold and *Cyclin D1* upregulated 4.1-fold in $Jnk^{f/f}$ liver, while mRNA *Cyclin A2* was increased 8.2-fold and *Cyclin D1* increased 2.8-fold in $Jnk^{\Delta hepa}$ mice after DEN/TAA (**Fig. 26D-F**). Specifically, compared to $Jnk^{f/f}$ mice, upregulation of mRNA *Cyclin E1* was statistically significantly in $Jnk^{\Delta hepa}$ mice (**Fig. 26D**). These results suggested that the deletion of *Jnk1/2* in hepatocytes triggers compensatory proliferation in response to DEN/TAA-induced liver damage.

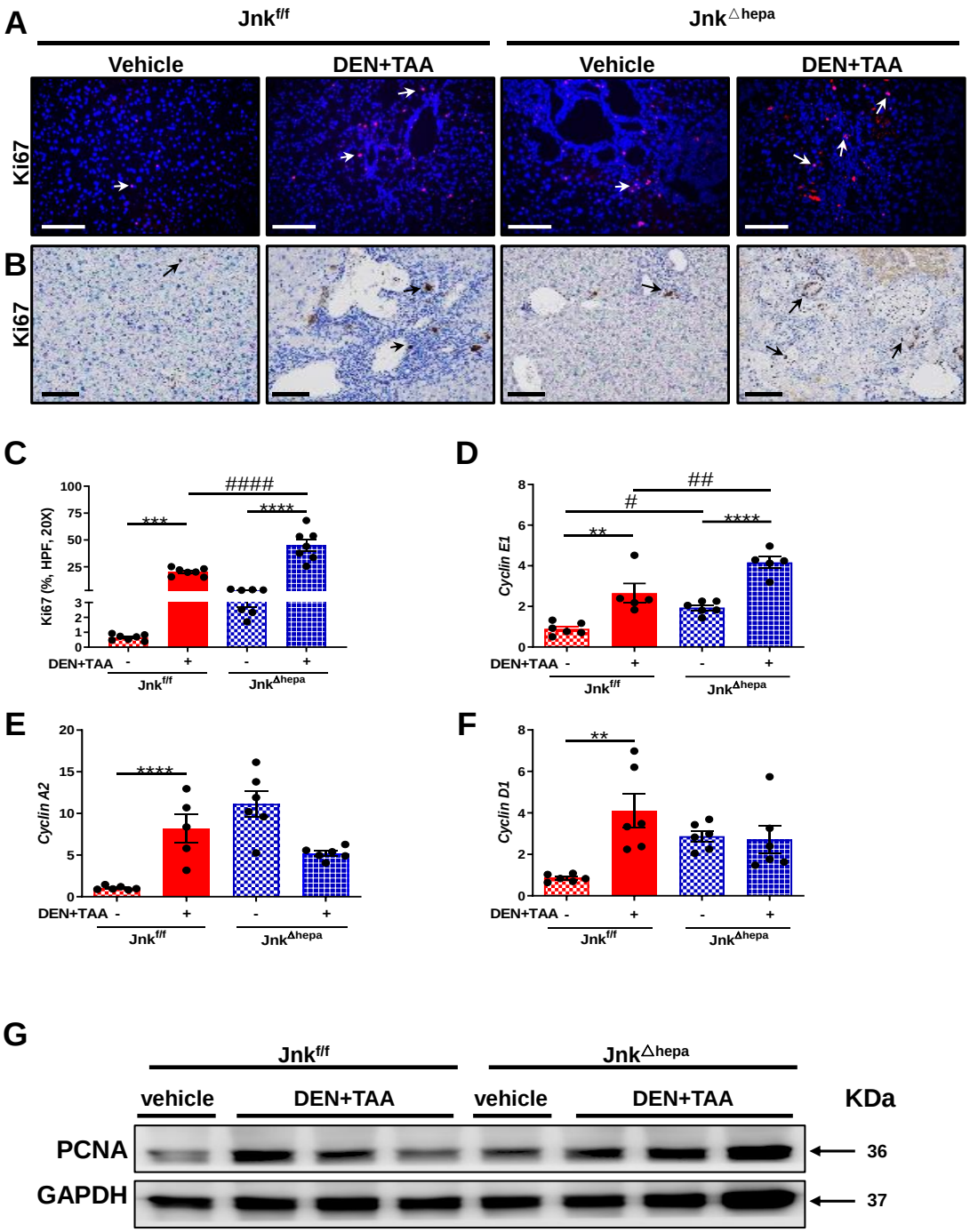

Figure 26. Proliferation after DEN/TAA treatment in Jnk$^{f/f}$ and Jnk$^{\Delta hepa}$ mice. Expression of Ki 67 was evaluated and graphed by both **A)** IF staining and **B)** IHC staining. IF: Scale bars, 50μm. IHC: Scale bars, 100μm. **C)** Data were represented as the mean ± SEM and graphed. **D-F)** Biomarkers of cell cycle mRNA *Cyclin E1, Cyclin A2, Cyclin D1,* were expressed according to the results of qRT-PCR, data were represented as the mean ± SEM and graphed (#p <0.05; **/##p <0.01; ****p <0.0001). **G)** Protein of PCNA was shown by WB as well. Numbers were denoted as the molecular weight (KDa) of proteins. GAPDH was used as a loading control.

6.24 Exacerbated fibrosis in $Jnk^{\Delta hepa}$ mice, after DEN/TAA treatment

After hyperproliferation was detected after DEN/TAA in *Jnk$^{\Delta hepa}$* mice. Then, we focused on the detection of fibrosis in each experimental group. Histologically, SR staining was used to analyze the degree of fibrosis. Simultaneously, αSMA was detected by IF and IHC staining, while expression of mRNA *αSMA* was measured by qRT-PCR (**Fig. 27)**. Significantly, fibrosis was promoted obviously in both *Jnk$^{f/f}$* and *Jnk$^{\Delta hepa}$* mice groups after the treatment of DEN/TAA according to SR staining (**Fig. 27A**). Compared to *Jnk$^{f/f}$* mice, *Jnk$^{\Delta hepa}$* mice developed significantly more liver fibrosis. The positive SR area was calculated and graphed (**Fig. 27D**). Compared with *Jnk$^{f/f}$* mice, activated fibrotic response area was upregulated in *Jnk$^{\Delta hepa}$* mice via both IF and IHC staining. After DEN/TAA, treatment, significant αSMA positive area was observed in both $Jnk^{f/f}$ and $Jnk^{\Delta hepa}$ livers, especially in $Jnk^{\Delta hepa}$ livers (**Fig. 27B-C**). Consistently, expression of mRNA *αSMA* was in line with the results of IF and IHC staining (**Fig. 27E**). These results suggested that loss function of DEN/TAA promotes liver fibrogenesis in mice with deletion of *Jnk1/2* in hepatocytes.

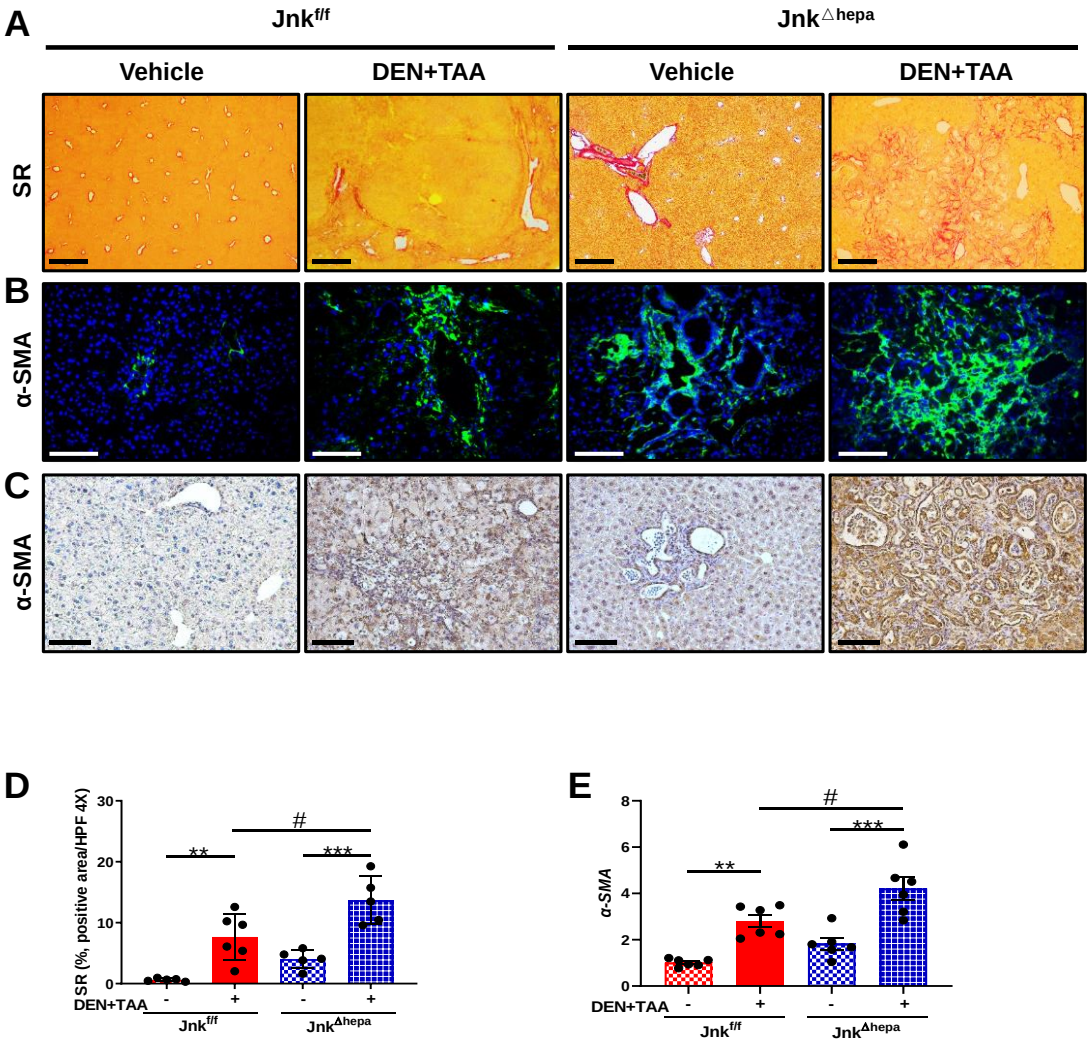

Figure 27. Deletion of *Jnk1/2* promotes fibrosis via DEN/TAA. A) Representative Sirius Red staining of paraffin sections from the indicated livers after the treatment of DEN/TAA as well as vehicle group mice. Scale bars, 500μm. **B)** Expression of αSMA was accessed via IHC staining. Scale bars, 100μm. **C)** αSMA was detected by IF staining at the same time. Scale bars, 50μm. **D)** Positive area of fibrosis was calculated by ImageJ with photographs of SR staining, data were represented as the mean ± SEM and graphed. **E)** Expression of mRNA *αSMA* was also detected via qRT-PCR (#p <0.05; **p <0.01; ***p <0.001).

6.25 Cytokine expression profile in Jnk$^{f/f}$ and Jnk$^{\Delta hepa}$ mice after DEN/TAA

After DEN/TAA, strong immune cells infiltration into the liver parenchyma in both Jnk$^{f/f}$ and Jnk$^{\Delta hepa}$ livers occurs, which correlate both with the degree of

liver damage combined with the expression of pro-inflammatory cytokines. We therefore evaluated the expression level of inflammatory cytokines, including TNFα, TGF-β, IL-6 and PDGFα by qRT-PCR (**Fig. 28A-D)**.

Tgf-β1 expression was increased 3-fold in $Jnk^{f/f}$ livers and increased 1.5-fold in $Jnk^{\Delta hepa}$ livers (**Fig. 28A**). Similarly, *Tnf-α* expression was increased 11-fold in $Jnk^{f/f}$ livers and 6.1-fold in $Jnk^{\Delta hepa}$ livers (**Fig. 28B**). *IL-6* expression was increased 6.4-fold in $Jnk^{f/f}$ livers and 1.6-fold in $Jnk^{\Delta hepa}$ livers after the treatment of DEN/TAA (**Fig. 28D**). Furthermore, compared to $Jnk^{f/f}$ livers, expressions of mRNA *Tgf-β1, Tnf-α,* and *IL-6* were significantly decreased in $Jnk^{\Delta hepa}$ livers. Interestingly, compared to $Jnk^{f/f}$ livers, mRNA expression of *pdgfα* was strongly increased in $Jnk^{\Delta hepa}$ livers, but no statistical difference was found (**Fig. 28C**).

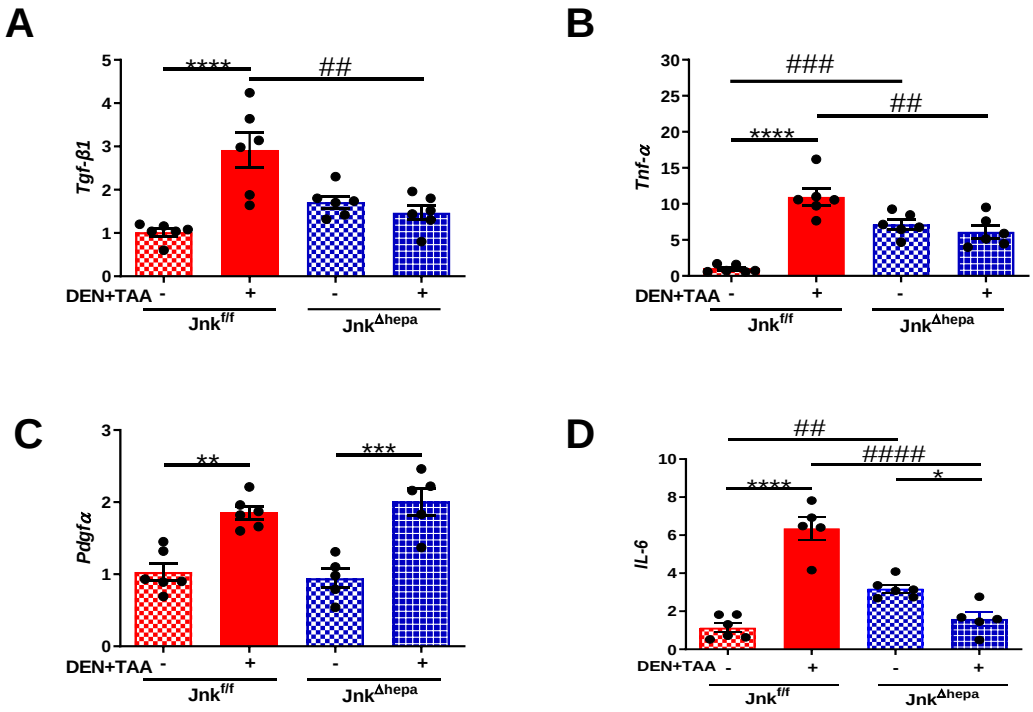

Figure 28. Expression of proinflammatory cytokines in *Jnk$^{\Delta hepa}$* mice after DEN/TAA. After DEN/TAA treatment, 26-week-old mice were sacrificed and analyzed for markers of inflammation. **A-D)** Total mRNA was isolated from the indicated livers, and the mRNA expression levels of *Tgf-β1*, *Tnf-α*, *pdgfα* and *IL-6* were examined by qRT-PCR (n=6). Date were represented as the mean ± SEM and graphed (*p <0.05; **/##p <0.01; ***p <0.001; ****/####p <0.0001).

6.26 Markers of biliary epithelial cells are strongly activated in $Jnk^{\Delta hepa}$ livers, after DEN/TAA

We next investigated markers of cholangiocytes. Typical markers of cholangiocytes or oval cells were detected, including CK19, SOX9, YAP1, MUC1, MUCIN2 and CD133, accompanied with expression of cholangiocarcinoma/tumor-enriched marker such as Dmbt1[134]. First, CK19, SOX9 and MUCIN2 were detected via IHC staining, which showed upregulation around the areas of ductogenesis or oval cell reaction triggered by DEN/TAA compared to vehicle groups. CK19, SOX9 and MUCIN2 were significantly upregulated in $Jnk^{\Delta hepa}$ compared with $Jnk^{f/f}$ livers (**Fig. 29A-C**). Expression of mRNA *Ck19* was upregulated 2-fold in $Jnk^{\Delta hepa}$ mice compared to $Jnk^{f/f}$ mice. After DEN/TAA treatment, mRNA *Ck19* was increased 2.5-fold in $Jnk^{f/f}$ mice and was significantly upregulated 4-fold in $Jnk^{\Delta hepa}$ mice, in line with expression of CK19 in IHC and WB (**Fig. 29D, J**). Additionally, expression of mRNA *Yap1* was upregulated 2-fold in $Jnk^{\Delta hepa}$ mice, compared to $Jnk^{f/f}$ mice. After DEN/TAA, *Yap1* expression increased 4-fold in $Jnk^{f/f}$ mice, while it was significantly upregulated 5.9-fold in $Jnk^{\Delta hepa}$ mice (**Fig. 29E**). Typical biomarkers of cholangiocyte/BECs and cholangiocarcinoma/tumor-enriched were evaluated by qRT-PCR, such as CD133, MUC1, ErbB2 and Dmbt1. Interestingly, after treatment with DEN/TAA, expression of these four markers, was strongly upregulated in $Jnk^{\Delta hepa}$ mice compared to vehicle group, *CD133* expression increased 5.3-fold, *MUC1* increased 35.2-fold, *ErbB2* increased 152.2-fold, *Dmbt1* increased 160-fold, separately (**Fig. 29F-I**). These results suggested that oval cells or Cholangiocyte/BECs were significantly activated in $Jnk^{\Delta hepa}$ mice after DEN/TAA treatment. Overexpression of cholangiocyte markers including CK19, YAP1, MUC1, MUCIN2 as well as CD133, accompanied with expression of cholangiocarcinoma/tumor-enriched marker Dmbt1 and ErbB2, together with the accumulation of SOX-9 positive cells in $Jnk^{\Delta hepa}$ liver after

challenged with DEN/TAA, suggested that DEN/TAA might induce mesenchymal epithelial transition in mice with hepatocyte-specific deletion of *Jnk1/2*.

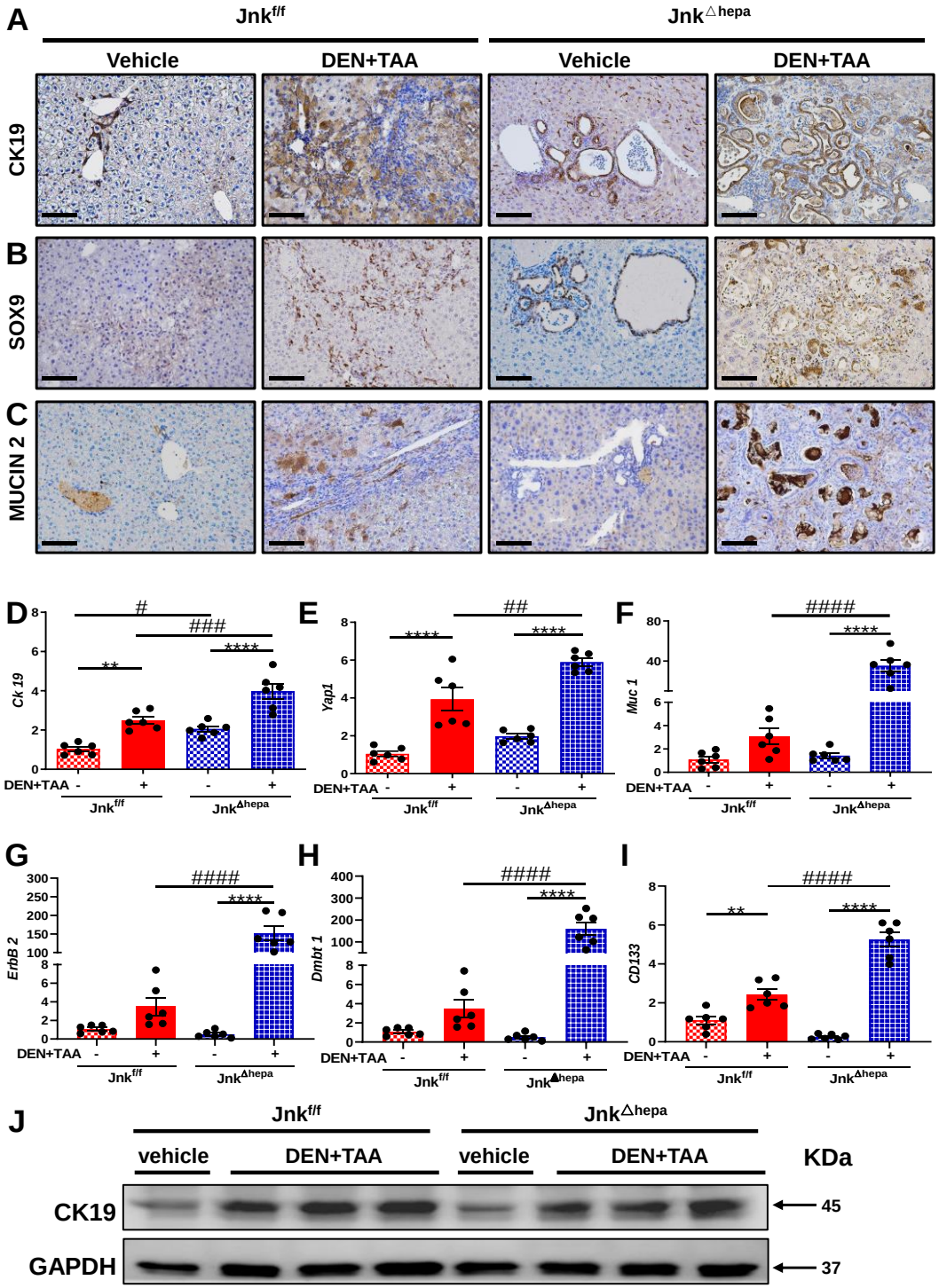

Figure 29. Cholangiocytes/BECs or oval cells were strongly activated in Jnk$^{\Delta hepa}$ mice by challenged with DEN/TAA. A) Representative IHC staining for biomarker of cholangiocytes, CK19 were accessed via IHC staining, as well as **B)** SOX9 and **C)**

MUCIN2. Scale bars, 100µm. **D-I)** Expression of mRNA *Ck19,* as well as *Yap1*, *Muc1, ErbB2*, *Dmbt1* and *CD133* were investigated by qRT-PCR, (#p <0.05; **/##p <0.01; ###p <0.001; ****/####p <0.0001). **J)** Protein of CK19 was shown by WB. Numbers were denoted as the molecular weight (KDa) of proteins. GAPDH served as loading control.

6.27 Involvement of the Notch signaling pathway in DEN/TAA-induced liver damage in Jnk$^{\Delta hepa}$ livers

The Notch and Wnt/β-Catenin signaling pathway involved and played a vital role in the development of CCA[135]. Activation of the Notch and Wnt signaling pathways stimulate the proliferation of the hepatic progenitor cell compartment. In particular, Notch signaling is related to the cell fate of BECs, while Wnt can trigger the differentiation toward hepatocytes[136]. Since conversion of oval cells to biliary epithelial cells requires Notch signaling[135], we assessed the relevance of Notch1 (A6) in each mice group via IHC staining. At the same time, expression of mRNA *Notch 1/3* accompanied with the ligand *Jag1*, and target effectors of Notch signaling *Hes1* and *Hey1*, as well as *HeyL* were detected via qRT-PCR (**Fig. 30**). Interestingly, Notch1/A6 staining was positive in clusters of immune cells as well as combined with ductular dilation in Jnk$^{\Delta hepa}$ livers. Compared to vehicle groups, livers sections stained for A6 by IHC were obviously detected in both *Jnk$^{f/f}$* and *Jnk$^{\Delta hepa}$* mice challenged with DEN/TAA, and positive A6 cells were strongly activated in *Jnk$^{\Delta hepa}$* mice. This revealed a strong activation of oval cells as indicated by overexpression of A6 positive cells in Jnk$^{\Delta hepa}$ liver, less evident in Jnk$^{f/f}$ livers (**Fig. 30A)**. This effect was mediated by the upregulation of *Notch1/3* expression accompanied by upregulated *Jag1* expression which was linked to the modulation of the transcription factors *Hes1* and *Hey1* through fold change of mRNA, but decreased in *HeyL* expression in *Jnk$^{\Delta hepa}$* mice after challenge with DEN/TAA (**Fig. 30B-G**). Simultaneously, protein expression of phospho-β-Catenin and β-catenin from whole liver extracts of each group mice were examined by WB. Overexpression of p-β-

Catenin was detected in *Jnk*$^{f/f}$ mice, but decreased in *Jnk*$^{\Delta hepa}$ mice after treated with DEN/TAA (**Fig. 30H**). Overall, these findings suggested that deletion of *Jnk1/2* in hepatocytes combined with chronic spontaneous hepatocytes damage induced a regenerative response with compensatory hepatocyte proliferation and activation of cholangiocyte of oval cells via Notch and Wnt/β-Catenin signaling pathway, eventually triggering the formation of CCA.

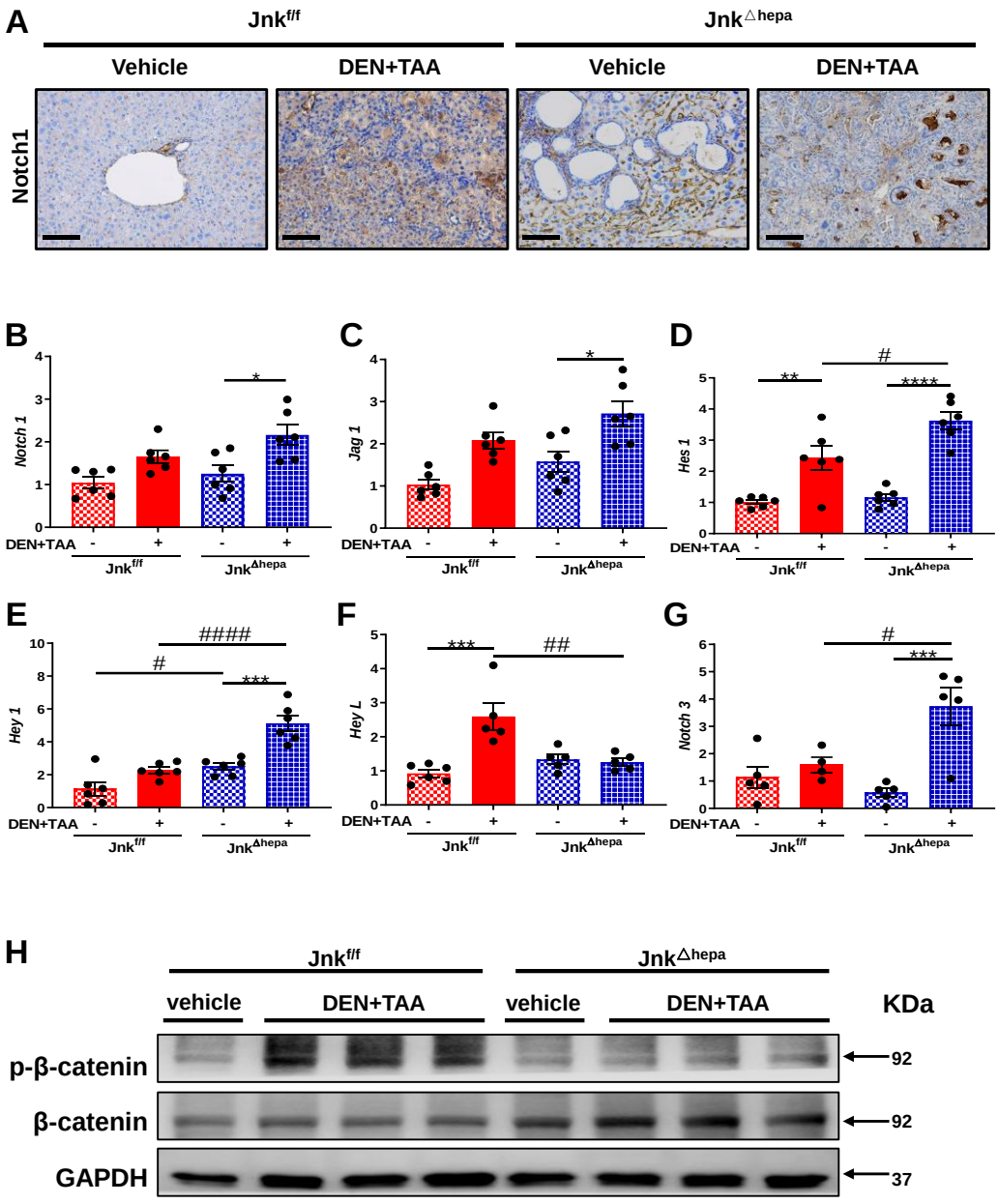

Figure 30. Activation of Notch and Wnt/β-Catenin in Jnk$^{\Delta hepa}$ mice. A) Representative IHC staining for biomarker of oval cells Notch1/A6, was evaluated by IHC staining after DEN/TAA, compared to vehicle group. Scale bars, 100μm. **B-G)** Expression of mRNA *Notch 1/3* accompanied with the ligand *Jag1*, and two

downstream effectors of Notch signaling *Hes1* and *Hey1*, as well as *HeyL,* were detected by qRT-PCR (*/#p <0.05; **/##p <0.01; ***p <0.001; ****/####p <0.0001). **H)** Protein expression of p-β-Catenin and β-Catenin from whole liver extracts of each group mice were analyzed by WB with the indicated antibodies. Numbers were denoted as the molecular weight (KDa) of proteins. GAPDH served as loading control.

6.28 The ERK signaling pathway was activated in Jnk$^{\Delta hepa}$ mice, after DEN/TAA administration

As mentioned earlier, DEN/TAA triggered liver tumorigenesis in both *Jnk$^{f/f}$* and *Jnk$^{\Delta hepa}$* mice. Based on loss function of JNK1/2 in hepatocytes, we detected the expression of MAPK/JNKs signaling pathway. After the treatment of DEN/TAA, overexpression of pJNK1 and pJNK2 were detected from whole liver extracts of the Jnk$^{f/f}$ mice via WB, but without expression in Jnk$^{\Delta hepa}$ mice. Simultaneously, WB analysis for pERK1/2 showed increased expression of proteins in Jnk$^{\Delta hepa}$ livers compared to the Jnk$^{f/f}$ animals (**Fig. 31**). Collectively, activation of ERK signaling pathway might be involved in the formation of liver tumor in Jnk$^{\Delta hepa}$ mice, after DEN/TAA.

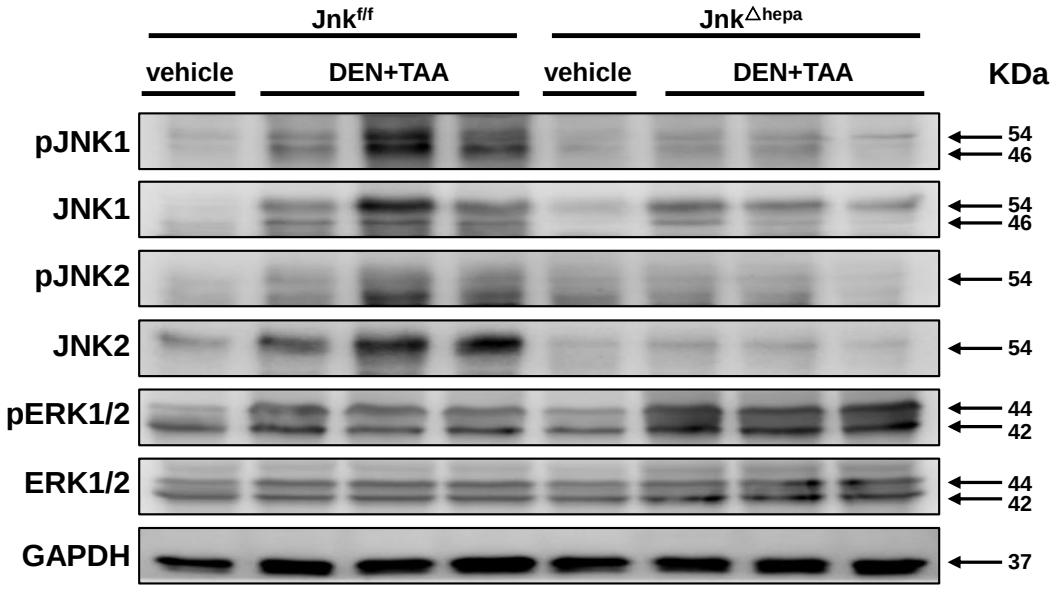

Figure 31. Overexpression of ERK1/2 is characteristic of mice with compound *Jnk1/2* deletion in hepatocytes after DEN/TAA treatment. Male 26-week-old mice were sacrificed and analyzed under the treatment of DEN/TAA. Protein expression of pJNK1/2, JNK1/2 pERK1/2 and total ERK1/2, from whole liver extracts of the mice.

Numbers were denoted as the molecular weight (KDa) of proteins. GAPDH served as loading control.

6.29 c-MYC plays a role of carcinogens in the formation of CCA in $Jnk^{\Delta hepa}$ mice

In our project, we pursued to create new animal model mimicking CCA for further mechanism study. In the DEN/TAA experiment group, expression of protein c-MYC was demonstrated in IHC staining together with expression of mRNA *c-Myc* by qRT-PCR. Simultaneously, tumor suppressor Klf6 and p21 which has been shown to prevent cell cycle arrest and promote DNA repair gene, thus acting as tumor suppressor[132, 133], expression of mRNA *Klf6* and *p21* was tested by qRT-PCR (**Fig. 32C, E**). C-MYC protein expression was characteristic of $Jnk^{\Delta hepa}$ compared to $Jnk^{f/f}$ livers after DEN/TAA. However, in vehicle groups, IHC staining was negative (**Fig. 32A**). Parallel to this, expression of mRNA *c-Myc* upregulated in experimental groups compared to vehicle groups, and more significantly in $Jnk^{\Delta hepa}$ mice, in line with the expression of c-MYC (**Fig. 32D**). Glutamine synthetase(GS), a diagnostic biomarker of HCC in human[137], has been shown by IHC staining compared with each group after the treatment of DEN/TAA. Expression of GS has been shown in both $Jnk^{f/f}$ mice and $Jnk^{\Delta hepa}$ mice. After DEN/TAA, the characteristics of map-like structure positive area nearly disappear instead of mosaic GS expression. However, positive GS also appeared around the hyperplastic and dilated cholangioma-like cells in $Jnk^{\Delta hepa}$ mice after DEN/TAA (**Fig. 32B**). Positive GS was calculated via ImageJ and graphed (**Fig. 32F**). Furthermore, markers of carcinogenesis including Klf6 and p21, expression of mRNA *Klf6* and *p21* were increased in both $Jnk^{f/f}$ mice and $Jnk^{\Delta hepa}$ mice after DEN/TAA administration, but strongly upregulated in $Jnk^{f/f}$ mice (**Fig. 32C, E**). Taken together, overexpression of c-MYC is involved in promoting the formation of CCA in $Jnk^{\Delta hepa}$ mice, which may present as carcinogenesis in chronic liver injury.

However, biomarkers of Klf6 and p21 may play as tumor suppressors in the formation of CCA after deletion of *Jnk1/2* in hepatocytes.

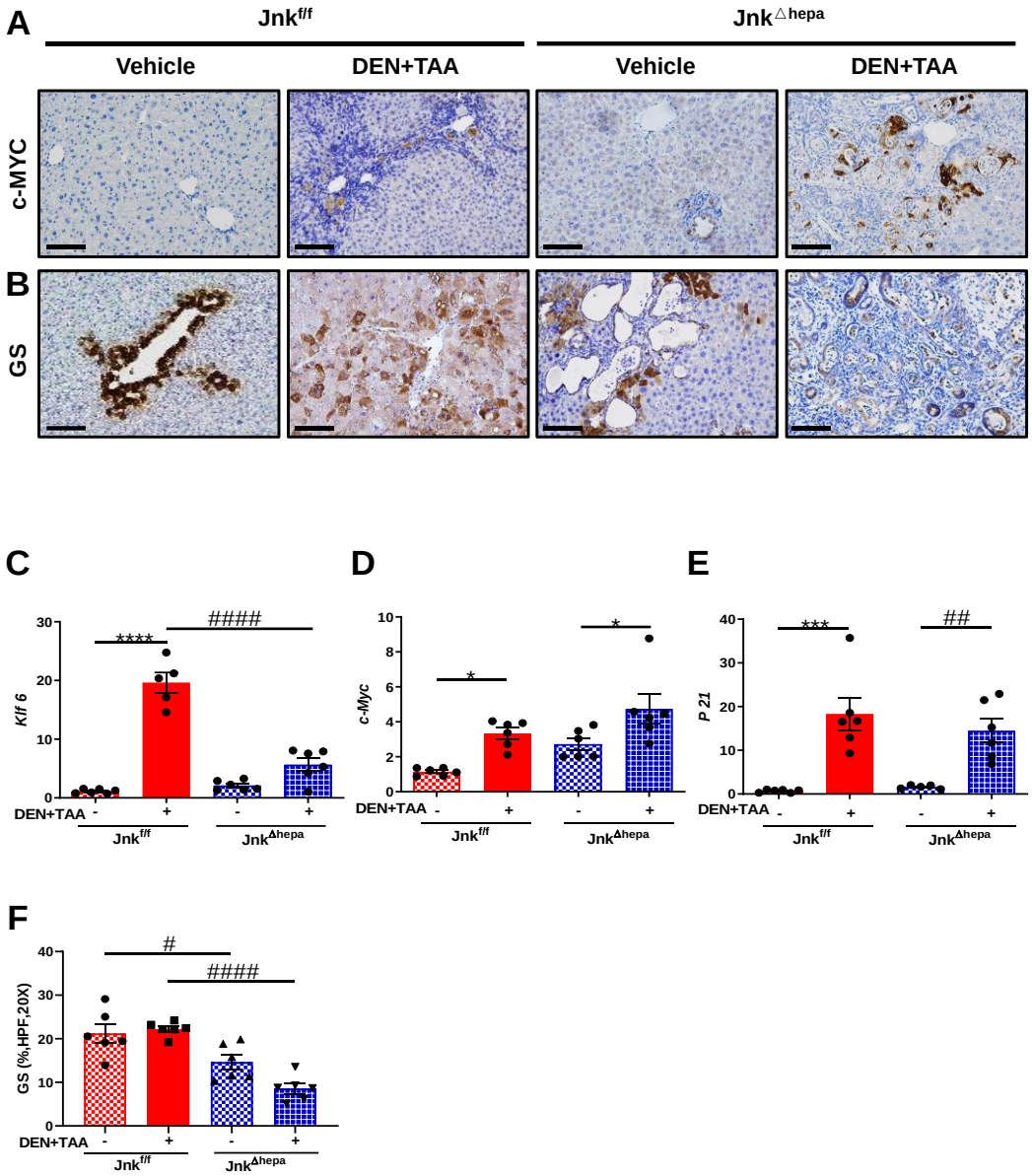

Figure 32. Carcinogenesis in *Jnk$^{\Delta hepa}$* mice. A-B) Representative images of paraffin liver sections staining for c-MYC and GS were evaluated by IHC. Scale bars, 100µm. **C-E)** Expression of mRNA *Klf6* was detected by qRT-PCR, as well as c-*Myc* and *p21.* **F)** Quantification of positive GS area was detected via ImageJ. Data were represented as the mean ± SEM and graphed (*p <0.05; ## p <0.01; *** p <0.001; ****/#### p <0.0001).

6.30 Protumorigenic and profibrogenic effect of DEN/CCl_4 in $Jnk^{f/f}$ and $Jnk^{\Delta hepa}$ mice

To confirm that tumorigenesis in *Jnk*$^{\Delta hepa}$ mice occurs in a proinflammatory setting, we subsequently used a second experimental model whereby these factors are induced by a single injection of DEN (25mg/Kg) followed by repeated administration of CCl_4 (0.5ml/Kg). After the administration of DEN and CCl_4, a significant increase in the incidence of liver tumors was observed, and 100% of wild type B6C3F1/J mice developed liver tumors, at 5 months of age[138]. DEN, a fixed concentration of 25mg/Kg, was chosen to IP injection in experimental group mice on the 14th day postpartum. Subsequently, mice were repeated with CCl_4 approach to IP injection at a fixed concentration of 0.5ml/kg twice per week. Mice were sacrificed at a 22-week, liver and blood were collected; nodules grown on the surface of the liver were annotated as well. Histopathology of the liver, serum parameters, as well as LW/BW ratio was also examined (**Fig. 33A-G)**. Compared to the vehicle groups, similar visible nodules ≥ 5 mm in diameter were detected, as well as a similar total number of liver nodules, in both $Jnk^{f/f}$ and $Jnk^{\Delta hepa}$ mice after the treatment of DEN/CCl_4. Compared to vehicle groups, LW was increased but BW decreased in $Jnk^{f/f}$ and $Jnk^{\Delta hepa}$ after DEN/CCl_4 treatment (**Fig. 33C-D**). Thus, DEN/CCl_4 increased LW/BW in $Jnk^{\Delta hepa}$ albeit no differences in tumorigenesis (**Fig. 33E**).

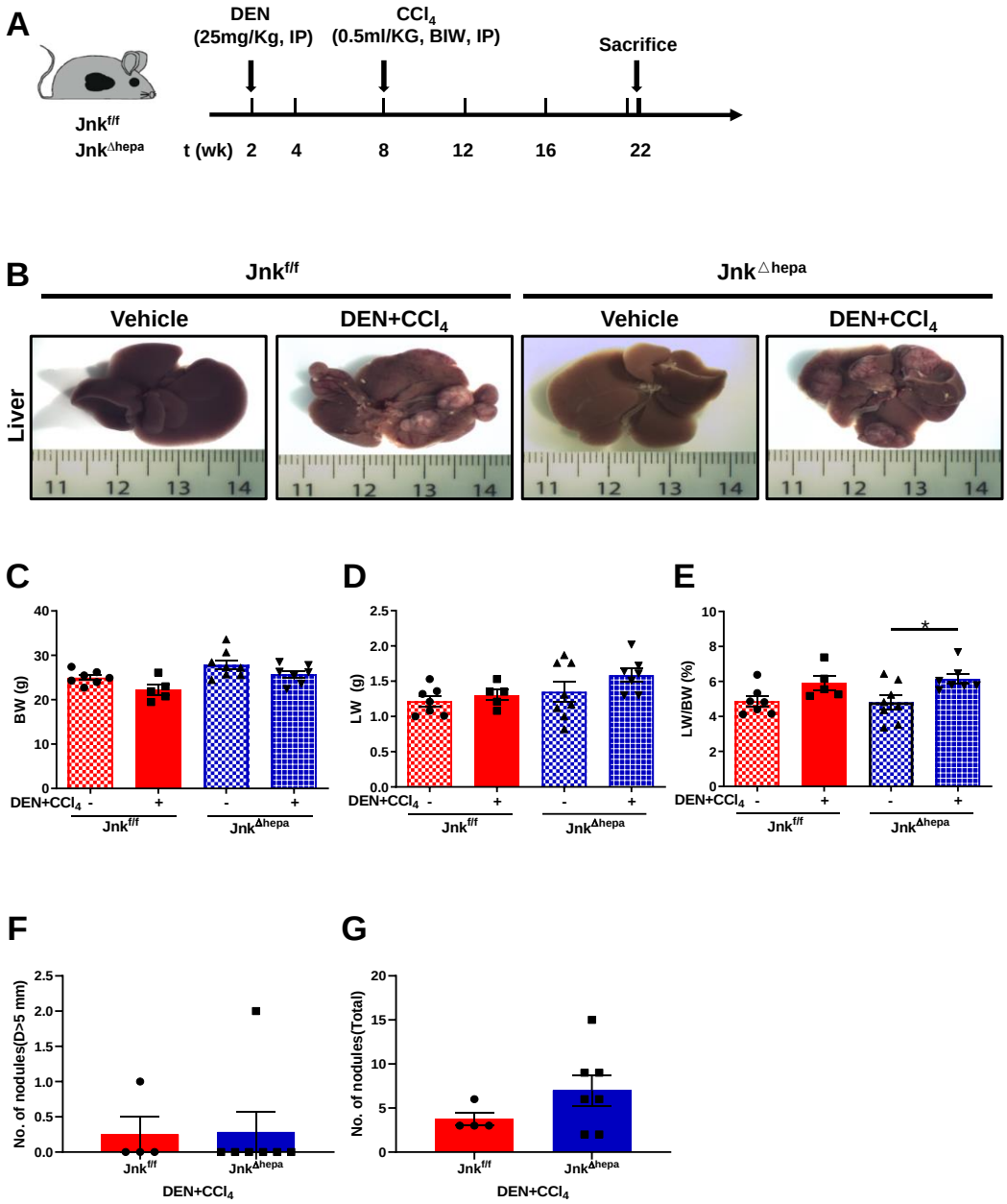

Figure 33. Effect of DEN/CCl_4 in $Jnk^{f/f}$ and $Jnk^{\Delta hepa}$ mice. A) 8-week-old *$Jnk^{f/f}$* and *$Jnk^{\Delta hepa}$* male mice were used for the experiments with the administration of CCl_4 (0.5ml/Kg, IP) twice per week after they received IP injections with a fixed dose DEN (25mg/Kg) at day 14 postnatally. **B)** Macroscopic pictures of the livers were taken. **C)** BW, **D)** LW and **E)** LW/BW ratio of mice and control littermates were calculated. **F)** Tumor burden for each individual mouse was characterized by calculating total number of visible tumors ≥ 5 mm in diameter and graphed. **G)** Total number of nodules were calculated and data was represented as the mean ± SEM and graphed (*p <0.05).

6.31 Histology and pathology in $Jnk^{f/f}$ and $Jnk^{\Delta hepa}$ mice after DEN/CCl_4

Histopathological examination of the livers was performed using H&E staining. Significantly proliferation of cholangiocytes combined with dilated ductular tracts in $Jnk^{\Delta hepa}$ mice group was visible, while abnormally differentiated hepatocytes were characteristic of $Jnk^{f/f}$ livers (**Fig. 34A**). No statistical differences in serum ALT and AST were found between *$Jnk^{f/f}$* and *$Jnk^{\Delta hepa}$* mice (**Fig. 34B-D**). However, LDH was significantly decreased in *$Jnk^{\Delta hepa}$* compared with *$Jnk^{f/f}$* mice indicating that hepatocyte damage might be enhanced in *$Jnk^{\Delta hepa}$* mice after DEN/CCl_4 treatment.

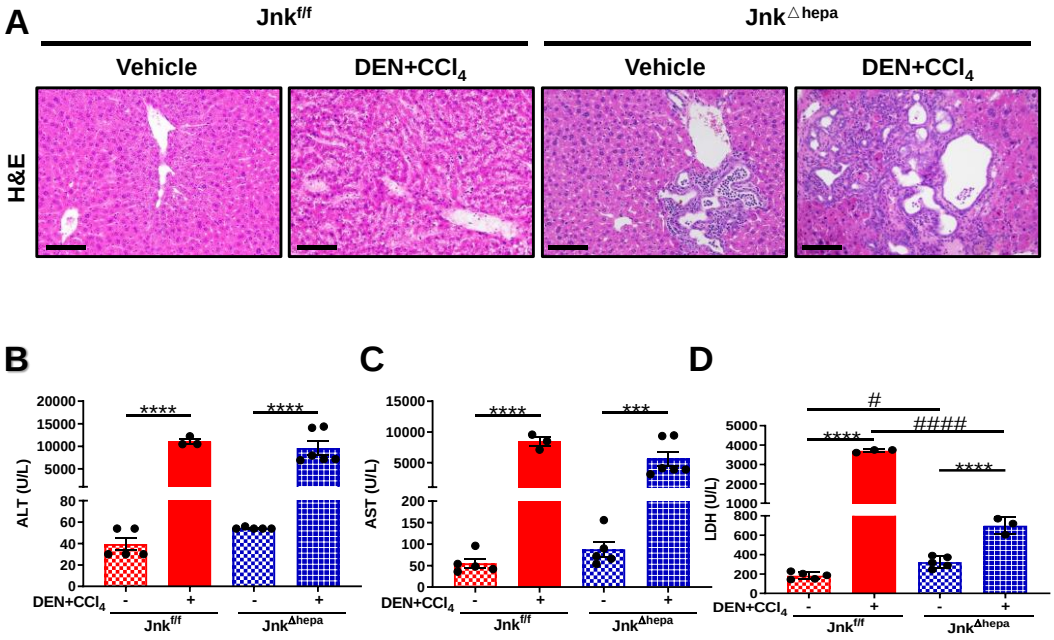

Figure 34. Histology and liver damage in $Jnk^{f/f}$ and $Jnk^{\Delta hepa}$ mice, after DEN/CCl_4. **A)** Representative images of liver sections with the indicated phenotypes that were stained with H&E. Scale bars, 100µm. **B-D)** Analysis of serum levels of ALT, AST and LDH from 22-week-old mice were accessed. Data were represented as the mean ± SEM and graphed (#p <0.05; **p <0.01; ***p <0.001; ****/####p <0.0001).

6.32 Cell death and compensatory prolifreaton in $Jnk^{f/f}$ and $Jnk^{\Delta hepa}$ mice, after DEN/CCl_4 treatment

First, TUNEL staining was analyzed to detect cell death in each group, photographs were taken and results calculated. Moreover, and according to the alteration pathological structure of the liver after DEN/CCl_4, Ki 67 and PCNA staining were performed, accompanied by SR to detect the degree of fibrosis. Positive TUNEL-cells, Ki 67-cells and SR positive area were calculated and graphed (**Fig. 35)**. After DEN/CCl_4, TUNEL staining suggested that cell death increased both in *Jnk*$^{f/f}$ mice and *Jnk*$^{\Delta hepa}$ mice. Compared to *Jnk*$^{f/f}$ mice, cell death was strongly elevated in *Jnk*$^{\Delta hepa}$ mice challenged with DEN/CCl_4 (**Fig. 35A, F**). This was in line with the expression of SR staining, which showed that SR positive area trended towards an increase in $Jnk^{\Delta hepa}$ compared with $Jnk^{f/f}$ mice (**Fig. 35E, H**). Expression of Ki 67 suggested that positive Ki 67-cells were increased to approximately 21.5% in $Jnk^{f/f}$ liver, and nearly 10.7% positive Ki 67 cells were detected in $Jnk^{\Delta hepa}$ liver challenged with DEN/CCl_4 (**Fig. 35B-C, G**). Additionally, expression of protein PCNA was analyzed via IHC. Compared to vehicle groups, overexpression of PCNA was demonstrated in both $Jnk^{f/f}$ and $Jnk^{\Delta hepa}$ groups after the treatment of DEN/CCl_4 (**Fig. 35D**). Altogether, these results showed that there were no differences in cell death or compensatory proliferation but a stronger fibrotic response in *Jnk*$^{\Delta hepa}$ mice.

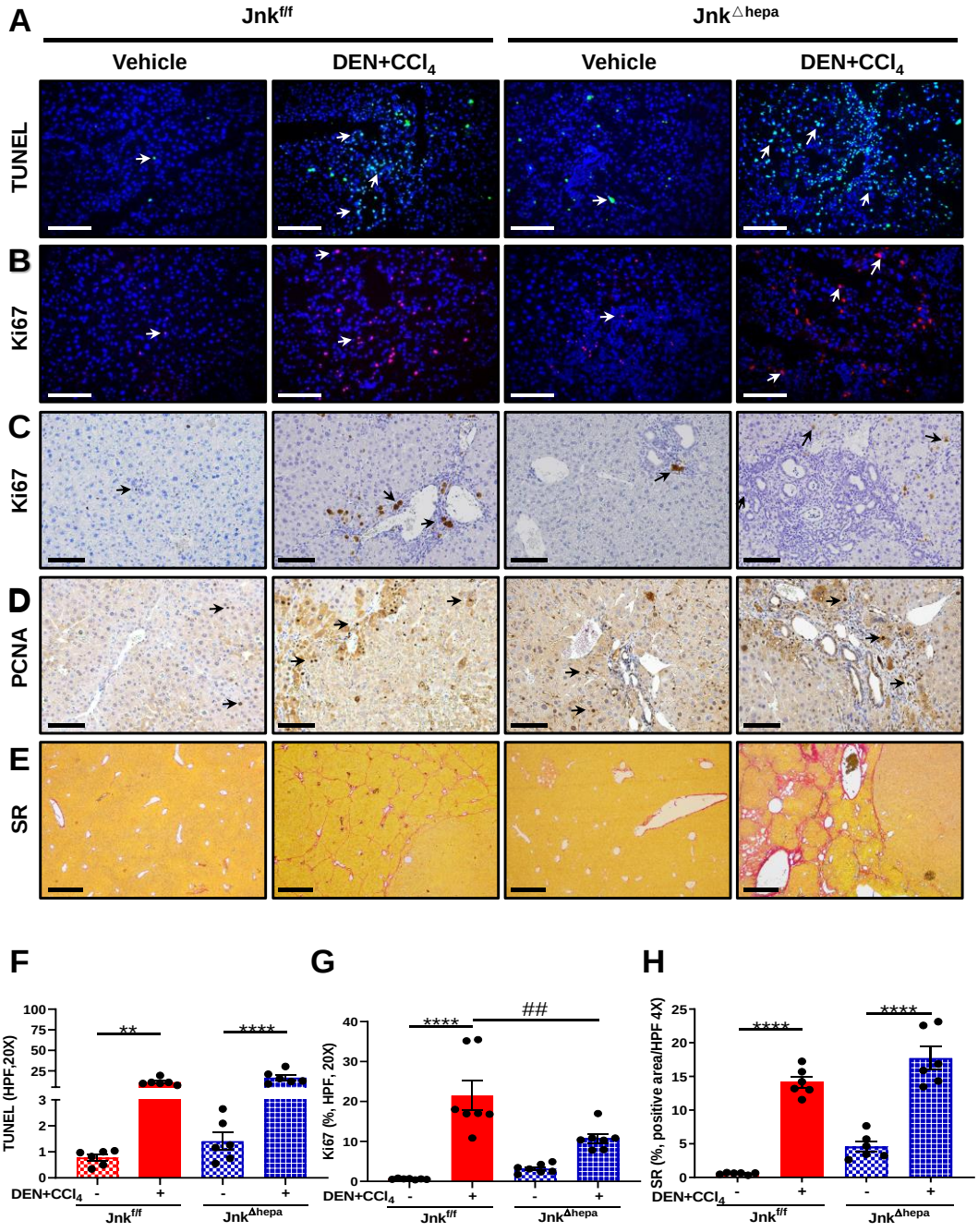

Figure 35. Cell death and compensatory proliferation in *Jnk*$^{f/f}$ and *Jnk*$^{\Delta hepa}$ mice after DEN/CCl_4. A) Cell death was evaluated using TUNEL staining in both *Jnk*$^{f/f}$ and *Jnk*$^{\Delta hepa}$ mice groups. Expression of Ki 67 was analyzed and graphed by both **B)** IF staining and **C)** IHC staining. IF Scale bars, 50μm. IHC Scale bars, 100μm. **D)** Expression of PCNA presented via IHC staining. Scale bars, 100μm. **E)** Representative SR staining of paraffin sections from the indicated livers after DEN/CCl_4 as well as vehicle groups mice. Scale bars, 500μm. **F)** Positive TUNEL-cells, **G)** positive-Ki 67 cells and **H)** SR positive area was calculated, data were represented as the mean ± SEM and graphed (**/##p <0.01; ****p <0.0001).

6.33 Hyperproliferation of BECs and increased cytokine signaling are characteristic of $Jnk^{\Delta hepa}$ mice, after DEN/CCl_4

Expression of CK19 was investigated using IHC staining. Compared to $Jnk^{f/f}$ mice, expression of this cholangiocytes marker was upregulated in $Jnk^{\Delta hepa}$ livers, after DEN/CCl_4, whereas in normal conditions CK19 stains BECs (**Fig. 36A**). Furthermore, expression of mRNA *Ck19* was in line with the IHC stain for CK19 (**Fig. 36B**). We therefore evaluated the expression level of inflammatory cytokines/chemokines, such as TNF-α and TGF-β1 by qRT-PCR. Both cytokines were strongly upregulated in experimental groups, compared to vehicle groups, especially significantly increased in $Jnk^{\Delta hepa}$ livers. After DEN/CCl_4 treatment, expression of mRNA *Tnf-α* was upregulated 12-fold in *Jnk$^{f/f}$* mice, and strongly increased 18-fold in $Jnk^{\Delta hepa}$ animals (**Fig. 36C**). Similarly, expression of mRNA *Tgf-β1* was upregulated 27.3-fold in *Jnk$^{f/f}$* mice, and significantly increased 105-fold in $Jnk^{\Delta hepa}$ animals challenged with DEN/CCl_4 (**Fig. 36D**). These results suggested that BECs hyperproliferation and a proinflammatory milieu are characteristic of $Jnk^{\Delta hepa}$ after DEN/CCl_4 treatment.

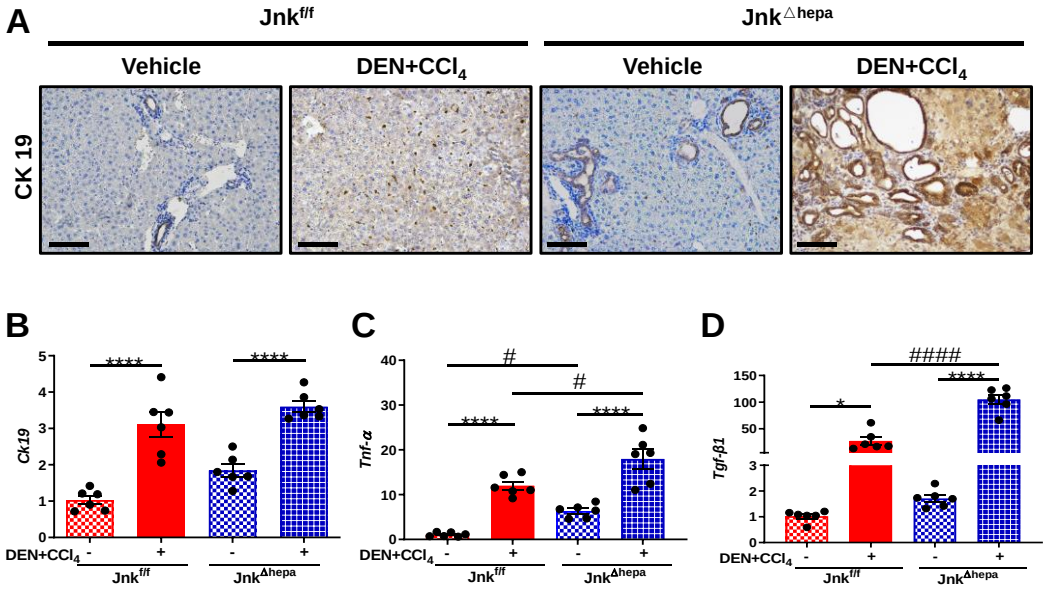

Figure 36. Hyperproliferation of BECs and increased cytokine signaling are characteristic of *$Jnk^{\Delta hepa}$* mice, after DEN/CCl_4. A) Representative images of paraffin

liver sections for CK19 by IHC staining. Scale bars, 100µm. **B)** Expression of mRNA *Ck19* was investigated by qRT-PCR, as well as **F)** *Tnf-α,* **G)** *Tgf-β1.* Data were represented as the mean ± SEM and graphed (#p <0.05; ****/####p <0.0001).

Collectively, JNKs adjust cell fate during liver carcinogenesis and play a vital role in balancing the differentiation and transformation of hepatocytes and cholangiocytes. This is essential for driving epithelial-mesenchymal transition (EMT) to induce the transdifferentiation of oval cells into cholangiocytes/BECs, and the formation of large-scale ducto/cystogenesis with common molecular characteristics of CCA (**Fig. 37**).

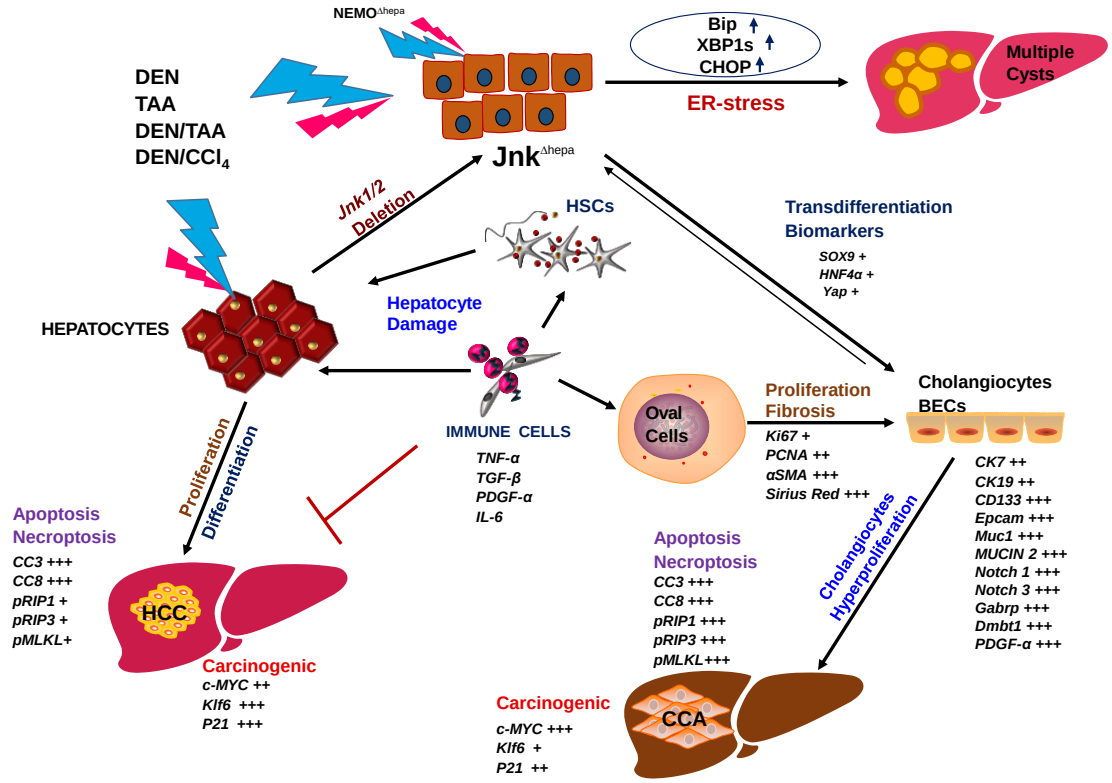

Figure 37. JNK1/2 play a vital role in balancing hepatic cell fate. Deletion of *Jnk1/2* in hepatocytes induces liver biliary hamartoma accompanied with liver dysfunction, related to hepatocellular vacuolation and exacerbated hyperproliferation of cholangiocyte/BECs via activation of ER-stress, eventually triggering multiple liver cysts. Overexpression of JNKs promotes the formation of HCC, while loss function of *Jnk1/2* in hepatocytes promotes the excessive proliferation of cholangiocyte/BECs and the expansion of the bile duct lumen, eventually leading to the formation of CCA in chronic liver disease.

7. Discussion

HCC and CCA are the two most common types of hepatic malignancies. Both of them have increased in incidence year by year. HCC is the fifth most common malignant tumor in Western countries. While the incidence of CCA is on the rise, up to 2.1 cases per 100,000 people in Western countries. Especially CCA, the cancer of the gallbladder and the biliary tract is nowadays a matter of tremendous concern. Lacking specific biomarkers make diagnosis difficult in early stages. The prognosis of CCA is miserable and surgery is the only effective treatment, but vast majority of patients with advanced disease and recurrence after resection are common. At the same time, CCA lacks the sensitivity of radiotherapy and chemotherapy, which has become a worldwide problem in clinical diagnosis and treatment. Patients who have been diagnosed with CCA and undergo radical surgery with 5-year survival are considered to be fortunate. Despite the diversity of treatment options, the 5-year survival rate of CCA has not been increased, remains only 5-10%, which has not significantly changed during the last 30 years[56, 139].

Recent progress has led to a deeper understanding of the role of MAPKs signaling pathways in liver tumor diseases. Among them, the JNKs signaling pathway involved in the development of CCA is not yet clear. Previously study showed that JNK plays an important role in regulating the interaction between different pro-apoptotic proteins and anti-apoptotic proteins in response to external and internal apoptotic stimuli[95]. Based on the spontaneous progression of $Jnk^{\Delta hepa}$ mice to multiple dilated cysts with age, we used improved CCA animal models to explore the important role of JNKs/MAPKs signaling pathways involved in the pathogenesis of CCA (Fig. 44).

Although the exact potential risk factors and molecular mechanisms of CCA have not been accurately identified, at least our research results give a potential direction. JNKs/MAPKs may become therapeutic targets for the treatment of CCA.

7.1 Loss function of JNK1/2 in hepatocytes triggers liver hamartoma with age in mice through ER-stress.

Fibrocystic liver disease is a type of disease associated with autosomal gene mutations, including PLD, Caroli's disease and CHF, characterized by the presence of multiple liver cysts of different shape and size filled with cystic fluid in normal liver tissue. PLD is usually associated with autosomal dominant polycystic kidney disease, with a prevalence ranging from 1/1,000,000-1/400, and about 8-10% of the patients have polycystic kidney disease[41]. Current research and effective treatments are limited. Even existing drugs can improve the symptoms of early patients, but they cannot prevent the progress of the disease. Liver transplantation is considered to be the most effective treatment at present. The previous PCK rat model[140] provides a lot of suggestion to the study of PLD, but still no breakthrough progress yet.

In our study, we specifically knocked out the *Jnk1/2* gene of mouse hepatocytes to promote their spontaneous progress into multiple liver cysts, maybe create a new animal model of PLD (**Fig. 5-11**). This not only provides a new animal model of PLD, but also expands our research direction. However, related genes and chromosomes still need to be further explored and clarified. Loss function of JNK1/2 in hepatocytes, we tried to detect the possible signaling pathway linked to JNKs/MAPKs. Overexpression of Bip/eIF2α/Chop, interacted with XBP1s but not IRE1α, showed us a new direction of activation of ER-stress (**Fig. 12**). We hypothesis that loss function of JNK1/2 in hepatocytes. The deposition of fibrosis is based on a paracrine interaction, which is mediated by the ability of RDC to secrete profibrotic and proinflammatory growth factors, including TNF-α[141].

Coincidentally, TGF-β is a key mediator in hepatic fibrogenesis[142], while TGFβ also induces JNKs/MAPKs signaling pathways via independently of Smads[143]. In the process of liver fibrosis, TGF-β is a main factor to secrete and

activate HSCs by fibroblasts and macrophages, and is responsible for depositing about 80% of the matrix protein[20]. As a response to injury, HSCs was converted to MF, which is characterized by new expression of αSMA, sensitivity to fibrogenic, and active secretion of ECM protein[14]. Here, we express the ER-stress signaling pathway activated by highly expressed upstream factors TNF-α or/and TGF-β. At the same time, overexpression of fibrosis biomarker αSMA also provides evidence of cholangiocellular hyperproliferation in $Jnk^{\Delta hepa}$ mice group.

All these data results supported our view that the lack of *Jnk1/2* in hepatocytes, continuing activation of ER-stress combined with activated Bip, contribute to promoting the progression of biliary hamartoma with age in mice.

7.2 Loss function of JNK1/2 in hepatocytes suppress HCC formation but promotes the progression of CCA.

Previously studies showed, JNKs/MAPKs signaling pathway was thought to play a significant role in the development of HCC[88]. Das et cl[90] suggested that JNK play a dual role in the development of hepatocellular carcinoma. While, the results of another study suggested that lack of JNK1 or JNK2 in hepatocytes may increase the tumor development, and the pro-tumor effect of JNK on HCC is related to inflammation[91]. Coincidentally, other data indicated that the JNKs, particularly JNK1, contribute to malignant transformation and tumor growth [92]. Possibly, JNK1 has a larger role than JNK2 in development of liver tumor [93].

Based on this information, we tried to treat these mice in approach to different methods as described above, in order to validate the relevance of JNK1/2 in mediating the shift from HCC to CCA. Sustained activation of JNKs/MAPKs promoted the formation of HCC was proved by H&E and IHC staining, as well as WB (in TAA and DEN/TAA groups). As seen the photographs presented in H&E staining, histopathology characteristic structure of the livers was obviously different between $Jnk^{f/f}$ mice and $Jnk^{\Delta hepa}$ mice after the treatment of drugs,

including TAA, DEN/TAA, DEN/CCl_4. It looks more significant proliferation of cholangiocytes combined with obvious fibrosis when loss function of JNK1/2 in hepatocytes according to the expression of biomarkers of BECs (including SOX9, CK19, Notch1 and MUCIN2), and fibrosis detection approach to Sirius Red staining (**Fig. 16, 27, 29, 35**).

Furthermore, under the administration of TAA/DEN+TAA, GS, which was one biomarker of HCC, showed map-like structure in normally liver area near the hepatic vein, but this characteristic performance was nearly disappeared in $Jnk^{f/f}$ mice, whilst overexpression positives dyed marked on the hyperproliferative cholangiocytes in $Jnk^{\Delta hepa}$ liver (such as CK19, SOX9, Notch1 and MUCIN2). At the same time, the investigations of mRNA *Dmbt1*, *Gabrp, ErbB2* and *Muc1* have been identified as oval cell/BECs markers in rodent, as well as CCA-enriched genes[134, 144] that were coincide with related expression of protein, such as Notch1, CK19, SOX9 and MUCIN2. These results suggested that the contribution of activated BECs in the cholangiocellular hyperproliferation was promoted in $Jnk^{\Delta hepa}$ animals. Considering that CCA tissues are characterized by the presence of mucin-secreting cells, this finding further supports the CCA diagnosis[145]. As identified in our experiments, upregulation of MUCIN2 in IHC staining coincide with overexpression of mRNA *Muc 1* in $Jnk^{\Delta hepa}$ experimental (DEN/TAA) group. Addition, the role of Klf6 in tumor growth regulation has been confirmed through a variety of ways. Upregulation of Klf6 in $Jnk^{f/f}$ mice show tumorigenicity in the HCC development progress, through developing liver damage (cirrhosis) via the formation of scar tissue[146], but depressed in $Jnk^{\Delta hepa}$ experimental (TAA, DEN/TAA) mice, which means Klf6 was consumed as tumor suppressor. The expression of Klf6 can attenuate the tumorigenicity of glioblastoma in vivo and in vitro, and can inhibit cell transformation induced by multiple oncogenes[147]. In line with PAS staining, positive mucins secreted around the hyperplastic cholangiocellular and ductular dilation (**Fig. 21, 24**), suggested that cirrhosis

induced in liver disease[148].

We therefore inferred that the lack of expression of JNKs promotes the proliferation and migration of hepatocytes to cholangiocytes in chronic liver disease. Which also means sustained overexpression of JNKs promotes the formation of HCC, but loss function of JNKs can shift to a destination of CCA.

7.3 Cell death was involved in CCA formation in $Jnk^{\Delta hepa}$ mice with chronic liver injury.

Regulating cell death is a powerful weapon for host defense. Therefore, we continued to investigate the mechanism of cell death in these models since these livers were characterized by cell death, inflammatory microenvironment or/and ECM deposition.

Since the 1980s, people have known the importance of mitochondrial damage in the pathogenesis of APAP-induced necrosis[149]. At that time, previous studies suggested that the mitochondria of the liver were damaged in APAP treated mice, and most importantly caused by activation of MAPKs pathway. Interference with various MAPK proteins, including MLK3, ASK1, MKK4 and JNK, as well as JNK binding Chaperone SH3BP (Sab) significantly prevents APAP-induced hepatocyte death[150, 151].

In normal liver, the JNKs family is minimally or transiently activated, the latter usually physiological, whereas sustained activation is pathological. In addition to their central role in hepatic physiological responses (such as cell death, apoptosis, and cell cycle regulation) [84, 85], JNKs play a carcinogenic role by promoting inflammation, proliferation, invasion, and angiogenesis, depending on the specific context and duration of JNK signaling pathway activation [86, 87].

In hepatocytes, the expansion of the cascade of mitochondrial permeability and apoptosis occurs in apoptosis induced by death receptors. This involves the release of mitochondrial mediators of apoptosis, which leads to the final activation of effector Caspase 3/7, positive feedback amplification of Caspase

8 activations. The activation of Caspase and then the resulting apoptosis is a highly regulated form of cell death, with multiple checkpoints and molecular mediators, which are activated through two different pathways (external pathway and internal pathway)[152]. As demonstrated in our study, Cleaved-Caspase 3 and Cleaved-Caspase 8 were activated in $Jnk^{\Delta hepa}$ mice, more than in $Jnk^{f/f}$ mice after the treatment of TAA or/and DEN/TAA. Which means loss function of JNKs in hepatocytes promoted cell death related to apoptosis.

Furthermore, Receptor-interacting protein kinase (RIP) 3 mediated programmed necrosis (RIP) 3 (also known as RIPK3) is activated by death receptors, pathogen sensors, interferon receptors, Ag-specific TCR and genotoxic stress via an alternative death pathway triggered. Necrosis causes cell leakage and acts as a "trap door", and is another kind of programmed cell death, independent of caspase activity, also is characterized by membrane swelling and rupture mediated by RIP1 and RIP3. Once RIP3 kinase activated, following with phosphorylating the downstream member pseudokinase MLKL[153, 154]. Finally, phosphorylated MLKL undergoes oligomerization and translocation to the cell membrane to perform a necroptosis[155] (**Fig. 18, 26**). According to the results that the deletion of JNKs cannot prevent cell death as presented by TUNEL staining *in vivo.* Based on TAA treatment, compared to $Jnk^{f/f}$ mice, upregulation of cytokines Cleave-Caspase 3/8 indicated apoptosis activated, combined with pRIP1/pRIP3/pMLKL which were evidence of necroptosis happened to $Jnk^{\Delta hepa}$ mice. However, caspase-dependent apoptosis was no more upregulated in DEN/TAA experiment model, but necroptosis was strongly activated according to the detection of protein expression, including pRIP1, pRIP3 and pMLKL.

In total, our results suggested that deletion of *Jnk1/2* in hepatocytes, promote cell death but not protect liver damage after the external stimulation, eventually induced the formation of CCA.

7.4 Deletion of *Jnk1/2* in hepatocytes promotes cholangiocellular hyperproliferation combined with strongly activated oval cells

As cell death was involved in the progression of CCA formation in $Jnk^{\Delta hepa}$ mice, liver damage with compensatory proliferation may be promoted via cholangiocellular hyperproliferation. One of the main consequences of the increased liver cells death is compensatory proliferation to compensate loss of liver cells. Compensatory proliferation has been implicated in the progression of many types of diseases including HCC [156, 157]. In our study, along with the increased hepatic cell death in $Jnk^{\Delta hepa}$ after the treatment of TAA or/and DEN/TAA or/and DEN/CCL_4, quantification of cell proliferation with expression of Ki 67 and PCNA via IF and/or IHC demonstrated exacerbated proliferation in $Jnk^{\Delta hepa}$ livers. Furthermore, increased proliferation was evident in both cholangiocytes and hepatocytes in $Jnk^{\Delta hepa}$ mice, especially cholangiocytes, which is consistent with the increased ductular proliferation found in these mice. These results were strengthened by detection of cholangiocyte biomarkers, such as overexpression of CK19, SOX9, Notch1, Muc1 and MUCIN2 in $Jnk^{\Delta hepa}$ mice. In fact, CCA development frequently requires conditions of chronic inflammation[158], which was proved by dysregulation of pro-inflammatory cytokines including *Tgf-β1, Tnf-α and pdgfα* in $Jnk^{\Delta hepa}$ livers. At the same time, these livers were characterized by cell death, inflammatory microenvironment and extracellular matrix deposition. Necroptosis-associated hepatic cytokine microenvironment induces the shift from HCC to CCA development [159].

In parallel with proliferating hepatocytes, marked expansion of the biliary epithelium, the liver parenchyma of $NEMO^{\Delta hepa}$/$Jnk^{\Delta hepa}$ animals were positive for CK19 and SOX9 and negative for HNF4α[60]. Moreover, CCA lesions were characterized by mucin-secreting cells, which might aid in CCA diagnosis[145]. Interestingly, analysis of gene expression showed the occurrence of

cholangiocarcinoma/tumor-enriched markers including Dmbt1 and Gabrp not only in NEMO$^{\Delta hepa}$/Jnk$^{\Delta hepa}$ but also in a second model of liver carcinogenesis, the DEN model[60]. Moreover, the microarray highlighted the pivotal role of JNK1/2 in modulating cell fate by promoting hepatocarcinogenesis and under-regulating cascades linked with cholangiocarcinogenesis. All of these results ssuggested that activation of strong proliferation and inflammatory microenvironment within the hepatic parenchyma involved in the progress of CCA formation after loss function of JNK1/2 hepatocytes in chronic liver damage.

7.5 Carcinogenesis was involved in promoting CCA formation in Jnk$^{\Delta hepa}$ mice

As described previously, Ras/Raf/ERK/MAPKs signaling pathway is helpful with contributory to the control of G1 phase. Combined with GSK3β, ERK played a key role in the critical phosphorylation of S62/T58 controlling c-MYC protein levels[160]. Overexpression of c-MYC is the cause of complete tumorigenesis, especially in the formation of CCA as described by Calvisi DF recently[129]. Similarly, c-MYC is one of the most frequently mutated genes in tumors and an important regulator of cell cycle and apoptosis, its dysregulated expression could be associated with many malignancies. c-MYC is instrumental in directly or indirectly regulating the progression through the G1 phase and G1/S transition, and transformation by c-MYC results in the perturbed cell cycle[130]. As previous published, Ki 67, one cellular marker for proliferation and is strictly associated with cell proliferation. Ki 67 protein is present in all active phases of the cell cycle (G1, S, G2, and mitosis), but not in resting (quiescent) cells (G0)[161]. mRNA of cell cycle *Cyclin E1* was demonstrated, evident upregulation of *Cyclin E1* in Jnk$^{\Delta hepa}$ experimental mice, in line with presentation of biomarker Ki 67 in IHC staining (TAA, DEN/TAA, DEN/CCl_4) which means cell proliferation was activated in cell cycle phase G1, which may be prominent

leading to CCA. This was in line with the results in our study that deletion of *Jnk1/2* in hepatocytes promoted the proliferation of cholangiocytes coincide with overexpression of mRNA *Cyclin E1* (**Fig. 26D**). On the other hand, PCNA was originally identified as an antigen that is expressed in the nuclei of cells during the DNA synthesis phase of the cell cycle, which is very important for both DNA synthesis and DNA repair[162].

However, Klf6 (Krüppel-like factor 6) is a transcription factor involved in the regulation of several cellular processes, is considered as a tumor suppressor. mRNA *Klf6* expression was accessed by qRT-PCR. After the treatment of TAA/DENTAA, *Klf6* expression significantly upregulated in $Jnk^{f/f}$ mice, while exhibited in $Jnk^{\Delta hepa}$ mice as described above (**Fig. 22C, 32C**). This was in live with expression of p21, functioned as a regulator of cell cycle progression and acting as tumor suppressor[132, 133]. According to these results, we speculated that mice loss function of JNK1/2 in hepatocytes were promoted CCA formation by activated c-MYC, but may be extenuated by tumor suppressor Klf6 and p21. Collectively, c-MYC plays as carcinogen in the formation of CCA, combined with dysregulation of cell cycle in chronic liver injury.

7.6 Deletion of *Jnk1/2* in hepatocytes contribute HPCs to bile duct repair via EMT transition in the formation of CCA.

Previously, cholangiocytes may be involved in liver fibrosis [67]. During acute and chronic cholestasis, liver fibrosis involving an increasing number of ductulus, is accompanied by polymorphonuclear leukocyte infiltration and increased extracellular matrix deposition, leading to periportal fibrosis and finally PBC[163]. Diaz et al. [164] presented histological data suggesting that EMT occurs in human liver fibrosis, particularly in diseases associated with prominent bile ductular proliferation including biliary atresia and PBC. Other studies indicated that cholangiocellular hyperproliferation play a vital role in the induction of fibrosis via EMT [67, 165, 166]. So that, EMT may also play an important

role in CCA progression, accompanied with dysregulation of JNKs/MAPKs signaling pathway.

EMT is critical then for embryonic development, wound healing, stem cell biology - and plays a key role in the tumorigenic process[64, 65]. The first change occurs when epithelial cells lose cell–cell adhesions (at specialized adherent junctions) with the disruption of two major components E-cadherin and β-catenin. We detected the expression of β-catenin via WB and results showed dysregulation of the Wnt/β-catenin signaling pathway (**Fig. 30H**).

In CCA, developmental changes seen in cholangiocytes may be due to the activation of HPCs, the proliferation of bile duct cells, or through ductal metaplasia of mature hepatocytes[29, 68]. However, alongside the progress seen in histopathological studies, there is now a better understanding of the origins of BECs. Both HPCs[69] and CCA stem cells [66] seem to be capable of differentiating into BECs, whilst CCA stem cells can also originate from HPCs [66, 70, 71]. Micrographs of in vivo fate-tracking experiments showed the contribution of hepatocytes and HPCs to bile duct repair or hepatocyte injury. In order to cope with biliary tract injury, signals derived from myofibroblasts mediate the activation and proliferation of the HPCs niche. This process can be triggered by NOTCH signal transduction, via Jag1, a NOTCH ligand provided by the stroma of the portal vein, which induces the differentiation of hepatocytes into BECs[167-169]. As seen in our results presented in **Figure 30**, which was in line with the studies previously published. These results indicate that CCA can be derived from common HPCs, which can differentiate into both hepatocytes and cholangiocytes [72, 73]. Also, chronic inflammatory processes can promote the development of CCA by affecting BEC function and proliferation [170, 171].

Interestingly, upregulation of mRNA *dmbt1*, *muc1* and *Gabrp* was found in experimental group, especially in *Jnk*$^{\Delta hepa}$ mice, these results also indicated that EMT may be modulated through a JNK-dependent mechanism. In line with CCA development, at the biochemical level, various morphogenetic and environmental signals including TGF-β, WNT, EGFR, and PDGF, inflammatory cytokines and integrin receptor ligands promote EMT [74, 75]. Furthermore, TGF-β is also involved in several steps of cancer progression, from tumorigenesis to

metastasis, which promotes cancer cell invasion and metastasis through an EMT process, although at later stages [76-80].

The canonical TGF-β pathway relies on the downstream SMAD family[172]. Interestingly, JNK-induced phosphorylation of R-SMAD can activate the EMT programming process. Both JNK and p38 can synergize with SMADs to promote non-canonical TGF-β-induced apoptosis[74, 81, 173, 174]. In SMAD-independent pathways, TGF-β can also induce AKT phosphorylation and rapidly activate PI3K, which is possibly involved in SMAD2-induced EMT[175]. Studies on keratinocytes indicate that the PI3K/AKT pathway contributes to completion of TGF-β-induced SMADs-dependent EMT. Therefore, we examined the expression of protein ERK1/2 in each group.

As the results showed, loss function of JNK1/2 in hepatocytes triggered the activation of ERK/MAPKs signaling pathway in our experiment model, which was in line with previous studies suggested that ERK/MAPKs pathway contributes to EMT induction, as ERK is required to remove cell adhesion junctions, which leads to increased cell migration[74, 81, 82].

8. Conclusions

We summarized a novel function of JNK1/2 in cholangiocyte/BECs hyperproliferation and transdifferentiation, aiming to open the new pathways involved in the targeted inhibition of CCA formation.

1) JNKs play an important role in hepatic cell fatal of transdifferentiation, inhibit JNK signaling pathway via DJNKI1 could revert hepatoblasts transdifferentiation.

2) Deletion of *Jnk1/2* in hepatocytes induces liver biliary hamartoma accompanied with liver dysfunction, related to hepatocellular vacuolation and exacerbated proliferation of cholangiocyte/BECs combined with exacerbated liver fibrosis, triggering multiple liver cysts.

3) Prominent activation of necroptosis combined with strong proinflammatory milieu were induced in mice after the deletion of *Jnk1/2* in hepatocytes in chronic liver injury.

4) Overexpression of JNKs promotes the formation of HCC, while loss function of *Jnk1/2* in hepatocytes promotes the excessive proliferation of cholangiocyte/BECs and the expansion of the bile duct lumen, eventually leading to the formation of CCA in chronic liver disease.

5) Activation of c-MYC may promote the formation of CCA while biomarkers of Klf6 and p21 may play as tumor suppressors after deletion of *Jnk1/2* in hepatocytes in chronic liver injury.

6) JNKs adjust cell fate during liver carcinogenesis and play a vital role in balancing the differentiation and transformation of hepatocytes and cholangiocytes.

9. Bibliography

1. Lindor, T. B. K., Zakim and Boyer's Hepatology 7th Edition. *Elsevier* **2017**, 1072.
2. Launois, B.; Jamieson, G. G.; Cherqui, D.; Randone, B.; Gayet, B.; Machado, M. A. C., *The Posterior Intrahepatic Approach in Liver Surgery*. Springer: 2013.
3. Chamberlain, R. S., Essential functional hepatic and biliary anatomy for the surgeon. *Hesham A. Hepatic surgery. Newark, NJ: InTech* **2013**, 41-60.
4. Corness, J. A.; McHugh, K.; Roebuck, D. J.; Taylor, A. M., The portal vein in children: radiological review of congenital anomalies and acquired abnormalities. *Pediatr Radiol* **2006,** *36* (2), 87-96, quiz 170-1.
5. Couinaud, C., Liver anatomy: portal (and suprahepatic) or biliary segmentation. *Dig Surg* **1999,** *16* (6), 459-67.
6. Lehman-McKeeman, L. D., Absorption, distribution, and excretion of toxicants. *Cassarett and Doull's Toxicology: The Basis Science of Poisons* **2008**, 131-159.
7. Dooley, J. S.; Lok, A. S.; Garcia-Tsao, G.; Pinzani, M., *Sherlock's diseases of the liver and biliary system*. John Wiley & Sons: 2018.
8. Gumucio, J. J., Structural and functional organization of the liver. *Liver and Biliary Disease* **1996**, 3-19.
9. Schleicher, J.; Tokarski, C.; Marbach, E.; Matz-Soja, M.; Zellmer, S.; Gebhardt, R.; Schuster, S., Zonation of hepatic fatty acid metabolism—the diversity of its regulation and the benefit of modeling. *Biochimica et Biophysica Acta (BBA)-Molecular and Cell Biology of Lipids* **2015,** *1851* (5), 641-656.
10. Tacke, F.; Weiskirchen, R., Update on hepatic stellate cells: pathogenic role in liver fibrosis and novel isolation techniques. *Expert review of gastroenterology & hepatology* **2012,** *6* (1), 67-80.
11. Braet, F.; Taatjes, D. J.; Wisse, E., Probing the unseen structure and function of liver cells through atomic force microscopy. *Semin Cell Dev Biol* **2018,** *73*, 13-30.
12. Wisse, E., Ultrastructure and function of Kupffer cells and other sinusoidal cells in the liver. **1977**.
13. Klaas, M.; Kangur, T.; Viil, J.; Maemets-Allas, K.; Minajeva, A.; Vadi, K.; Antsov, M.; Lapidus, N.; Jarvekulg, M.; Jaks, V., The alterations in the extracellular matrix composition guide the repair of damaged liver tissue. *Sci Rep* **2016,** *6*, 27398.
14. Mallat, A.; Lotersztajn, S., Cellular mechanisms of tissue fibrosis. 5. Novel insights into liver fibrosis. *Am J Physiol Cell Physiol* **2013,** *305* (8), C789-99.
15. Sørensen, K. K.; Smedsrød, B., The liver sinusoidal endothelial cell: basic biology and pathobiology. *The Liver: Biology and Pathobiology* **2020**, 422-434.
16. Jenne, C. N.; Kubes, P., Immune surveillance by the liver. *Nat Immunol* **2013,** *14* (10), 996-1006.
17. Cheung, A. C.; Lorenzo Pisarello, M. J.; LaRusso, N. F., Pathobiology of biliary epithelia. *Biochim Biophys Acta Mol Basis Dis* **2018,** *1864* (4 Pt B), 1220-1231.
18. Elborn, J. S., Cystic fibrosis. *Lancet* **2016,** *388* (10059), 2519-2531.
19. Bilzer, M.; Roggel, F.; Gerbes, A. L., Role of Kupffer cells in host defense and liver disease. *Liver Int* **2006,** *26* (10), 1175-86.
20. Kisseleva, T.; Brenner, D. A., Mechanisms of fibrogenesis. *Exp Biol Med (Maywood)* **2008,** *233* (2), 109-22.
21. Kieffer, D. A.; Martin, R. J.; Adams, S. H., Impact of Dietary Fibers on Nutrient

Management and Detoxification Organs: Gut, Liver, and Kidneys. *Adv Nutr* **2016,** *7* (6), 1111-1121.
22. Carpentier, R.; Suner, R. E.; van Hul, N.; Kopp, J. L.; Beaudry, J. B.; Cordi, S.; Antoniou, A.; Raynaud, P.; Lepreux, S.; Jacquemin, P.; Leclercq, I. A.; Sander, M.; Lemaigre, F. P., Embryonic ductal plate cells give rise to cholangiocytes, periportal hepatocytes, and adult liver progenitor cells. *Gastroenterology* **2011,** *141* (4), 1432-8, 1438 e1-4.
23. Boyer, J. L., Bile formation and secretion. *Compr Physiol* **2013,** *3* (3), 1035-78.
24. Itoh, T., Stem/progenitor cells in liver regeneration. *Hepatology* **2016,** *64* (2), 663-8.
25. Banales, J. M.; Huebert, R. C.; Karlsen, T.; Strazzabosco, M.; LaRusso, N. F.; Gores, G. J., Cholangiocyte pathobiology. *Nat Rev Gastroenterol Hepatol* **2019,** *16* (5), 269-281.
26. Jensen, J. M.; Brix, F.; Kohr, P., General and specific aspects of experimental dose measurement in total body irradiation (TBI). *Strahlenther Onkol* **1986,** *162* (4), 250-3.
27. Mederacke, I.; Hsu, C. C.; Troeger, J. S.; Huebener, P.; Mu, X.; Dapito, D. H.; Pradere, J. P.; Schwabe, R. F., Fate tracing reveals hepatic stellate cells as dominant contributors to liver fibrosis independent of its aetiology. *Nat Commun* **2013,** *4*, 2823.
28. Raynaud, P.; Carpentier, R.; Antoniou, A.; Lemaigre, F. P., Biliary differentiation and bile duct morphogenesis in development and disease. *Int J Biochem Cell Biol* **2011,** *43* (2), 245-56.
29. Roskams, T. A.; Theise, N. D.; Balabaud, C.; Bhagat, G.; Bhathal, P. S.; Bioulac-Sage, P.; Brunt, E. M.; Crawford, J. M.; Crosby, H. A.; Desmet, V.; Finegold, M. J.; Geller, S. A.; Gouw, A. S.; Hytiroglou, P.; Knisely, A. S.; Kojiro, M.; Lefkowitch, J. H.; Nakanuma, Y.; Olynyk, J. K.; Park, Y. N.; Portmann, B.; Saxena, R.; Scheuer, P. J.; Strain, A. J.; Thung, S. N.; Wanless, I. R.; West, A. B., Nomenclature of the finer branches of the biliary tree: canals, ductules, and ductular reactions in human livers. *Hepatology* **2004,** *39* (6), 1739-45.
30. Franchitto, A.; Onori, P.; Renzi, A.; Carpino, G.; Mancinelli, R.; Alvaro, D.; Gaudio, E., Recent advances on the mechanisms regulating cholangiocyte proliferation and the significance of the neuroendocrine regulation of cholangiocyte pathophysiology. *Ann Transl Med* **2013,** *1* (3), 27.
31. Roskams, T. A.; Libbrecht, L.; Desmet, V. J., Progenitor cells in diseased human liver. *Semin Liver Dis* **2003,** *23* (4), 385-96.
32. Kisseleva, T.; Brenner, D. A., Is it the end of the line for the EMT? *Hepatology* **2011,** *53* (5), 1433-5.
33. Zeisberg, M.; Yang, C.; Martino, M.; Duncan, M. B.; Rieder, F.; Tanjore, H.; Kalluri, R., Fibroblasts derive from hepatocytes in liver fibrosis via epithelial to mesenchymal transition. *J Biol Chem* **2007,** *282* (32), 23337-47.
34. Poncy, A.; Antoniou, A.; Cordi, S.; Pierreux, C. E.; Jacquemin, P.; Lemaigre, F. P., Transcription factors SOX4 and SOX9 cooperatively control development of bile ducts. *Dev Biol* **2015,** *404* (2), 136-48.
35. Mansini, A. P.; Peixoto, E.; Thelen, K. M.; Gaspari, C.; Jin, S.; Gradilone, S. A., The cholangiocyte primary cilium in health and disease. *Biochim Biophys Acta Mol Basis Dis* **2018,** *1864* (4 Pt B), 1245-1253.

36. Medzhitov, R., Origin and physiological roles of inflammation. *Nature* **2008,** *454* (7203), 428-35.
37. Masyuk, T.; Masyuk, A.; LaRusso, N., Cholangiociliopathies: genetics, molecular mechanisms and potential therapies. *Curr Opin Gastroenterol* **2009,** *25* (3), 265-71.
38. Santos-Laso, A.; Izquierdo-Sanchez, L.; Lee-Law, P. Y.; Perugorria, M. J.; Marzioni, M.; Marin, J. J.; Bujanda, L.; Banales, J. M., New Advances in Polycystic Liver Diseases. *Semin Liver Dis* **2017,** *37* (1), 45-55.
39. van Aerts, R. M. M.; van de Laarschot, L. F. M.; Banales, J. M.; Drenth, J. P. H., Clinical management of polycystic liver disease. *J Hepatol* **2018,** *68* (4), 827-837.
40. Masyuk, T. V.; Masyuk, A. I.; LaRusso, N. F., Polycystic liver disease: The interplay of genes causative for hepatic and renal cystogenesis. *Hepatology* **2018,** *67* (6), 2462-2464.
41. Masyuk, T.; Masyuk, A.; LaRusso, N., Polycystic Liver Diseases: Genetics, Mechanisms, and Therapies. *The Liver: Biology and Pathobiology* **2020**, 408-421.
42. Cadamuro, M.; Fiorotto, R.; Strazzabosco, M., Cholangiocyte Biology and Pathobiology. *The Liver: Biology and Pathobiology* **2020**, 391-407.
43. Lorenzo Pisarello, M.; Masyuk, T. V.; Gradilone, S. A.; Masyuk, A. I.; Ding, J. F.; Lee, P. Y.; LaRusso, N. F., Combination of a Histone Deacetylase 6 Inhibitor and a Somatostatin Receptor Agonist Synergistically Reduces Hepatorenal Cystogenesis in an Animal Model of Polycystic Liver Disease. *Am J Pathol* **2018,** *188* (4), 981-994.
44. Perugorria, M. J.; Masyuk, T. V.; Marin, J. J.; Marzioni, M.; Bujanda, L.; LaRusso, N. F.; Banales, J. M., Polycystic liver diseases: advanced insights into the molecular mechanisms. *Nat Rev Gastroenterol Hepatol* **2014,** *11* (12), 750-61.
45. Waanders, E.; Van Krieken, J. H.; Lameris, A. L.; Drenth, J. P., Disrupted cell adhesion but not proliferation mediates cyst formation in polycystic liver disease. *Mod Pathol* **2008,** *21* (11), 1293-302.
46. Masyuk, A. I.; Masyuk, T. V.; Lorenzo Pisarello, M. J.; Ding, J. F.; Loarca, L.; Huang, B. Q.; LaRusso, N. F., Cholangiocyte autophagy contributes to hepatic cystogenesis in polycystic liver disease and represents a potential therapeutic target. *Hepatology* **2018,** *67* (3), 1088-1108.
47. Banales, J. M.; Cardinale, V.; Carpino, G.; Marzioni, M.; Andersen, J. B.; Invernizzi, P.; Lind, G. E.; Folseraas, T.; Forbes, S. J.; Fouassier, L.; Geier, A.; Calvisi, D. F.; Mertens, J. C.; Trauner, M.; Benedetti, A.; Maroni, L.; Vaquero, J.; Macias, R. I.; Raggi, C.; Perugorria, M. J.; Gaudio, E.; Boberg, K. M.; Marin, J. J.; Alvaro, D., Expert consensus document: Cholangiocarcinoma: current knowledge and future perspectives consensus statement from the European Network for the Study of Cholangiocarcinoma (ENS-CCA). *Nat Rev Gastroenterol Hepatol* **2016,** *13* (5), 261-80.
48. Bridgewater, J.; Galle, P. R.; Khan, S. A.; Llovet, J. M.; Park, J. W.; Patel, T.; Pawlik, T. M.; Gores, G. J., Guidelines for the diagnosis and management of intrahepatic cholangiocarcinoma. *J Hepatol* **2014,** *60* (6), 1268-89.
49. Komuta, M.; Govaere, O.; Vandecaveye, V.; Akiba, J.; Van Steenbergen, W.; Verslype, C.; Laleman, W.; Pirenne, J.; Aerts, R.; Yano, H.; Nevens, F.; Topal, B.; Roskams, T., Histological diversity in cholangiocellular carcinoma reflects the different cholangiocyte phenotypes. *Hepatology* **2012,** *55* (6), 1876-88.
50. Aishima, S.; Oda, Y., Pathogenesis and classification of intrahepatic cholangiocarcinoma:

different characters of perihilar large duct type versus peripheral small duct type. *J Hepatobiliary Pancreat Sci* **2015,** *22* (2), 94-100.
51. Rizvi, S.; Gores, G. J., Pathogenesis, diagnosis, and management of cholangiocarcinoma. *Gastroenterology* **2013,** *145* (6), 1215-29.
52. Nakamura, H.; Arai, Y.; Totoki, Y.; Shirota, T.; Elzawahry, A.; Kato, M.; Hama, N.; Hosoda, F.; Urushidate, T.; Ohashi, S.; Hiraoka, N.; Ojima, H.; Shimada, K.; Okusaka, T.; Kosuge, T.; Miyagawa, S.; Shibata, T., Genomic spectra of biliary tract cancer. *Nat Genet* **2015,** *47* (9), 1003-10.
53. Cardinale, V.; Carpino, G.; Reid, L.; Gaudio, E.; Alvaro, D., Multiple cells of origin in cholangiocarcinoma underlie biological, epidemiological and clinical heterogeneity. *World J Gastrointest Oncol* **2012,** *4* (5), 94-102.
54. Nakanuma, Y.; Sato, Y.; Harada, K.; Sasaki, M.; Xu, J.; Ikeda, H., Pathological classification of intrahepatic cholangiocarcinoma based on a new concept. *World J Hepatol* **2010,** *2* (12), 419-27.
55. Yuan, D.; Huang, S.; Berger, E.; Liu, L.; Gross, N.; Heinzmann, F.; Ringelhan, M.; Connor, T. O.; Stadler, M.; Meister, M.; Weber, J.; Ollinger, R.; Simonavicius, N.; Reisinger, F.; Hartmann, D.; Meyer, R.; Reich, M.; Seehawer, M.; Leone, V.; Hochst, B.; Wohlleber, D.; Jors, S.; Prinz, M.; Spalding, D.; Protzer, U.; Luedde, T.; Terracciano, L.; Matter, M.; Longerich, T.; Knolle, P.; Ried, T.; Keitel, V.; Geisler, F.; Unger, K.; Cinnamon, E.; Pikarsky, E.; Huser, N.; Davis, R. J.; Tschaharganeh, D. F.; Rad, R.; Weber, A.; Zender, L.; Haller, D.; Heikenwalder, M., Kupffer Cell-Derived Tnf Triggers Cholangiocellular Tumorigenesis through JNK due to Chronic Mitochondrial Dysfunction and ROS. *Cancer Cell* **2017,** *31* (6), 771-789 e6.
56. Khan, S. A.; Thomas, H. C.; Davidson, B. R.; Taylor-Robinson, S. D., Cholangiocarcinoma. *Lancet* **2005,** *366* (9493), 1303-14.
57. Sirica, A. E., Cholangiocarcinoma: molecular targeting strategies for chemoprevention and therapy. *Hepatology* **2005,** *41* (1), 5-15.
58. Doherty, B.; Nambudiri, V. E.; Palmer, W. C., Update on the Diagnosis and Treatment of Cholangiocarcinoma. *Curr Gastroenterol Rep* **2017,** *19* (1), 2.
59. Hama, T.; Nakanishi, K.; Sato, M.; Mukaiyama, H.; Togawa, H.; Shima, Y.; Miyajima, M.; Nozu, K.; Nagao, S.; Takahashi, H.; Sako, M.; Iijima, K.; Yoshikawa, N.; Suzuki, H., Aberrant Smad3 phosphoisoforms in cyst-lining epithelial cells in the cpk mouse, a model of autosomal recessive polycystic kidney disease. *Am J Physiol Renal Physiol* **2017,** *313* (6), F1223-F1231.
60. Cubero, F. J.; Mohamed, M. R.; Woitok, M. M.; Zhao, G.; Hatting, M.; Nevzorova, Y. A.; Chen, C.; Haybaeck, J.; de Bruin, A.; Avila, M. A.; Boekschoten, M. V.; Davis, R. J.; Trautwein, C., Loss of c-Jun N-terminal Kinase 1 and 2 Function in Liver Epithelial Cells Triggers Biliary Hyperproliferation Resembling Cholangiocarcinoma. *Hepatol Commun* **2020,** *4* (6), 834-851.
61. Yang, Y. M.; Kim, S. Y.; Seki, E., Inflammation and Liver Cancer: Molecular Mechanisms and Therapeutic Targets. *Semin Liver Dis* **2019,** *39* (1), 26-42.
62. Manieri, E.; Folgueira, C.; Rodriguez, M. E.; Leiva-Vega, L.; Esteban-Lafuente, L.; Chen, C.; Cubero, F. J.; Barrett, T.; Cavanagh-Kyros, J.; Seruggia, D.; Rosell, A.; Sanchez-Cabo, F.; Gomez, M. J.; Monte, M. J.; JJ, G. M.; Davis, R. J.; Mora, A.;

Sabio, G., JNK-mediated disruption of bile acid homeostasis promotes intrahepatic cholangiocarcinoma. *Proc Natl Acad Sci U S A* **2020,** *117* (28), 16492-16499.
63. Hay, E. D., Organization and fine structure of epithelium and mesenchyme in the developing chick embryo. *Epithel. Mesenchymal Interact.* **1968,** *2*, 31-35.
64. Brabletz, T.; Kalluri, R.; Nieto, M. A.; Weinberg, R. A., EMT in cancer. *Nat Rev Cancer* **2018,** *18* (2), 128-134.
65. Zhang, Q.; Agoston, A. T.; Pham, T. H.; Zhang, W.; Zhang, X.; Huo, X.; Peng, S.; Bajpai, M.; Das, K.; Odze, R. D.; Spechler, S. J.; Souza, R. F., Acidic Bile Salts Induce Epithelial to Mesenchymal Transition via VEGF Signaling in Non-Neoplastic Barrett's Cells. *Gastroenterology* **2019,** *156* (1), 130-144 e10.
66. Kokuryo, T.; Yokoyama, Y.; Nagino, M., Recent advances in cancer stem cell research for cholangiocarcinoma. *J Hepatobiliary Pancreat Sci* **2012,** *19* (6), 606-13.
67. Glaser, S. S.; Gaudio, E.; Miller, T.; Alvaro, D.; Alpini, G., Cholangiocyte proliferation and liver fibrosis. *Expert Rev Mol Med* **2009,** *11*, e7.
68. Alvaro, D.; Mancino, M. G.; Glaser, S.; Gaudio, E.; Marzioni, M.; Francis, H.; Alpini, G., Proliferating cholangiocytes: a neuroendocrine compartment in the diseased liver. *Gastroenterology* **2007,** *132* (1), 415-31.
69. Lee, J. S.; Heo, J.; Libbrecht, L.; Chu, I. S.; Kaposi-Novak, P.; Calvisi, D. F.; Mikaelyan, A.; Roberts, L. R.; Demetris, A. J.; Sun, Z.; Nevens, F.; Roskams, T.; Thorgeirsson, S. S., A novel prognostic subtype of human hepatocellular carcinoma derived from hepatic progenitor cells. *Nat Med* **2006,** *12* (4), 410-6.
70. Zhang, F.; Chen, X. P.; Zhang, W.; Dong, H. H.; Xiang, S.; Zhang, W. G.; Zhang, B. X., Combined hepatocellular cholangiocarcinoma originating from hepatic progenitor cells: immunohistochemical and double-fluorescence immunostaining evidence. *Histopathology* **2008,** *52* (2), 224-32.
71. Kumar, M.; Zhao, X.; Wang, X. W., Molecular carcinogenesis of hepatocellular carcinoma and intrahepatic cholangiocarcinoma: one step closer to personalized medicine? *Cell Biosci* **2011,** *1* (1), 5.
72. Theise, N. D.; Yao, J. L.; Harada, K.; Hytiroglou, P.; Portmann, B.; Thung, S. N.; Tsui, W.; Ohta, H.; Nakanuma, Y., Hepatic 'stem cell' malignancies in adults: four cases. *Histopathology* **2003,** *43* (3), 263-71.
73. Chiba, T.; Kita, K.; Zheng, Y. W.; Yokosuka, O.; Saisho, H.; Iwama, A.; Nakauchi, H.; Taniguchi, H., Side population purified from hepatocellular carcinoma cells harbors cancer stem cell-like properties. *Hepatology* **2006,** *44* (1), 240-51.
74. Zhang, J.; Tian, X. J.; Xing, J., Signal Transduction Pathways of EMT Induced by TGF-beta, SHH, and WNT and Their Crosstalks. *J Clin Med* **2016,** *5* (4).
75. Vaquero, J.; Guedj, N.; Claperon, A.; Nguyen Ho-Bouldoires, T. H.; Paradis, V.; Fouassier, L., Epithelial-mesenchymal transition in cholangiocarcinoma: From clinical evidence to regulatory networks. *J Hepatol* **2017,** *66* (2), 424-441.
76. Jakowlew, S. B., Transforming growth factor-beta in cancer and metastasis. *Cancer Metastasis Rev* **2006,** *25* (3), 435-57.
77. Heldin, C. H.; Landstrom, M.; Moustakas, A., Mechanism of TGF-beta signaling to growth arrest, apoptosis, and epithelial-mesenchymal transition. *Curr Opin Cell Biol* **2009,** *21* (2), 166-76.

78. Seoane, J., Escaping from the TGFbeta anti-proliferative control. *Carcinogenesis* **2006,** *27* (11), 2148-56.
79. Sheahan, S.; Bellamy, C. O.; Dunbar, D. R.; Harrison, D. J.; Prost, S., Deficiency of G1 regulators P53, P21Cip1 and/or pRb decreases hepatocyte sensitivity to TGFbeta cell cycle arrest. *BMC Cancer* **2007,** *7*, 215.
80. Connolly, E. C.; Freimuth, J.; Akhurst, R. J., Complexities of TGF-beta targeted cancer therapy. *Int J Biol Sci* **2012,** *8* (7), 964-78.
81. Yamamura, Y.; Hua, X.; Bergelson, S.; Lodish, H. F., Critical role of Smads and AP-1 complex in transforming growth factor-beta -dependent apoptosis. *J Biol Chem* **2000,** *275* (46), 36295-302.
82. Giannelli, G.; Koudelkova, P.; Dituri, F.; Mikulits, W., Role of epithelial to mesenchymal transition in hepatocellular carcinoma. *J Hepatol* **2016,** *65* (4), 798-808.
83. Chen, C.; Nelson, L. J.; Avila, M. A.; Cubero, F. J., Mitogen-Activated Protein Kinases (MAPKs) and Cholangiocarcinoma: The Missing Link. *Cells* **2019,** *8* (10).
84. Win, S.; Than, T. A.; Zhang, J.; Oo, C.; Min, R. W. M.; Kaplowitz, N., New insights into the role and mechanism of c-Jun-N-terminal kinase signaling in the pathobiology of liver diseases. *Hepatology* **2018,** *67* (5), 2013-2024.
85. Win, S.; Than, T. A.; Min, R. W.; Aghajan, M.; Kaplowitz, N., c-Jun N-terminal kinase mediates mouse liver injury through a novel Sab (SH3BP5)-dependent pathway leading to inactivation of intramitochondrial Src. *Hepatology* **2016,** *63* (6), 1987-2003.
86. Mingo-Sion, A. M.; Marietta, P. M.; Koller, E.; Wolf, D. M.; Van Den Berg, C. L., Inhibition of JNK reduces G2/M transit independent of p53, leading to endoreduplication, decreased proliferation, and apoptosis in breast cancer cells. *Oncogene* **2004,** *23* (2), 596-604.
87. Vivanco, I.; Palaskas, N.; Tran, C.; Finn, S. P.; Getz, G.; Kennedy, N. J.; Jiao, J.; Rose, J.; Xie, W.; Loda, M.; Golub, T.; Mellinghoff, I. K.; Davis, R. J.; Wu, H.; Sawyers, C. L., Identification of the JNK signaling pathway as a functional target of the tumor suppressor PTEN. *Cancer Cell* **2007,** *11* (6), 555-69.
88. Wang, J.; Tai, G., Role of C-Jun N-terminal Kinase in Hepatocellular Carcinoma Development. *Target Oncol* **2016,** *11* (6), 723-738.
89. Cubero, F. J.; Zhao, G.; Nevzorova, Y. A.; Hatting, M.; Al Masaoudi, M.; Verdier, J.; Peng, J.; Schaefer, F. M.; Hermanns, N.; Boekschoten, M. V.; Grouls, C.; Gassler, N.; Kiessling, F.; Muller, M.; Davis, R. J.; Liedtke, C.; Trautwein, C., Haematopoietic cell-derived Jnk1 is crucial for chronic inflammation and carcinogenesis in an experimental model of liver injury. *J Hepatol* **2015,** *62* (1), 140-9.
90. Das, M.; Garlick, D. S.; Greiner, D. L.; Davis, R. J., The role of JNK in the development of hepatocellular carcinoma. *Genes Dev* **2011,** *25* (6), 634-45.
91. Han, M. S.; Barrett, T.; Brehm, M. A.; Davis, R. J., Inflammation Mediated by JNK in Myeloid Cells Promotes the Development of Hepatitis and Hepatocellular Carcinoma. *Cell Rep* **2016,** *15* (1), 19-26.
92. Chen, F., JNK-induced apoptosis, compensatory growth, and cancer stem cells. *Cancer Res* **2012,** *72* (2), 379-86.
93. Seki, E.; Brenner, D. A.; Karin, M., A liver full of JNK: signaling in regulation of cell function and disease pathogenesis, and clinical approaches. *Gastroenterology* **2012,** *143* (2),

307-20.
94. Chang, Q.; Zhang, Y.; Beezhold, K. J.; Bhatia, D.; Zhao, H.; Chen, J.; Castranova, V.; Shi, X.; Chen, F., Sustained JNK1 activation is associated with altered histone H3 methylations in human liver cancer. *J Hepatol* **2009,** *50* (2), 323-33.
95. Dhanasekaran, D. N.; Reddy, E. P., JNK signaling in apoptosis. *Oncogene* **2008,** *27* (48), 6245-51.
96. Zhong, F.; Tong, Z. T.; Fan, L. L.; Zha, L. X.; Wang, F.; Yao, M. Q.; Gu, K. S.; Cao, Y. X., Guggulsterone-induced apoptosis in cholangiocarcinoma cells through ROS/JNK signaling pathway. *Am J Cancer Res* **2016,** *6* (2), 226-37.
97. Kamiya, A.; Gonzalez, F. J., TNF-alpha regulates mouse fetal hepatic maturation induced by oncostatin M and extracellular matrices. *Hepatology* **2004,** *40* (3), 527-36.
98. In *Guide for the Care and Use of Laboratory Animals*, th, Ed. Washington (DC), 2011.
99. Cubero, F. J.; Zoubek, M. E.; Hu, W.; Peng, J.; Zhao, G.; Nevzorova, Y. A.; Al Masaoudi, M.; Bechmann, L. P.; Boekschoten, M. V.; Muller, M.; Preisinger, C.; Gassler, N.; Canbay, A. E.; Luedde, T.; Davis, R. J.; Liedtke, C.; Trautwein, C., Combined Activities of JNK1 and JNK2 in Hepatocytes Protect Against Toxic Liver Injury. *Gastroenterology* **2016,** *150* (4), 968-81.
100. Donato, M. T.; Tolosa, L.; Gomez-Lechon, M. J., Culture and Functional Characterization of Human Hepatoma HepG2 Cells. *Methods Mol Biol* **2015,** *1250*, 77-93.
101. McGill, M. R.; Yan, H. M.; Ramachandran, A.; Murray, G. J.; Rollins, D. E.; Jaeschke, H., HepaRG cells: a human model to study mechanisms of acetaminophen hepatotoxicity. *Hepatology* **2011,** *53* (3), 974-82.
102. Pfaffl, M. W., A new mathematical model for relative quantification in real-time RT-PCR. *Nucleic Acids Res* **2001,** *29* (9), e45.
103. An, L.; Wang, X.; Cederbaum, A. I., Cytokines in alcoholic liver disease. *Arch Toxicol* **2012,** *86* (9), 1337-48.
104. Kurien, B. T.; Scofield, R. H., Western blotting. *Methods* **2006,** *38* (4), 283-93.
105. Das, M.; Jiang, F.; Sluss, H. K.; Zhang, C.; Shokat, K. M.; Flavell, R. A.; Davis, R. J., Suppression of p53-dependent senescence by the JNK signal transduction pathway. *Proc Natl Acad Sci U S A* **2007,** *104* (40), 15759-64.
106. Das, M.; Sabio, G.; Jiang, F.; Rincon, M.; Flavell, R. A.; Davis, R. J., Induction of hepatitis by JNK-mediated expression of TNF-alpha. *Cell* **2009,** *136* (2), 249-60.
107. Stocker, J. T.; Ishak, K. G., Mesenchymal hamartoma of the liver: report of 30 cases and review of the literature. *Pediatr Pathol* **1983,** *1* (3), 245-67.
108. Luedde, T.; Kaplowitz, N.; Schwabe, R. F., Cell death and cell death responses in liver disease: mechanisms and clinical relevance. *Gastroenterology* **2014,** *147* (4), 765-783 e4.
109. Quante, M.; Tu, S. P.; Tomita, H.; Gonda, T.; Wang, S. S.; Takashi, S.; Baik, G. H.; Shibata, W.; Diprete, B.; Betz, K. S.; Friedman, R.; Varro, A.; Tycko, B.; Wang, T. C., Bone marrow-derived myofibroblasts contribute to the mesenchymal stem cell niche and promote tumor growth. *Cancer Cell* **2011,** *19* (2), 257-72.
110. Petersen, B. E.; Goff, J. P.; Greenberger, J. S.; Michalopoulos, G. K., Hepatic oval cells express the hematopoietic stem cell marker Thy-1 in the rat. *Hepatology* **1998,** *27* (2), 433-45.
111. Tarlow, B. D.; Finegold, M. J.; Grompe, M., Clonal tracing of Sox9+ liver progenitors in

mouse oval cell injury. *Hepatology* **2014,** *60* (1), 278-89.
112. Ferrarotto, R.; Mitani, Y.; Diao, L.; Guijarro, I.; Wang, J.; Zweidler-McKay, P.; Bell, D.; William, W. N., Jr.; Glisson, B. S.; Wick, M. J.; Kapoun, A. M.; Patnaik, A.; Eckhardt, G.; Munster, P.; Faoro, L.; Dupont, J.; Lee, J. J.; Futreal, A.; El-Naggar, A. K.; Heymach, J. V., Activating NOTCH1 Mutations Define a Distinct Subgroup of Patients With Adenoid Cystic Carcinoma Who Have Poor Prognosis, Propensity to Bone and Liver Metastasis, and Potential Responsiveness to Notch1 Inhibitors. *J Clin Oncol* **2017,** *35* (3), 352-360.
113. Hyun, J.; Oh, S. H.; Premont, R. T.; Guy, C. D.; Berg, C. L.; Diehl, A. M., Dysregulated activation of fetal liver programme in acute liver failure. *Gut* **2019,** *68* (6), 1076-1087.
114. Masyuk, T. V.; Radtke, B. N.; Stroope, A. J.; Banales, J. M.; Gradilone, S. A.; Huang, B.; Masyuk, A. I.; Hogan, M. C.; Torres, V. E.; Larusso, N. F., Pasireotide is more effective than octreotide in reducing hepatorenal cystogenesis in rodents with polycystic kidney and liver diseases. *Hepatology* **2013,** *58* (1), 409-21.
115. Santos-Laso, A.; Izquierdo-Sanchez, L.; Rodrigues, P. M.; Huang, B. Q.; Azkargorta, M.; Lapitz, A.; Munoz-Garrido, P.; Arbelaiz, A.; Caballero-Camino, F. J.; Fernandez-Barrena, M. G.; Jimenez-Aguero, R.; Argemi, J.; Aragon, T.; Elortza, F.; Marzioni, M.; Drenth, J. P. H.; LaRusso, N. F.; Bujanda, L.; Perugorria, M. J.; Banales, J. M., Proteostasis disturbances and endoplasmic reticulum stress contribute to polycystic liver disease: New therapeutic targets. *Liver Int* **2020,** *40* (7), 1670-1685.
116. Hetz, C.; Chevet, E.; Oakes, S. A., Proteostasis control by the unfolded protein response. *Nat Cell Biol* **2015,** *17* (7), 829-38.
117. Hernandez-Alvarez, M. I.; Sebastian, D.; Vives, S.; Ivanova, S.; Bartoccioni, P.; Kakimoto, P.; Plana, N.; Veiga, S. R.; Hernandez, V.; Vasconcelos, N.; Peddinti, G.; Adrover, A.; Jove, M.; Pamplona, R.; Gordaliza-Alaguero, I.; Calvo, E.; Cabre, N.; Castro, R.; Kuzmanic, A.; Boutant, M.; Sala, D.; Hyotylainen, T.; Oresic, M.; Fort, J.; Errasti-Murugarren, E.; Rodrigues, C. M. P.; Orozco, M.; Joven, J.; Canto, C.; Palacin, M.; Fernandez-Veledo, S.; Vendrell, J.; Zorzano, A., Deficient Endoplasmic Reticulum-Mitochondrial Phosphatidylserine Transfer Causes Liver Disease. *Cell* **2019,** *177* (4), 881-895 e17.
118. Uskokovic-Markovic, S.; Milenkovic, M.; Topic, A.; Kotur-Stevuljevic, J.; Stefanovic, A.; Antic-Stankovic, J., Protective effects of tungstophosphoric acid and sodium tungstate on chemically induced liver necrosis in wistar rats. *J Pharm Pharm Sci* **2007,** *10* (3), 340-9.
119. J. F. L. Childs, E. A. S., Controlling orange decay. *Ind. Eng. Chem.,* **1946,** *38 (1)*, pp 82–87.
120. Dyroff, M. C.; Neal, R. A., Studies of the mechanism of metabolism of thioacetamide s-oxide by rat liver microsomes. *Mol Pharmacol* **1983,** *23* (1), 219-27.
121. Gordon, C. T.; Tan, T. Y.; Benko, S.; Fitzpatrick, D.; Lyonnet, S.; Farlie, P. G., Long-range regulation at the SOX9 locus in development and disease. *J Med Genet* **2009,** *46* (10), 649-56.
122. Chiang, J. Y., Hepatocyte nuclear factor 4alpha regulation of bile acid and drug metabolism. *Expert Opin Drug Metab Toxicol* **2009,** *5* (2), 137-47.
123. Carotenuto, P.; Fassan, M.; Pandolfo, R.; Lampis, A.; Vicentini, C.; Cascione, L.;

Paulus-Hock, V.; Boulter, L.; Guest, R.; Quagliata, L.; Hahne, J. C.; Ridgway, R.; Jamieson, T.; Athineos, D.; Veronese, A.; Visone, R.; Murgia, C.; Ferrari, G.; Guzzardo, V.; Evans, T. R. J.; MacLeod, M.; Feng, G. J.; Dale, T.; Negrini, M.; Forbes, S. J.; Terracciano, L.; Scarpa, A.; Patel, T.; Valeri, N.; Workman, P.; Sansom, O.; Braconi, C., Wnt signalling modulates transcribed-ultraconserved regions in hepatobiliary cancers. *Gut* **2017,** *66* (7), 1268-1277.

124. Rittie, L., Method for Picrosirius Red-Polarization Detection of Collagen Fibers in Tissue Sections. *Methods Mol Biol* **2017,** *1627*, 395-407.

125. Grasl-Kraupp, B.; Ruttkay-Nedecky, B.; Koudelka, H.; Bukowska, K.; Bursch, W.; Schulte-Hermann, R., In situ detection of fragmented DNA (TUNEL assay) fails to discriminate among apoptosis, necrosis, and autolytic cell death: a cautionary note. *Hepatology* **1995,** *21* (5), 1465-8.

126. Fan, Y.; Bergmann, A., Apoptosis-induced compensatory proliferation. The Cell is dead. Long live the Cell! *Trends Cell Biol* **2008,** *18* (10), 467-73.

127. Dolmans, R. A.; Boel, C. H.; Lacle, M. M.; Kusters, J. G., Clinical Manifestations, Treatment, and Diagnosis of Tropheryma whipplei Infections. *Clin Microbiol Rev* **2017,** *30* (2), 529-555.

128. Kasprzak, A.; Adamek, A., Mucins: the Old, the New and the Promising Factors in Hepatobiliary Carcinogenesis. *Int J Mol Sci* **2019,** *20* (6).

129. Wang, J.; Wang, H.; Peters, M.; Ding, N.; Ribback, S.; Utpatel, K.; Cigliano, A.; Dombrowski, F.; Xu, M.; Chen, X.; Song, X.; Che, L.; Evert, M.; Cossu, A.; Gordan, J.; Zeng, Y.; Chen, X.; Calvisi, D. F., Loss of Fbxw7 synergizes with activated Akt signaling to promote c-Myc dependent cholangiocarcinogenesis. *J Hepatol* **2019,** *71* (4), 742-752.

130. Lutterbach, B.; Hann, S. R., Hierarchical phosphorylation at N-terminal transformation-sensitive sites in c-Myc protein is regulated by mitogens and in mitosis. *Mol Cell Biol* **1994,** *14* (8), 5510-22.

131. Reeves, H. L.; Narla, G.; Ogunbiyi, O.; Haq, A. I.; Katz, A.; Benzeno, S.; Hod, E.; Harpaz, N.; Goldberg, S.; Tal-Kremer, S.; Eng, F. J.; Arthur, M. J.; Martignetti, J. A.; Friedman, S. L., Kruppel-like factor 6 (KLF6) is a tumor-suppressor gene frequently inactivated in colorectal cancer. *Gastroenterology* **2004,** *126* (4), 1090-103.

132. Ehedego, H.; Boekschoten, M. V.; Hu, W.; Doler, C.; Haybaeck, J.; Gabetaler, N.; Muller, M.; Liedtke, C.; Trautwein, C., p21 ablation in liver enhances DNA damage, cholestasis, and carcinogenesis. *Cancer Res* **2015,** *75* (6), 1144-55.

133. Willenbring, H.; Sharma, A. D.; Vogel, A.; Lee, A. Y.; Rothfuss, A.; Wang, Z.; Finegold, M.; Grompe, M., Loss of p21 permits carcinogenesis from chronically damaged liver and kidney epithelial cells despite unchecked apoptosis. *Cancer Cell* **2008,** *14* (1), 59-67.

134. Mu, X.; Pradere, J. P.; Affo, S.; Dapito, D. H.; Friedman, R.; Lefkovitch, J. H.; Schwabe, R. F., Epithelial Transforming Growth Factor-beta Signaling Does Not Contribute to Liver Fibrosis but Protects Mice From Cholangiocarcinoma. *Gastroenterology* **2016,** *150* (3), 720-33.

135. Sekiya, S.; Suzuki, A., Intrahepatic cholangiocarcinoma can arise from Notch-mediated conversion of hepatocytes. *J Clin Invest* **2012,** *122* (11), 3914-8.

136. Carpino, G.; Cardinale, V.; Folseraas, T.; Overi, D.; Floreani, A.; Franchitto, A.; Onori, P.; Cazzagon, N.; Berloco, P. B.; Karlsen, T. H.; Alvaro, D.; Gaudio, E., Hepatic

Stem/Progenitor Cell Activation Differs between Primary Sclerosing and Primary Biliary Cholangitis. *Am J Pathol* **2018,** *188* (3), 627-639.
137. Long, J.; Wang, H.; Lang, Z.; Wang, T.; Long, M.; Wang, B., Expression level of glutamine synthetase is increased in hepatocellular carcinoma and liver tissue with cirrhosis and chronic hepatitis B. *Hepatol Int* **2011,** *5* (2), 698-706.
138. Uehara, T.; Pogribny, I. P.; Rusyn, I., The DEN and CCl4 -Induced Mouse Model of Fibrosis and Inflammation-Associated Hepatocellular Carcinoma. *Curr Protoc Pharmacol* **2014,** *66*, 14 30 1-10.
139. Shaib, Y.; El-Serag, H. B., The epidemiology of cholangiocarcinoma. *Semin Liver Dis* **2004,** *24* (2), 115-25.
140. Lager, D. J.; Qian, Q.; Bengal, R. J.; Ishibashi, M.; Torres, V. E., The pck rat: a new model that resembles human autosomal dominant polycystic kidney and liver disease. *Kidney Int* **2001,** *59* (1), 126-36.
141. Fabris, L.; Strazzabosco, M., Epithelial-mesenchymal interactions in biliary diseases. *Semin Liver Dis* **2011,** *31* (1), 11-32.
142. Inagaki, Y.; Okazaki, I., Emerging insights into Transforming growth factor beta Smad signal in hepatic fibrogenesis. *Gut* **2007,** *56* (2), 284-92.
143. Lee, Y. A.; Friedman, S. L., Stellate Cells and Fibrosis. *The Liver: Biology and Pathobiology* **2020**, 444-454.
144. Yovchev, M. I.; Grozdanov, P. N.; Joseph, B.; Gupta, S.; Dabeva, M. D., Novel hepatic progenitor cell surface markers in the adult rat liver. *Hepatology* **2007,** *45* (1), 139-49.
145. Mall, A. S.; Tyler, M. G.; Ho, S. B.; Krige, J. E.; Kahn, D.; Spearman, W.; Myer, L.; Govender, D., The expression of MUC mucin in cholangiocarcinoma. *Pathol Res Pract* **2010,** *206* (12), 805-9.
146. Strnad, P.; McElvaney, N. G.; Lomas, D. A., Alpha1-Antitrypsin Deficiency. *N Engl J Med* **2020,** *382* (15), 1443-1455.
147. Kimmelman, A. C.; Qiao, R. F.; Narla, G.; Banno, A.; Lau, N.; Bos, P. D.; Nunez Rodriguez, N.; Liang, B. C.; Guha, A.; Martignetti, J. A.; Friedman, S. L.; Chan, A. M., Suppression of glioblastoma tumorigenicity by the Kruppel-like transcription factor KLF6. *Oncogene* **2004,** *23* (29), 5077-83.
148. Patel, D.; Teckman, J. H., Alpha-1-Antitrypsin Deficiency Liver Disease. *Clin Liver Dis* **2018,** *22* (4), 643-655.
149. Walker, R. M.; Racz, W. J.; McElligott, T. F., Scanning electron microscopic examination of acetaminophen-induced hepatotoxicity and congestion in mice. *Am J Pathol* **1983,** *113* (3), 321-30.
150. Dara, L.; Kaplowitz, N., Drug‐Induced Liver Injury. *The Liver: Biology and Pathobiology* **2020**, 701-713.
151. Win, S.; Than, T. A.; Han, D.; Petrovic, L. M.; Kaplowitz, N., c-Jun N-terminal kinase (JNK)-dependent acute liver injury from acetaminophen or tumor necrosis factor (TNF) requires mitochondrial Sab protein expression in mice. *J Biol Chem* **2011,** *286* (40), 35071-8.
152. Malhi, H.; Gores, G. J., Hepatocyte Apoptosis: Mechanisms and Relevance in Liver Diseases. *The Liver: Biology and Pathobiology* **2020**, 195-205.
153. Sun, L.; Wang, H.; Wang, Z.; He, S.; Chen, S.; Liao, D.; Wang, L.; Yan, J.; Liu, W.; Lei, X.; Wang, X., Mixed lineage kinase domain-like protein mediates necrosis

signaling downstream of RIP3 kinase. *Cell* **2012,** *148* (1-2), 213-27.
154. Zhao, J.; Jitkaew, S.; Cai, Z.; Choksi, S.; Li, Q.; Luo, J.; Liu, Z. G., Mixed lineage kinase domain-like is a key receptor interacting protein 3 downstream component of TNF-induced necrosis. *Proc Natl Acad Sci U S A* **2012,** *109* (14), 5322-7.
155. Wang, H.; Sun, L.; Su, L.; Rizo, J.; Liu, L.; Wang, L. F.; Wang, F. S.; Wang, X., Mixed lineage kinase domain-like protein MLKL causes necrotic membrane disruption upon phosphorylation by RIP3. *Mol Cell* **2014,** *54* (1), 133-146.
156. Fausto, N., Mouse liver tumorigenesis: models, mechanisms, and relevance to human disease. *Seminars in liver disease* **1999,** *19* (3), 243-52.
157. Grivennikov, S. I.; Greten, F. R.; Karin, M., Immunity, inflammation, and cancer. *Cell* **2010,** *140* (6), 883-99.
158. Labib, P. L.; Goodchild, G.; Pereira, S. P., Molecular Pathogenesis of Cholangiocarcinoma. *BMC Cancer* **2019,** *19* (1), 185.
159. Seehawer, M.; Heinzmann, F.; D'Artista, L.; Harbig, J.; Roux, P. F.; Hoenicke, L.; Dang, H.; Klotz, S.; Robinson, L.; Dore, G.; Rozenblum, N.; Kang, T. W.; Chawla, R.; Buch, T.; Vucur, M.; Roth, M.; Zuber, J.; Luedde, T.; Sipos, B.; Longerich, T.; Heikenwalder, M.; Wang, X. W.; Bischof, O.; Zender, L., Necroptosis microenvironment directs lineage commitment in liver cancer. *Nature* **2018,** *562* (7725), 69-75.
160. Chang, L.; Karin, M., Mammalian MAP kinase signalling cascades. *Nature* **2001,** *410* (6824), 37-40.
161. Cuylen, S.; Blaukopf, C.; Politi, A. Z.; Muller-Reichert, T.; Neumann, B.; Poser, I.; Ellenberg, J.; Hyman, A. A.; Gerlich, D. W., Ki-67 acts as a biological surfactant to disperse mitotic chromosomes. *Nature* **2016,** *535* (7611), 308-12.
162. Bowman, G. D.; O'Donnell, M.; Kuriyan, J., Structural analysis of a eukaryotic sliding DNA clamp-clamp loader complex. *Nature* **2004,** *429* (6993), 724-30.
163. Roskams, T.; Desmet, V., Ductular reaction and its diagnostic significance. *Semin Diagn Pathol* **1998,** *15* (4), 259-69.
164. Diaz, R.; Kim, J. W.; Hui, J. J.; Li, Z.; Swain, G. P.; Fong, K. S.; Csiszar, K.; Russo, P. A.; Rand, E. B.; Furth, E. E.; Wells, R. G., Evidence for the epithelial to mesenchymal transition in biliary atresia fibrosis. *Hum Pathol* **2008,** *39* (1), 102-15.
165. Burns, W. C.; Kantharidis, P.; Thomas, M. C., The role of tubular epithelial-mesenchymal transition in progressive kidney disease. *Cells Tissues Organs* **2007,** *185* (1-3), 222-31.
166. Robertson, H.; Ali, S.; McDonnell, B. J.; Burt, A. D.; Kirby, J. A., Chronic renal allograft dysfunction: the role of T cell-mediated tubular epithelial to mesenchymal cell transition. *J Am Soc Nephrol* **2004,** *15* (2), 390-7.
167. Planas-Paz, L.; Orsini, V.; Boulter, L.; Calabrese, D.; Pikiolek, M.; Nigsch, F.; Xie, Y.; Roma, G.; Donovan, A.; Marti, P.; Beckmann, N.; Dill, M. T.; Carbone, W.; Bergling, S.; Isken, A.; Mueller, M.; Kinzel, B.; Yang, Y.; Mao, X.; Nicholson, T. B.; Zamponi, R.; Capodieci, P.; Valdez, R.; Rivera, D.; Loew, A.; Ukomadu, C.; Terracciano, L. M.; Bouwmeester, T.; Cong, F.; Heim, M. H.; Forbes, S. J.; Ruffner, H.; Tchorz, J. S., The RSPO-LGR4/5-ZNRF3/RNF43 module controls liver zonation and size. *Nat Cell Biol* **2016,** *18* (5), 467-79.
168. Guest, R. V.; Boulter, L.; Dwyer, B. J.; Forbes, S. J., Understanding liver regeneration

to bring new insights to the mechanisms driving cholangiocarcinoma. *NPJ Regen Med* **2017,** *2*, 13.
169. Zong, Y.; Panikkar, A.; Xu, J.; Antoniou, A.; Raynaud, P.; Lemaigre, F.; Stanger, B. Z., Notch signaling controls liver development by regulating biliary differentiation. *Development* **2009,** *136* (10), 1727-39.
170. Al-Bahrani, R.; Abuetabh, Y.; Zeitouni, N.; Sergi, C., Cholangiocarcinoma: risk factors, environmental influences and oncogenesis. *Ann Clin Lab Sci* **2013,** *43* (2), 195-210.
171. Isomoto, H.; Kobayashi, S.; Werneburg, N. W.; Bronk, S. F.; Guicciardi, M. E.; Frank, D. A.; Gores, G. J., Interleukin 6 upregulates myeloid cell leukemia-1 expression through a STAT3 pathway in cholangiocarcinoma cells. *Hepatology* **2005,** *42* (6), 1329-38.
172. Heldin, C. H.; Miyazono, K.; ten Dijke, P., TGF-beta signalling from cell membrane to nucleus through SMAD proteins. *Nature* **1997,** *390* (6659), 465-71.
173. Zhang, Y. E., Non-Smad pathways in TGF-beta signaling. *Cell Res* **2009,** *19* (1), 128-39.
174. Yamashita, M.; Fatyol, K.; Jin, C.; Wang, X.; Liu, Z.; Zhang, Y. E., TRAF6 mediates Smad-independent activation of JNK and p38 by TGF-beta. *Mol Cell* **2008,** *31* (6), 918-24.
175. Bakin, A. V.; Tomlinson, A. K.; Bhowmick, N. A.; Moses, H. L.; Arteaga, C. L., Phosphatidylinositol 3-kinase function is required for transforming growth factor beta-mediated epithelial to mesenchymal transition and cell migration. *J Biol Chem* **2000,** *275* (47), 36803-10.

10. Appendix

10.1 Publications

10.1.1 Conference abstracts

Poster presentation at the International Liver Congress 2019 in Vienna Austria, abstract published:

1) **Chen, C**., Nelson, L. J., Avila, M. A., & Cubero, F. J. (2019). FRI-426-Overexpression of c-Jun N-terminal Kinase-1 coincides with the acquisition of cholangiocytic markers in experimental cholangiocarcinoma. *J Hepatol*, 70(1), e581.

2) Leticia Colyn, Gloria Álvarez-Sola, Maria U Latasa, Iker Uriarte, Marina Bárcena-Varela, Maria Arechederra, Maddalen Jimenez, Sergio Morini, Simone Carotti, Julen Oyarzabal, Felipe Prosper, Matteo Canale, Andrea Casadei Gardini, Maria Iraburu Elizalde, Jesus Urman, **Chaobo Chen**, Francisco Javier Cubero, Leonard J Nelson, Bruno Sangro, María Luz Martínez-Chantar, Jesús María Banales, Jose Marin, Carmen Berasain, Maite G Fernandez-Barrena, Matías A Avila. (2019). PS-043-Dual targeting of G9a and DNM-methyltransferase-1 for the treatment of experimental cholangiocarcinoma. *J Hepatol*, 70(1), e27-e28.

3) Raquel Benedé, Olga Estévez, Laura Moran Blanco, Nuria López-Alcántara, Feifei Guo, **Chaobo CHEN**, Ricardo Macias-Rodriguez, Astrid Ruiz-Margain, kang Zheng, Pierluigi Ramadori, Francisco Javier Cubero, Yulia Nevzorova (2019). THU-254-Cumulative effects of western diet and alcohol abuse: A novel model of ASH/NASH-derived liver injury. *J Hepatol*, 70(1), e274.

4) F Guo, K Zheng, R Benedé-Ubieto, O Estévez Vázquez, P Ramadori, MM Woitok, **C Chen**, C Trautwein, C Liedtke, FJ Cubero, YA Nevzorova (2019). c-Myc overexpression in hepatocytes is associated with spontaneous development of non-alcoholic steatohepatitis (NASH) in mice. Zeitschrift für Gastroenterologie, 57(01), P3-4.

10.1.2 Original Publication

1) **Chen C**, Nelson LJ, Ávila MA, Cubero FJ, Mitogen-Activated Protein Kinases (MAPKs) and Cholangiocarcinoma: The Missing Link. *Cells*. 2019 Sep 28;8(10):1172. DOI: 10.3390/cells8101172. PMID: 31569444.

2) Francisco Javier Cubero, Mohamed Ramadan Mohamed, Marius M. Woitok, Gang Zhao, Maximilian Hatting, Yulia A. Nevzorova, **Chaobo Chen**, Johannes Haybaeck, Alain de Bruin, Matias A. Avila, Mark V. Boekschoten, Roger J. Davis Christian Trautwein, Loss of c‐Jun N‐terminal Kinase 1 and 2 Function in Liver Epithelial Cells Triggers Biliary Hyperproliferation Resembling Cholangiocarcinoma. *Hepatol Commun.*2020. 4(6): 834-851. DOI: 10.1002/hep4.1495. PMID: 32490320.

3) Manieri E, Folgueira C, Rodríguez ME, Leiva-Vega L, Esteban-Lafuente L, **Chen C**, Cubero FJ, Barrett T, Cavanagh-Kyros J, Seruggia D, Rosell A, Sanchez-Cabo F, Gómez MJ, Monte MJ, G Marin JJ, Davis RJ, Mora A, Sabio G. JNK-mediated disruption of bile acid homeostasis promotes intrahepatic cholangiocarcinoma. *Proc Natl Acad Sci U S A*. 2020 Jun 29:202002672. doi: 10.1073/pnas.2002672117. Epub ahead of print. PMID: 32601222.

4) Colyn L, Bárcena-Varela M, Álvarez-Sola G, Latasa MU, Uriarte I, Santamaría E, Herranz JM, Santos-Laso A, Arechederra M, Ruiz de Gauna M, Aspichueta P, Canale M, Casadei-Gardini A, Francesconi M, Carotti S, Morini S, Nelson LJ, Iraburu MJ, **Chen C**, Sangro B, Marin JJ, Martinez-Chantar ML, Banales JM, Arnes R, Huch M, Patino J, Dar AA, Nosrati M, Oyarzábal J, Prósper F, Urman J, Cubero FJ, Trautwein C, Berasain C, Fernandez-Barrena MG, Avila MA. Dual targeting of G9a and DNMT1 for the treatment of experimental cholangiocarcinoma. Hepatology. 2020 Nov 22. doi: 10.1002/hep.31642. Epub ahead of print. PMID: 33222246.

10.1.3 Awards

04.2019 **Free registration award** of the EASL (European Association for the Study of the Liver)

TESIS DOCTORAL

MADRID, 2020.